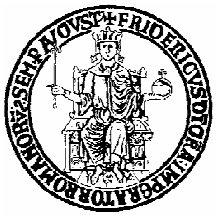

UNIVERSITY OF NAPLES "FEDERICO II"

FACULTY OF MATHEMATICS, PHYSICS AND NATURAL SCIENCES

PH.D. IN CHEMISTRY - XX CYCLE

2004-2007

Synthesis and structural characterization of artificial metalloproteins

Candidate:

Giancarlo Del Gatto

Tutor: ***Prof. Vincenzo Pavone***

Supervisor: ***Prof. Lelio Mazzarella***

Coordinator: ***Prof. Aldo Vitagliano***

Contents

Experimental Section

Appendix

References

List of abbreviations

Abs	Absorbance
Ac	Acetyl
Arg	Arginine
Asn	Asparagine
Asp	Aspartic acid
Boc	t-Butoxycarbonyl
CD	Circular dichroism
DCC	Dicyclohexylcarbodiimide
DCM	Dichloromethane
DIEA	Diisopropylethylamine
DMF	Dimethylformamide
EDT	Ethanedithiol
EtOH	Ethanol
Fmoc	9-Fluorenylmethoxycarbonyl
Gln	Glutamine
Glu	Glutamic acid
HATU	*N*-[(dimethylamino)-1*H*-1,2,3-triazolo[4,5-*b*]pyridin-1-ylmethylene]-*N*-methylmethanaminium hexafluorophosphate *N*-oxide
Hb	Hemoglobin
HBTU	2-(1H-Benzotriazole-1-yl)-1,1,3,3-tetramethyluronium hexafluorophosphate
His	Histidine
HOBt	N-hydroxybenzotriazole
Leu	Leucine
Lys	Lysine
MALDI	Matrix Assisted Laser Desorption Ionization
Mb	Myoglobin
MeOH	Methanol
Mmt	Methoxytrityl
MP	Microperoxidases
NMR	Nuclear magnetic resonance
Pbf	2,2,4,6,7-Pentamethyldihydrobenzofurane-5-sulfonyl

RMD	Restrained molecular dynamics
RP-HPLC	Reverse Phase High Pressure Liquid Chromatography
Ser	Serine
SPPS	Solid Phase Peptide Synthesis
t-Bu	tert-Butyl
TFA	Trifluoroacetic acid
TFE	Trifluoroethanol
TLC	Thin Layer Chromatography
TRT	Trityl

Summary

Metalloproteins are involved in fundamental biological processes and utilize a relatively small number of metal-based prosthetic groups to serve numerous and diverse chemical functions.[1,2]

The hemeproteins family represents a fascinating example in this respect: a single prosthetic group, the heme, promotes a variety of functions, such as dioxygen storage and transport, electron transfer, hydroxylation and oxidation of organic substrates, and hydrogen peroxide disproportion. One of most interesting aspect is how the local protein environment surrounding the heme more finely regulates the heme-protein properties, such as the iron redox potential.

With the aim of understanding the effects of the composition and conformation of the peptide chain in the modulation of the heme redox potential, it has been undertaken the development of porphyrin-peptide molecules, called mimochromes.

They are pseudo-C_2 symmetric systems, composed of two helical peptides covalently linked to the deuteroporphyrin. The use of C_2 symmetry is particularly advantageous, because it simplifies the design, synthesis and characterization. However, it leaves the problem of possible diastereomeric forms. In the cobalt complex of the first derivative, mimochrome I, Λ and Δ isomers were indeed experimentally observed. All the insights derived from the Co(III) mimochrome I structure were used to obtain a re-designed molecule, mimochrome IV. The spectroscopic characterization of the iron and cobalt derivatives suggested the presence of the Λ isomer as unique species. The NMR solution structure of the diamagnetic Co(III)-mimochrome IV confirmed the ability of the molecule to adopt a unique topology, and revealed the peptide chains to be in helical conformation, as designed. The stereochemically stable structure of mimochrome IV provides an attractive model for modulating the redox potential of the heme, by simple changing the peptide chain composition around the heme. To this goal two new analogues, which are characterized by different charges, have been development mimochrome IV 8Lys and

[1] Lippard, S. J.; Berg, J. M. *Principles of Bioinorganic Chemistry*; University Science Books: Mill Valley

[2] Holm, R. H.; Kennepohl, P.; Solomon, E. I. *Chem. Rev*. 1996, *96*, 2239.

mimochrome IV 8Glu, which contain into their sequences eight Lys residues and eight Glu residues, respectively (see figure 1).

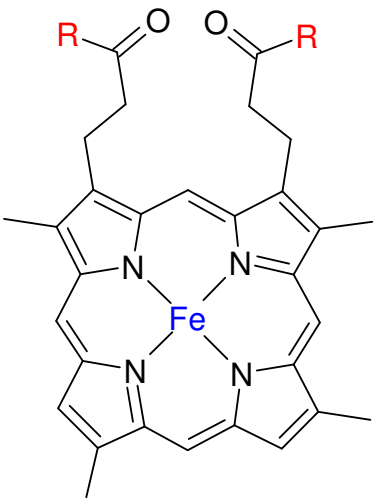

R=R_1; *Peptide mimchromes*

Mimochrome	***Peptide Sequence***
8Glu	Ac-Glu-Glu-Glu-Leu-His-Glu-Glu-Lys-Arg-NH_2
8Lys	Ac-Glu-Lys-Lys-Leu-His-Lys-Lys-Lys-Arg-NH_2
IV	Ac-Glu-Ser-Gln-Leu-His-Ser-Asn-Lys-Arg-NH_2

Figure 1: Structure of Fe mimochromes

The effect of such different charges on the peptide conformation and on the coordination strength has been investigated in detail, by UV-vis and CD spectroscopies while the effect of the charge distributions on redox properties of metal centre, was determined by experiments of square wave voltammetry.

Introduction

Chapter 1: Hemeprotein, structures and functions

Metalloproteins are involved in fundamental biological processes and utilize a relatively small number of metal-based prosthetic groups to serve numerous and diverse chemical functions[1,2]. The hemeprotein family represents a fascinating example in this respect: a single prosthetic group, the heme, promotes a variety of functions, such as dioxygen storage and transport, electron transfer, hydroxylation and oxidation of organic substrates, and hydrogen peroxide disproportion[3]. How different proteins are able to fine-tune the environment of the heme cofactor, thus producing such different chemistries, is becoming increasingly clear through the study of natural and artificial model systems.

High-resolution X-ray crystallographic data as well NMR analysis available for an increasing number of heme-proteins, have deeply contributed to understanding their reactivity and structural and electronic properties at the molecular level[4-16]. It is now well ascertained that the protein matrix, which surrounds the heme active site, controls the intrinsic reactivity of the prosthetic group, selecting one reaction as the only or predominant one.

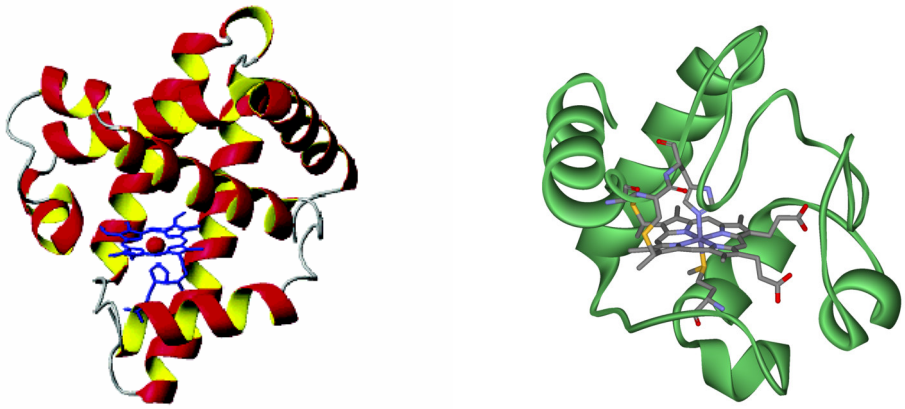

Myoglobin ***Cytochrome c with heme c***

Figure 1.1:two natural heme proteins

However the inherent complexity of natural heme proteins continues to obscure the full description of the factors governing the heme properties.

Therefore, a large number of artificial model systems are being developed in an attempt to (i) provide further insights for structure-activity relationships, (ii) understand the minimal requirements for function, (iii) reproduce the properties of the parent natural proteins in smaller molecules, and (iv) most importantly construct new, tailor-made molecules useful for biomedical, pharmaceutical, biological, and environmental applications.

1.1 Heme structure

1.1.1 Properties of the porphyrin macrocycle

The basic structure of natural heme protein is a tetrapyrrole macrocycle called porphyrin. The porphyrin (shown in figure 1.2) consists of four pyrrole-like five-membered units, A, B, C and D, which are linked by four methine bridges, 5, 10, 15, 20 (*meso* positions). The porphyrin macrocycle is an aromatic system containing 22 π electrons, but only 18 of them are involved in a delocalization pathway. Porphyrin obeys Huckel's rule of aromaticity (4n + 2 π electrons, n = 4) and is shown by X-ray crystallography to be planar. The aromatic character of porphyrins can also be seen by NMR spectroscopy. Due to the anisotropic effect from the porphyrin ring current, the NMR signals for the deshielded *meso* protons appear at low field (8 to 10 ppm), whereas the signals for the shielded protons (on the inner nitrogen atoms) appear at very high field (-2 to -4 ppm).

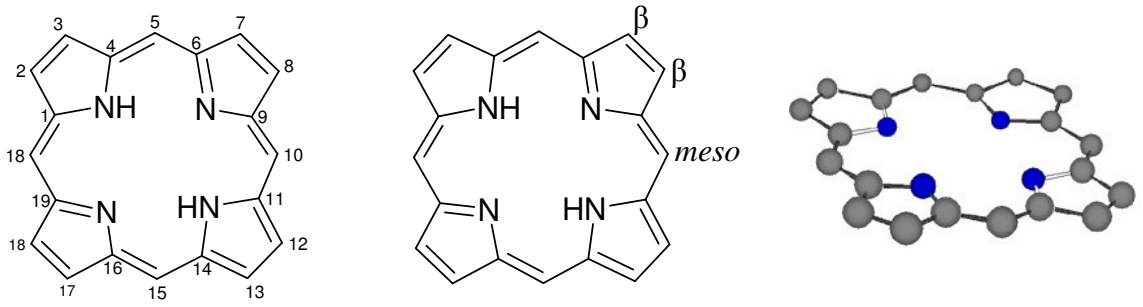

Figure1.2: Basic structure of the porphyrin macrocycle: numbering, functionalization sites and planarity.

The identity of porphyrin in natural heme proteins is distinguished by its peripheral β-pyrrolic substituents, as shown in Figure 1.3. The most common heme tetrapyrrole macrocycle is heme *b* or iron(II) protoporphyrin IX[17]. The term "heme" specifically refers to the ferrous complex of protoporphyrin IX, with the ferric-hydroxy and ferric-chloride complexes referred to as hematin and hemin, respectively. Heme *b*, also called protoheme, has methyl groups at positions 3, 8, 13, and 17, vinyl groups at positions 7 and 12, and propionates at positions 2 and 18 on the macrocycle.

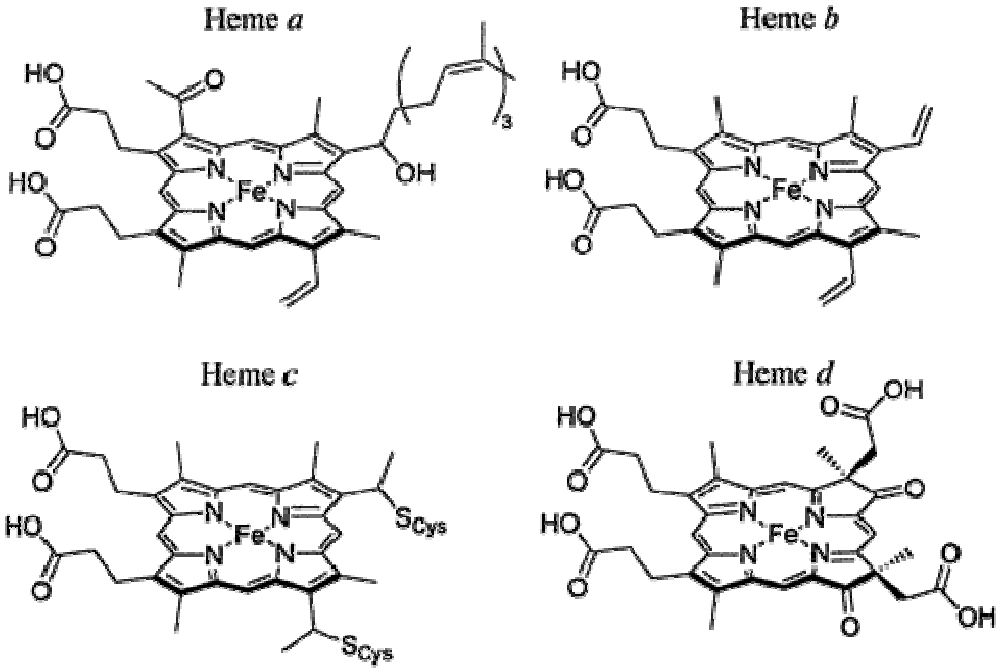

Figure1.3: *Chemical structures of commonly occurring natural hemes a, b, c, and d.*

All the porphyrins are synthesized in vivo as the free base forms before incorporation of the iron(II) by the enzyme ferrocheletase[18, 19]. Additionally, heme *b* serves as the structure from which hemes *a* and *c* are biosynthetically derived. Heme *c* is structurally similar to heme *b* except that thioether bonds to cysteine residues replace one or both of the vinyl groups and covalently link the heme macrocycle directly to the protein scaffold[20]. The covalent attachment of heme to the protein is effected by the enzyme heme lyase,[21] but *in vitro* chemical synthesis has also been used to form the thioether bonds in *b*-type cytochrome and *c*-type cytochrome scaffolds[22-24]. Instead Heme *a* is biosynthesized from heme *b* by conversion of the vinyl group at position 2 into a hydroxyethylfarnesyl side chain, yielding heme *o*, followed by subsequent oxidation of the methyl at position 8 to a formyl group[23]. These alterations render heme *a* both more hydrophobic and more electron-withdrawing as an equatorial ligand to iron than heme *b*. Other less common heme architectures include heme *d*[25], heme P-460[26], siroheme[27], and chlorocruoroheme[28].

1.1.2 Coordination properties

It is now well ascertained that the protein matrix, which surrounds the heme active site, controls the intrinsic reactivity of the prosthetic group, selecting one reaction as the only or predominant one. The protein composition and structural organization of the peptide chain dictate the properties of the primary (metal coordination geometry, number, type, and donor properties of the axial ligands) and secondary (local dielectric constant, hydrophobicity, and hydrogenbonding interactions near the active site coordination sphere) coordination shells. Further, the protein directs long-range interactions[29]. These factors all contribute to the functional specificity of the heme.

It has been well recognized that in the primary coordination sphere, therefore the axial ligands to the iron in eme proteins, play important roles in modulation of structure and function of heme proteins, such as redox potentials, electronic structure, spin states, electron-transfer rates, and catalytic properties[30-37].

Several amino acids are known to serve as axial or proximal ligands to heme proteins[30-32]. In cytochromes (cyt), histidine, methionine, lysine, and cysteine are common axial ligands that coordinate the heme. *Bis*-His and His-Met coordination, found in cyt *b*5 and cyt *c*, respectively, are by far the most common ligation states of the cytochromes (Figure 1.4a). Other ligation states, such as *bis*-Met and His-Lys, have also been found. Interesting ligation from the terminal α-amino group of a peptide bond has been observed in cyt *f* (Figure 1.4a)[38]. Heme-based sensors and enzymes are mostly five coordinate with an open site for binding small molecules such as O_2 and CO. In those proteins, histidine is by far the most common axial ligand, with cysteine and tyrosine found in a few classes of heme enzymes such as cyt P450, chloroperoxidase (CPO), and catalase (Figure 1.4b). Recently, a new axial ligand, the N-terminal nitrogen of proline, was discovered in the CO sensing heme protein called CooA (Figure 1.4b)[39].

While the axial ligands to heme iron establish the basic coordination chemistry, the interaction of amino acids beyond the primary coordination sphere is critical to modulating the chemical properties of the heme, allowing it to perform a variety of biochemical functions.

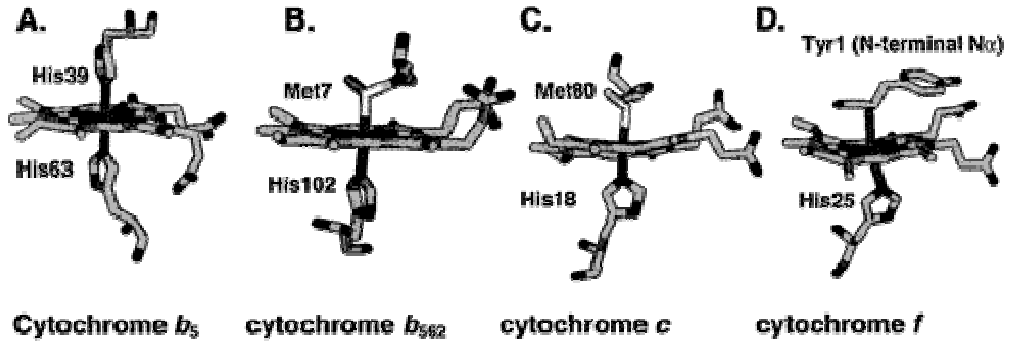

Figure 1.4a: Cytochromes with different axial ligand coordination

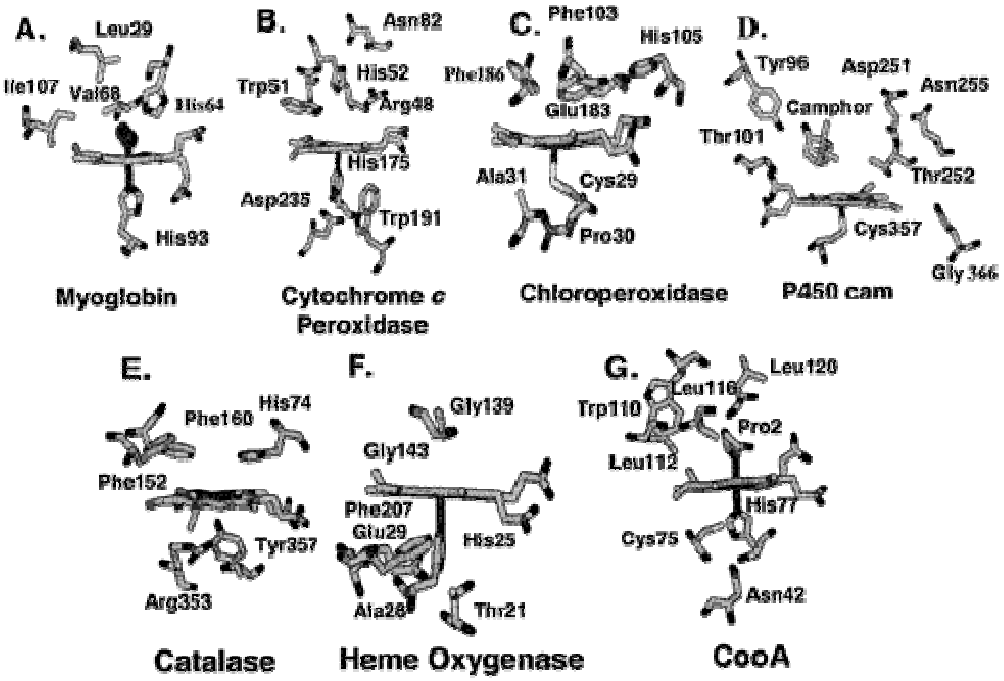

Figure 1.4b*:* Heme proteins with one open coordination site

The local protein environment surrounding the heme more finely regulates the heme-protein properties, such as the iron redox potential[40-45]. For instance, a large number of positively charged residues around the heme in hemoglobin and myoglobin may favor a low oxidation state for the iron, making it ready to bind dioxygen. On the contrary, the progressive change in the polarity of the surrounding peptide environment, from a negative charge distribution in cytochromes *b* to a positive one in cytochromes *c*, determines a

gradual increase in the Fe(III)/Fe(II) redox potential. The resulting stabilization of the matching Fe(II) and Fe(III) states enables cytochromes to mediate the electron transfer.

While the control of the functional specificity by the primary coordination sphere is well understood, the contribution of medium- and long-range interactions is still not completely rationalized, and their molecular description remains to be determined. Therefore, a large number of artificial model systems are being developed in an attempt to

- provide further insights for structure-activity relationships;
- understand the minimal requirements for function;
- reproduce the properties of the parent natural proteins in smaller molecules;
- construct new, tailor-made molecules useful for biomedical, pharmaceutical, biological, and environmental applications.

Chapter 2: Design of new metalloporphyrin scaffold

2.1 Covalent Peptide-Porphyrin Systems

In order to better understand the role of the peptide chain composition and folding in the control of the physico-chemical properties of the heme-proteins, a great deal of attention was devoted to the design of low molecular weight peptide based heme proteins mimetics. These molecules have been developed using quite different strategies. They differ in molecular structures, ranging from simple *meso*-substituted *tetra*-arylmetalloporphyrins to more complex peptide-porphyrin conjugates[46]. The chemical structures of porphyrins usually employed in model systems are illustrated in Figure 2.1.

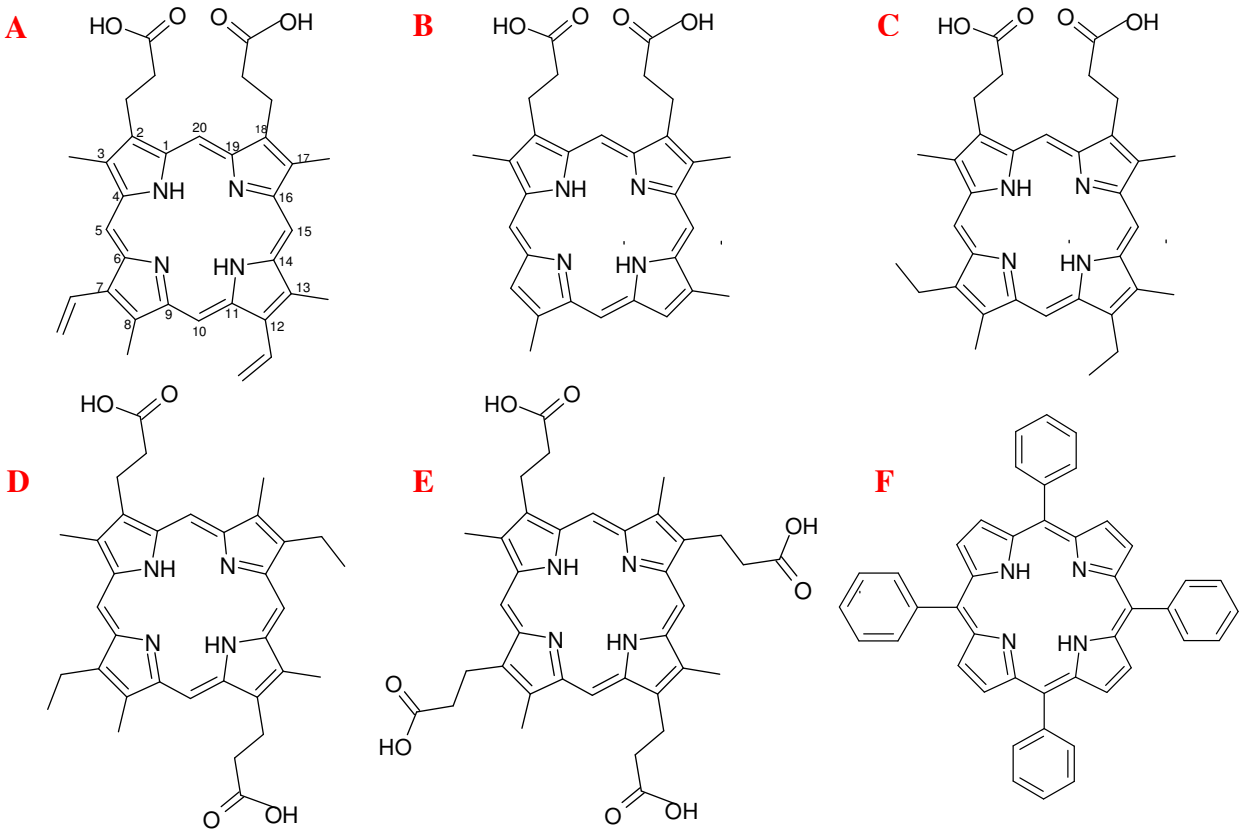

Figure 2.1: Chemical structures of porphyrin rings: (A) protoporphyrin IX; (B) deuteroporphyrin IX; (C) mesoporphyrin IX; (D) mesoporphyrin II; (E) coproporphyrin; (F) *meso*-tetraphenylporphyrin. Commonly, the 5, 10, 15, and 20 positions have been also referred to as *meso*-positions.

A common feature in the compounds so far developed is the assembly, around the porphyrin ring, of several different chemical components, which are intended to fulfill the features of the protein matrix and make the heme ready to accomplish specific functions.

As an example, to obtain oxygen carrier models, two main requirements are needed: (1) stabilization of a five-coordinate heme complex having an imidazole proximal ligand and (2) prevention from further oxidation of the iron-dioxygen complex[47-50].

In the natural systems these mandatory conditions for efficient reversible oxygen binding are accomplished by the presence of the steric bulkiness of the protein moiety, which blocks the formation of a μ-oxo bridge between two heme complexes and brings the axial ligand in the correct coordination position.

On the other hand, a chemical model system for the dioxygen activation, resembling the cytochrome-P450 catalytic cycle and efficiency, should embody the following features. (1) An axial thiolate ligand should be present, as it fundamentally contributes to the heterolytic cleavage of O-O bond and modulates the intrinsic reactivity of the high valent iron-oxo species. (2) A steric protection of the porphyrin ring is required to prevent the rapid degradation of the catalyst by the oxidizing species produced during the reaction. (3) Further, to control the chemio-, regio-, and stereoselectivity in oxygenation reactions, a chiral environment, able to selectively recognize a defined substrate, should be constructed around the heme group[51-54].

The first studies on low molecular weight heme-protein models was based on the construction around the heme of bulky moieties by covalently linking aromatic or aliphatic substituents to the porphyrin ring [47-54].Unfortunately the low functionality of these model systems have not permitted their use in pratical applications. Nevertheless these molecules have gained considerable success at a molecular level, because they have better helped to better understand the properties of the natural heme-proteins. (Figure2.2)

In more recent years, the field of heme-protein mimetics broadens to include more elaborate peptide based models. Peptide-based models are having an enormous impact on our understanding of the factors governing the heme properties, as they seem to be better candidates to mimic both the structural characteristics and reactivity of the natural systems.

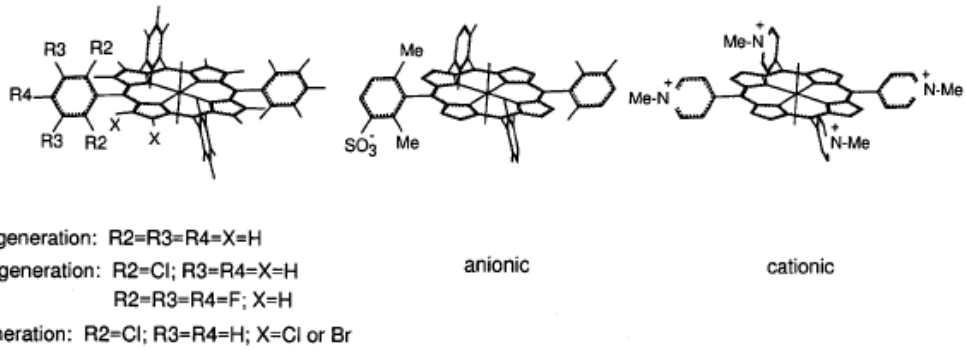

Figure 2.2: Schematic representations of substituted porphyrins as cytochrome P450 models: (a) *first*-, *second*-, and *third*-generation *meso*-tetraaryl substituted porphyrins [51,52], (b) anionic porphyrin[55], and (c) cationic porphyrin [56].

Peptide architecture around the heme can serve for substrate recognition and to reproduce the efficient chemio-, regio-, and stereoselectivity of natural heme-proteins. Peptide models stand at the crossroads of small molecule models and large proteins. Their structures are simple and hence more easily understood than their natural counterparts. They simultaneously have sufficient size and chemical diversity to allow the construction of functional binding and catalytic sites [57-62].

The development of peptide-based models takes advantage of recent progress in both the design and synthesis of peptides and proteins. It is now possible to construct rigid scaffolds able to accommodate substantial changes in their sequence without loosing their three-dimensional structure because the principles governing folding and stability of peptides and proteins are better understood and advanced tools for their design are available [63-72]. Hence, it is possible to build recognition and catalytic sites in a scaffold and to systematically vary the amino acid composition, thus allowing one to (1) optimize the structural and functional properties of the initial target, in terms of stability, catalytic activity and selectivity, (2) test how small changes in the sequence affect the properties of the heme and whether they are able to switch the heme function from one to another, and (3) investigate not only the effect of variation in the first coordination sphere but also the influence on the activity of medium- and long-range interactions.

Peptide models offer the additional advantage of solubilizing the high hydrophobic heme in aqueous solution by simply accommodating the heme group in a hydrophobic pocket of an amphiphilic structure.

2.2 Spectral Properties of Metal-Porphyrins and Heme-Proteins

UV-vis spectroscopy has been widely applied for the characterization of peptide-based heme-protein models because it is one of the most powerful techniques for the analysis of the heme properties. Useful information on artificial porphyrin-containing systems can be obtained by comparing their spectral properties with those of natural heme-proteins and viceversa. This section will provide a brief survey of the main spectral features of metalloporphyrins and heme-proteins, which could be helpful to nonspecialists in understanding the subsequent sections. For a more detailed description of porphyrin and metalloporphyrin spectra together with the theoretical aspects of the spectral transitions, the readers can refer to many excellent reviews on the arguments [73-76].

The porphyrins and their various metal complexes show very distinct spectra, and UV-vis spectroscopy can be conveniently applied to ascertain the insertion of the metal into the porphyrin ring, the oxidation and spin state of the metal, and the nature of the axial ligands. The highly conjugated π-electron system of the porphyrin ring is responsible for its intense color. Two $\pi \rightarrow \pi^*$ electronic transitions are responsible for the absorption bands, typically found in the porphyrin spectra[73-76]. An intense band (molar extinction coefficient $\approx 10^5$ M^{-1} cm^{-1}) is detected around 400 nm, and it is referred to as the *B* band, Soret band, or γ band; much weaker bands (molar extinction coefficient $\approx 10^4$ M^{-1} cm^{-1}) are observed in the 500-600 nm visible region. These weaker bands are referred to as *Q* bands or β-α bands. The α band corresponds to the lowest porphyrin $\pi \rightarrow \pi^*$ singlet transition Q_o and the β band to the vibronic envelope Q_v[73,74]. The visible bands are very sensitive to the metal inserted into the porphyrin ring and to peripheral substituent groups. The Q_o and Q_v transitions are polarized in the *x*, *y* plane of the porphyrin; for a metal porphyrin with D_{4h} symmetry, the dipole transitions in the *x* and *y* directions are equivalent and both the Q_o and Q_v transitions are doubly degenerate. Thus, the spectrum of a metal porphyrin usually shows two bands in the visible region. In free base porphyrins, two protons are linked to two opposite inner nitrogens (see Figure 1). In this case, the porphyrin plane no longer possess the 4-fold symmetry and β and α bands splits. In fact, the degenerate Q_o transition is replaced by transitions polarized along each of the nonequivalent *x* and *y* axes, Q_o^x and Q_o^y.

Each transition has its vibronic envelope (Q_v^x and Q_v^y), and, as a consequence, four distinct bands characterize the spectrum of free base porphyrins in the visible region[73-76].

The positions of the Soret, *β,* and α bands depend on the metal electron configuration, and the energy of the transitions varies as a consequence of the coupling between the metal and the porphyrin orbitals. The absorption spectra of metalloporphyrins are thus classified into three types, *normal*, *hypso*, and *hyper* [76].

Normal-type spectra are observed for a majority of metalloporphyrins with closed-shell metal ions, where the relevant porphyrin π orbitals do not significantly interact with the metal orbitals. The Soret, α*,* and *β* bands are often found around 400, 570, and 530 nm, respectively.

Hypso-type spectra follow the *normal* absorption pattern, but all bands are blue-shifted, due to filled metal d orbitals to porphyrin π^* back-donation. Metal ions that cause *hypso*-type spectra are limited to those of d^6-d^9 electron configurations.

Finally, *hyper*-type spectra show charge-transfer bands in addition to a significant red-shift of the porphyrin π-π^* bands. They are difficult to analyze because the number of extra bands varies from one metal ion to another and the positions of all bands are far more dependent on the axial ligands than in the other types [76]. Metal ions with d^1-d^5 electron configurations show these *hyper*-type spectra. Most of them can be easily found in lower oxidation states within the porphyrin, causing *normal*- or *hypso*-type spectra. Mn(III)- and Fe(III)-porphyrins are the best known examples in this respect.

The UV-vis spectra of heme-proteins show absorption patterns quite similar to those observed in simple metalloporphyrins. They are very sensitive to the oxidation and spin state of the iron, which are modulated by the protein environment. In addition to the Soret, *β*, and α bands, four extra bands are found in the lower energy of the visible region, and they are usually referred to as IV, III, II, and I. The typical UV-Vis absorption data for several hemoproteins are reported in Table 2.1[74,75,77-80].

			Soret		β		α	
Protein	**axial ligands**	**spin state**	**λ_{max} (nm)**	**$\varepsilon \times 10^{-3}$ ($M^{-1}cm^{-1}$)**	**λ_{max} (nm)**	**$\varepsilon \times 10^{-3}$ (M^{-1} cm^{-1})**	**λ_{max} (nm)**	**$\varepsilon \times 10^{-3}$ (M^{-1} cm^{-1})**
Sperm whale Mb[a]								
MbO_2	His/O_2	LS	418	128	543	14.6	581	13.6
MbCO	His/CO	LS	423	187	542	14.0	579	12.2
Mb	His/H_2O	HS	434	115	556	11.8	588	s[g]
Horse Hb[b]								
HbO_2	His/O_2	LS	415	129	540	14.1	576	14.9
HbCO	His/CO	LS	419	192	539	13.9	569	13.9
Hb[h]	His/H_2O	HS	430	130	555	12.9	590	s[g]
cyanomet-Hb	His/CN	LS	422	114	542	10.9	575	s[g]
aquomet-Hb[i]	His/H_2O	HS	405	169	500	9.0	540	s[g]
Cytochromes								
E. coli b_{562} red[c]	His/Met	LS	427	180	531	17.6	562	32.1
E. coli b_{562} ox[c]	His/Met	LS	419	117	531	11.3	564	9.30
chloroplast b_{559} red[d]	His/His	LS	427	-	530	-	559	-
chloroplast b_{559} ox[d]	His/His	LS	413	-	534	-	562	-
michrosomes b_5 red[e]	His/His	LS	423	-	527	-	555	-
michrosomes b_5 ox[e]	His/His	LS	413	117	530	11.0	560	9.16
P450-CAM[f]	Cys/H_2O	LS	417	115	536	10.6	569	11.1

Table 2.1: [a] Data from ref 74.[b] Data from ref 75.[c] Data from ref 77.[d] Data from ref 78.[e] Data from ref 79.[f] Data from ref 80[g] s indicates that the band produces a shoulder.[h] The III and I bands are detected at 758 nm (ε = 375 M^{-1} cm^{-1}) and 910 nm (ε = 195 M^{-1} cm^{-1}), respectively, and are diagnostic for the HS state.[i] The IV and III bands are detected at 580 nm (ε = 3400 M^{-1} cm^{-1}) and 633 nm (ε = 3900 M^{-1} cm^{-1}), respectively, and are diagnostic for the HS state.

2.3 Microperoxidases

Peptide-based hemoprotein models have been developed in order to reproduce better in model systems the physical-chemical properties of the natural systems. Microperoxidases (MP8 and MP11) have been widely employed as biomimetic models for heme-containing enzymes.

The microperoxidases (MPs) are the heme-protein containing the consensus cyt *c* CXXCH sequence motif, as shown in Figure 2.3. They can be obtained by the cytochrome *c* proteolysis with digestive enzymes. The most important microperoxidase are Microperoxidase-11 (MP-11), isolated from pepsin digestion, and microperoxidase-8 (MP-8), isolated from trypsin digestion, contain 11 and 8 amino acids, respectively. While the number of residues contained in microperoxidases depends on the proteolysis conditions, all contain the covalently linked *c*-type heme with a histidine axial ligand.

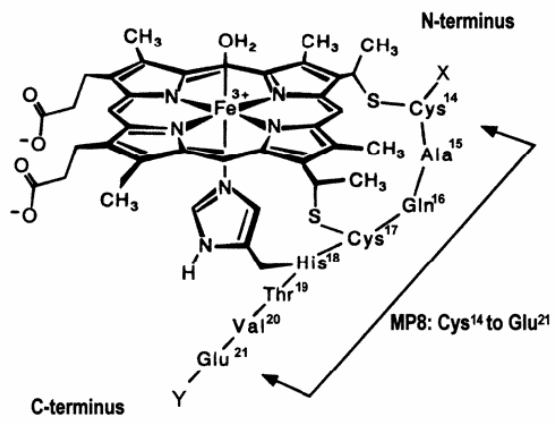

Figure 2.3: Schematic representation of the microperoxidase framework

In the MP8, the porphyrin is covalently attached to the protein fragment through thioether linkages with Cys residues at positions 14 and 17; in the MP11, the peptide fragment corresponds to the 11–21 amino acid sequence of the protein. The His residue at position 18 in both systems acts as axial ligand to the iron ion, leaving the sixth coordination site able to accommodate exogenous ligands or substrates. MP8 and MP11 have been tested in a wide number of catalytic reactions, such as peroxidase like and cytochrome P450-like

reactions. They are able to activate hydrogen peroxide to give high valence iron *oxo* species.

The applications of these systems are limited low stability under the catalytic conditions: the porphyrin ring is rapidly degraded either by the direct action of H_2O_2 or by intermolecular reactions between the iron-*oxo* species and a non-activated molecule of the catalyst. However, their stability is higher than that of simple protoporphyrin systems, thus indicating that the presence of a small peptide chain can play an important protective role. Recently [81], the influence of peptide chain length and composition on the stability of the microperoxidases has been investigated. An increase in the size of, the attached polypeptide results in an increase in stability. The peptide chains can: (a) function as a scavenger for hydroxyl or superoxide radicals; (b) make a barrier for the formation of the inactive μ-oxo diiron dimer; (c) act as an alternative source of H-atoms, thus reducing the inactivation of the microperoxidase by H-atom abstraction from the *meso* position of the porphyrin ring. The analysis of the features of microperoxidases highlights the role of the peptide chains in modulating the reactivity of the heme ring. Furthermore, these molecules also serve as useful probes for the interpretation of some spectroscopic properties of synthetic heme-peptide adducts [82].

2.4 Peptide based-synthetic porphyrins

The search for artificial catalytic systems able to reproduce the properties of natural hemeproteins is a key field in bioinorganic chemistry. The pioneering example of an artificial hemeprotein, based on a peptide-porphyrin conjugate system, was developed by Sasaki and Kaiser in an effort of using a porphyrin ring as a template to direct helical folding into the attached peptides [83-84]. The resulting molecule, named “helichrome”, is characterized by four identical 15-residue peptide chains N-terminally linked to the four propionic groups of coproporphyrin I, shown in Figure 2.4.

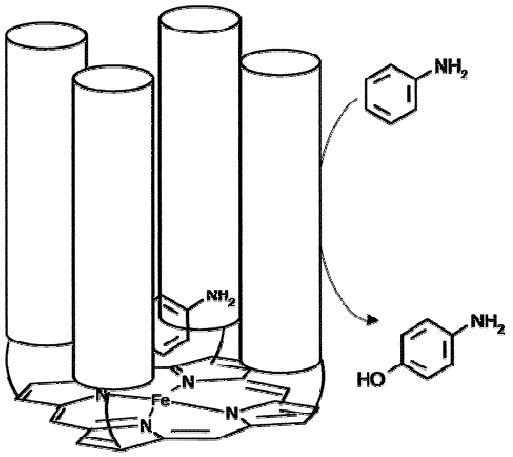

Figure 2.4: Schematic representation of the helichrome molecule

Helichrome was designed to mimic the hydroxylase activity of cytochrome P450, whose structure is characterized by the presence of several α-helices surrounding the heme group and forming a hydrophobic recognition site. Therefore, the peptide sequence in helichrome was chosen such that it could stabilize an amphiphilic helix and create, in the folded state, a substrate binding hydrophobic pocket proximal to the porphyrin ring.

Helichrome, by structural and functional characterization, showed quite remarkable features:

- soluble in water above pH 3;
- the peptide chain exhibits a high α-helical content as assessed by CD measurements;
- is monomeric under the experimental conditions of the spectroscopic measurements;
- The free energy of folding (-4.4 kcal mol^{-1}) was determined to be comparable to that of native globular proteins.

These properties have induced to use the helicrome in catalytic reactions. The aniline hydroxylase activity of the helichrome-iron(III) complex, from K_{cat} and K_m values, showed to be similar to those of natural heme-proteins that possess this activity.

Interestingly, the rigid hydrophobic pocket formed by the peptide chains plays key role for helichrome activity because the iron(III) complex of the isolated coproporphyrin showed negligible catalytic activity under the same conditions.

A quite similar approach was followed in the development of tetraphilins[84]. These molecules were designed with the aim of mimicking the activity of ion-channel proteins.

To provide assemblies of defined aggregation state and drive amphiphilic peptides into four helix bundles, ion-channel-forming peptides were covalently attached to a tetraphenylporphyrin derivative (shown in Figure 2.5).

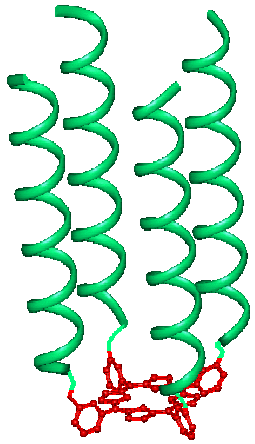

***Figure 2.5*:** Molecular model of tetraphyillin.

Four copies of the 21-residue peptide $(LSLBLSL)_3$ (B= α-aminoisobutyric acid) were covalently linked through the peptide N-terminus to *meso*-tetrakis (*m*carboxyphenyl) porphyrin via *m*-carboxamido linkages. *Meta* substitution provides optimal interhelical spacing for ion transport. The tetraphilins properties in forming ion channels in planar diphytanoyl phosphatidylcoline bilayers indicated that the attachment of the peptide to the template stabilizes the conducting state of the peptide. Therefore, thetetraphenylporphyrin template exerts a major influence on the lifetime and voltage dependence of $(LSLBLSL)_3$ channels, possibly through changes in the overall hydrophobicity and geometric restrictions imposed on the peptide.

In summary, heliochrome and tetraphilins are excellent examples of using a porphyrin template to direct the folding of peptides into a helical conformation.

The use of porphyrin templates for inducing helical conformation in peptide sequences is as well reported in the papers of Benson[85–87]. With the aim of elucidating the forces which impart stabilization to protein structures, they developed peptide sandwiched mesoheme molecules[85,87], in which a random coil–helix transition of two identical peptides, covalently attached to a iron III–mesoporphyrin IX moiety, occurs upon histidine to iron binding.

In a subsequent work[86], the same effects have been investigated by using a cystine-dimerized peptide containing two histidine residues. In the presence of cobalt (III)–coproporphyrin I, the peptide self assembled around the macrocyclic ring. The authors concluded that these non-covalent model systems could be applied to probe the influence of peptide sequence and porphyrin structure on peptide conformational stability. A similar approach was followed by Mihara et al. in the design of heme-binding peptides[88]. A 14-residue peptide segment was designed to stabilize an amphiphilic α-helix structure. To construct a parallel 2α-helix structure the two segments were dimerized by the disulfide linkage of Cys^{16}.

Furthermore, a His residue was introduced at the position 6 of the sequence in order to coordinate a heme group. The CD and UV-Visible spectroscopic characterizations showed that the heme binding is controlled by the peptide conformation. Moreover, the formation of the heme–peptide complex enhances the N demethylase activity of the heme.

2.5 Peptide-Sandwiched Deuteroheme: Mimochromes

Our laboratory has approached the challenge of constructing heme-protein models using a miniaturization process[46]. A miniaturized heme-protein is a peptide-based model which contains a minimum set of constituents necessary for

- an accurate reconstruction of a well-defined structure and
- a fine tuned reproduction of a defined function.

This strategy leads to the development of a class of miniaturized heme-proteins, named mimochromes[89-93]. The schematic structures of mimochromes are reported in Figure 2.6.

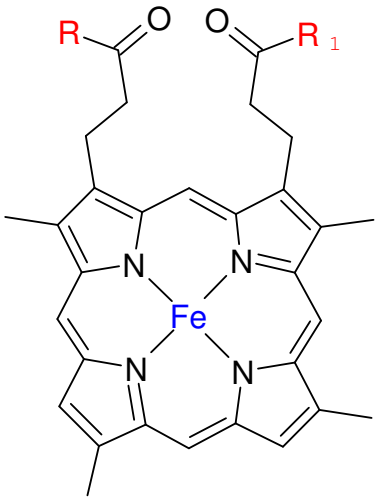

R=R1 *peptides sequence*

Mimochrome	*Peptide sequence*
I	Ac–L–A–Q–L–H–A–N–K–L–NH_2
II	Ac–D–L–S–D–L–H–S–K–K–L–K–I–T–L–NH_2
IV	Ac–E–S–Q–L–H–S–N–K–R–NH_2

Figure 2.6: Schematic representation of mimochromes

Mimochromes are peptide-porphyrin conjugates, with *pseudo-*C_2 symmetry. They are made up of deuteroporphyrin, covalently linked to two peptides (nine or fourteen residues), *via* an amide bond between the porphyrin propionyl groups and the side chains of two Lys residues[89-92]. The peptide fragments, which face the porphyrin plane, are in α-helical conformation, a common feature of several natural heme-proteins. The α-helix is a well-defined rigid scaffold, which can accommodate several amino acid substitutions without severe structural perturbations; therefore, numerous model compounds, based on helical

peptides, have been developed[94,95]. The peptide sandwiched mesoheme[85-87], the disulfide linked α-helices-mono-heme adducts[96-98], the MOP derivatives[99-101], and the heme-maquettes[102-105] are examples of either covalent or non-covalent artificial heme-peptide conjugates.

The prototype mimochrome I was designed an the β-chain of human deoxyhemoglobin as template structure. The X-ray structure of deoxyhemoglobin[106] showed that the proximal His[89] residue is located in the central position of the Leu[88]-Leu[96] protein fragment. This protein fragment adopts an helical conformation. It represents a rigid framework both for properly positioning His[89] in the correct coordination site, and for completely covering one face of the heme. The helix axis is about parallel to the porphyrin plane; hydrophobic residues surround the axial coordinating residue and face the heme directly.

All the information derived from the analysis of the natural systems served as starting points for engineering the mimochrome models. As a first step in this direction, we used the Leu[88]-Leu[96] fragment as a scaffold for building an nine residue polypeptide sequence able to fold into an α-helical conformation[89](see Figure 2.6). We appropriately changed the natural sequence by considering the factors that affect helix stability.

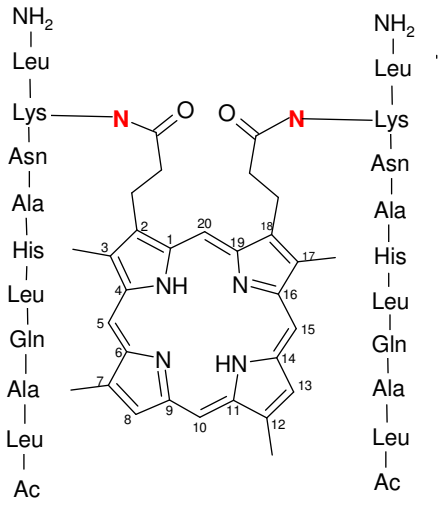

Figure 2.6: Formula of mimochrome I: (3, 7, 12,17-tetramethyl-porphyrin-of N^{ε}_{8}-(Ac-Leu[1]-Ala[2]-Gln[3]-Leu[4]-His[5]-Ala[6]-Asn[7]-Lys[8]-Leu[9]-NH_2)-propionamide)

Therefore we replaced Ser[89] and Cys[93] with alanine, which is known to have a high preference for the α-helical conformation. The resulting sequence contained five helix inducing residues, Leu[1,4,9] and Ala[2,6]. Moreover, Glu[90] and Asp[94] were substituted with Gln

and Asn respectively, in order to obtain an uncharged compound. N- and C-terminal ends were acetylated and amidated, respectively, in order to avoid unfavorable end-charge to helix-dipole interactions. The peptide chain was then covalently linked to the porphyrin propionic group through the ε-amino function of Lys^{8}. Molecular modeling showed that changing the side chain conformation of Lys^{95} as found on the β chain of deoxyemoglobin and the conformation of the closest propionyl carboxyl group, the lysine ε-amino group may approach the carboxyl group at bonding distance. Finally, an identical peptide chain was placed on the other side of the heme by applying a C2 symmetry operation (Figure 2.7)
.

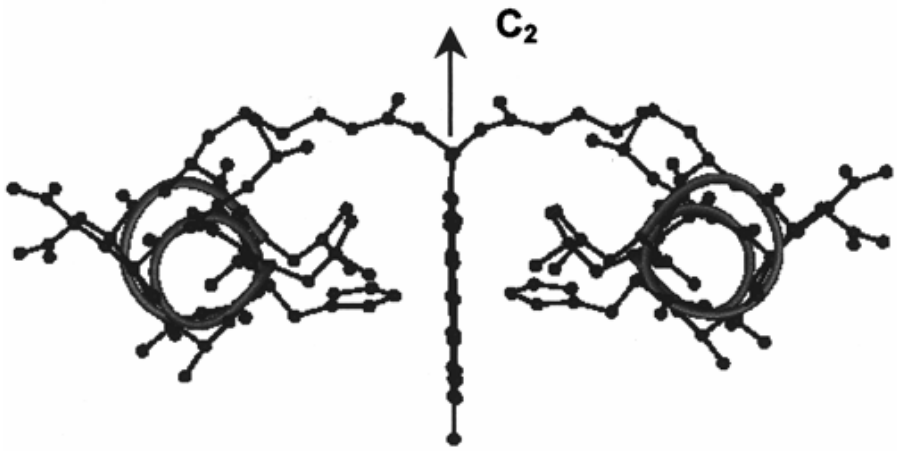

Figure 2.7: helix-heme-helix sandwich obtained by applying a C2 symmetry operation.

The two covalent bridges between the peptide moiety and the porphyrin, together with the coordination of the two His residues, would make the peptide chains able to cover both heme faces. These factors would also serve as a strong local constraint to firmly keep the prosthetic group inside the hydrophobic cavity created by the two peptide chains. Finally, deuteroporphyrin was preferred to the most common protoporphyrin IX to avoid degradation of the sensitive vinyl substituents during the synthesis.

The fully characterization of mimochrome I iron and cobalt complexes confirmed the design, even though some unexpected features were observed. The iron complex showed quite low solubility in water (in the μm range), in a wide range of experimental conditions[90-92]. Its detailed characterization was henceforth strongly limited. On the

opposite, the cobalt complex was soluble in water (up to mm concentration), but two equally abundant isomers were obtained (see Figure 2.8).

Because of the flexibility of the linker between the peptide and the deuteroporphyrin ring, each peptide chain can be positioned either above or below the porphyrin plane, giving rise to Λ and Δ diastereomers (see Figure 2.9)[91].

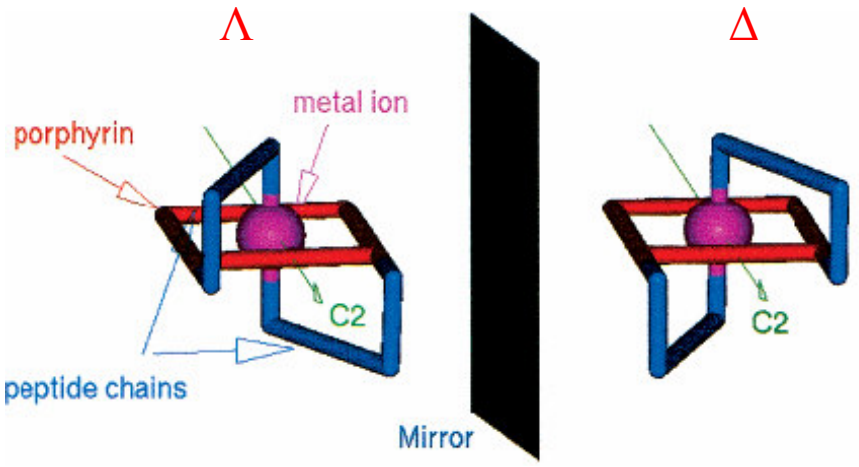

Figure2.8: Schematic representation of the two possible orientations of the peptide chains around the metal center, which give rise to the two Λ and Δ diastereomers.

This finding was confirmed by the solution structural characterization[89]. In fact, the NMR structures of the two diamagnetic Co(III) isomers (Figure 2.9), which represent the first example of structure determination of a designed heme-protein models, allowed a definitive identification of the two isomers as the Λ and Δ diastereomers and a straightforward correlation between their structure and spectral properties. As expected, the peptide chains adopt an almost regular α-helical conformation; the helices lie parallel to the porphyrin plane, and they are antiparallel to each other in the Λ isomer and about orthogonal in the Δ isomer (see Figure 2.9). The analysis of the three-dimensional structure of the two cobalt isomers was important in understanding the properties of the Fe(II) and Fe(III) complexes, which could not be studied by NMR spectroscopy because of their poor solubility

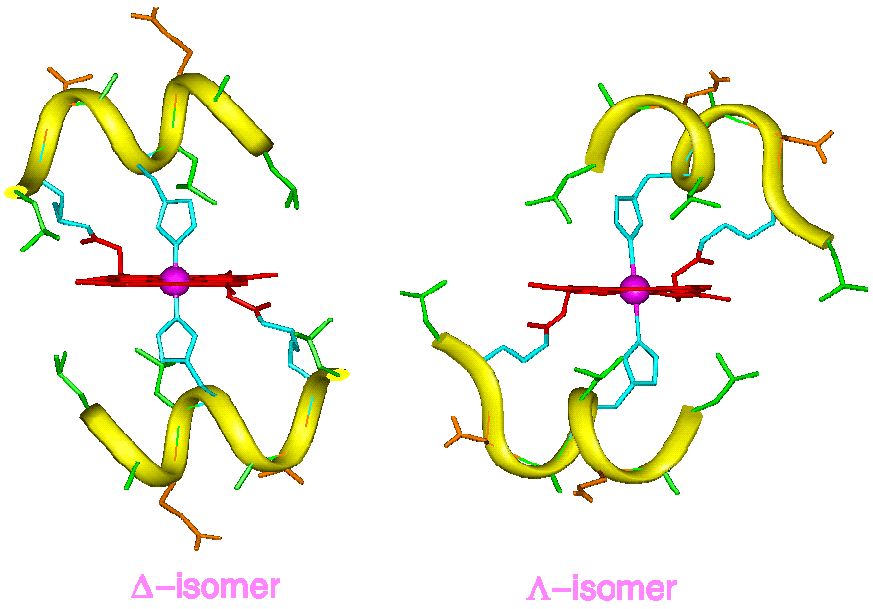

Figure 2.9: Average molecular structures of Co(III) mimochrome I Δ and Λ isomers, as obtained from NMR experimental data and RMD calculations.

The remarkably different solubility between the iron and cobalt complexes was tentatively attributed to the simultaneous presence of the two diastereomers, for the iron complex, in fast interconverting equilibrium. During this process both peptide chains might be displaced from the porphyrin plane. The porphyrin ring is thus exposed to the solvent, and aggregation by stacking of the porphyrin ring may occur. Confirmation for this hypothesis came from the CD spectral properties in the Soret region, which are an average of those corresponding to the two separate diastereomers (see Table 2.2).

The unpredicted but experimentally observed Λ and Δ isomers of Co(III)-mimochrome I clarify the concept of diastereomerism that may occur when polypeptides coordinate to metal ions. The use of local *pseudo*-*C*2 symmetry is particularly advantageous to construct symmetric molecules with minimized size, because it simplifies the design, reduces the size of the molecules to be synthesized, and may simplify their structural characterization[107,108]. However, great attention should be paid in the design to overcome the problem of diastereomer formation.

	UV region	Soret region	
	$[\theta]_{222}$	$[\theta]$	sign
mimochrome I	■■	not detected	not detected
Fe(III)-mimochrome I	■■	(-) ■■■; (+) ■	S-shaped
*Co(III)-mimochrome I*Δ	■■	■■■■■	negative
*Co(III)-mimochrome I*Λ	■■	■■■	positive
mimochrome II	■■■	not detected	not detected
Co(III)-mimochrome II	■■■	■■	negative
mimochrome III	■■■	■	negative
Fe(III)-mimochrome III	■■■	■■	positive
mimochrome IV	■	not detected	not detected
Fe(III)-mimochrome IV	■■	■■■■	positive
Co(III)-mimochrome IV	■■	■■■	positive

Table 2.2: CD parameters for Mimochrome Derivatives[a]; *(a),* The intensities of the cotton effect are proportional to the number of ■

The information derived from mimochrome I was fruitfully applied for improving the structure by design. Two strategies were used to reduce the peptide flexibility:

- by elongating the peptide chain at the C-termini, with a four residue fragment, modeled in an extended conformation;
- by amino acid substitutions that may provide *intra*-molecular, *inter*-chain interactions.

The first strategy was successfully applied, as reported for mimochrome II, where the stabilization of the Λ isomer was achieved[91]. The second strategy led to the design of mimochrome IV, namely 3,7,12,17-tetramethylporphyrin-2,18-di-N_8ε-(Ac-Glu^1-Ser^2-Gln^3-Leu^4-His^5-Ser^6-Asn^7-Lys^8-Arg^9-NH_2)-propionamide.

Mimochrome IV was designed by using the NMR structures of Co(III) mimochrome I Δ and Λ isomers as templates[90]. Mimochrome I contains two leucine residues at both the N- and C-termini. These residues were selected in the initial design of mimochrome I, because

of their high propensity to be accommodated in α-helical conformation[109]. Further, we expected that hydrophobic interactions, between the leucine side chains and the porphyrin, would drive the helices to lay on the porphyrin. Nevertheless as mentioned previously , the sandwich was stable for the Co(III) derivative, and not for the Fe^{III} [89,90]. In order to provide an extra contribution to the stability of the sandwich, beside the metal coordination force, we modified the sequence of mimochrome I, by introducing *intra*-molecular, *inter*-helical interactions.

The Cα atoms of Leu^1 of one helix and of Leu^9 of the other helix are about 12 Å apart in both isomers. At this distance, the carboxylate side chain of a Glu residue at position 1 of one peptide chain could ion pair with the guanidine group of an Arg residue at position 9 of the other peptide chain. Thus, Glu^1 and Arg^9, which replace Leu^1 and Leu^9, was inserted to stabilize one of the two possible diastereomers. Further, the solvent exposed Ala^2 and Ala^6 in mimochrome I were replaced by Ser residues in mimochrome IV in order to further increase the water solubility of the new molecule.

The insertion of Glu and Arg residues at position 1 and 9 of the sequence, respectively, was successful in stabilizing the sandwich structure and in favoring the formation of Λ isomer (figure 2.10) over the other, both in the Fe(III) and Co(III) complexes. These results were confirmed by NMR data and RMD calculations[110].

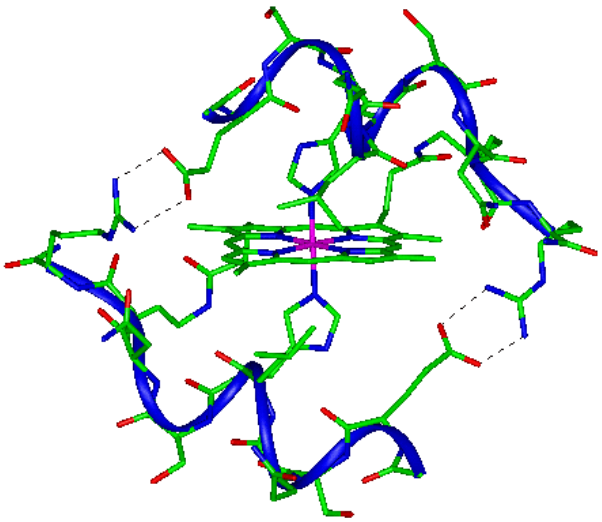

Figure 2.10: Co(III)-mimochrome IV average structure as obtained from NMR data and RMD calculations

The UV-vis pH titration showed the iron *bis*-His coordination is strong enough to bring the His pK_{app} value around 3.8. The *bis*-His coordination is even stronger in Co(III) complex, and it occurs at very acidic conditions (pH < 2). This finding is related to the high preference of cobalt for nitrogen donor ligands, and to the exchange- inertness of low-spin Co(III) complexes. These low pKa values of the axially coordinating His (with values very close to what observed in several myoglobins, hemoglobins and cytochromes in the oxidized and reduced forms) strongly support the designed sandwich structure[111,112].

CD spectra in the far UV region confirmed the peptide chain to be predominantly in an α-helical conformation in both the *apo* and metalated species, even at low TFE concentration. We also observed that the sign of the Cotton effect depends on the relative orientation of the peptide chains respect to the porphyrin plane. In the cobalt complexes of mimochrome I and II, the Λ configuration gives rise to a positive Cotton effect, whereas the Δ configuration gives rise to a negative effect; in the Fe(III) mimochrome I complex, the observed S-shaped Soret Cotton effect was attributed to the simultaneous presence of the two diastereomeric forms. Consequently, the presence of a positive Cotton effect in both Fe(III) and Co(III) mimochrome IV complexes indicates that both systems assume a Λ configuration. A single positive Cotton effect detected even in the iron complex confirmed the effectiveness of the inter-helical interactions in reinforcing the sandwich structure and in driving the peptide chains to fold into a unique topology around the heme. The definitive answer of the structural identity of the diastereomer stabilized in mimochrome IV was obtained by NMR structural characterization of the cobalt complex. The NMR analysis fully confirms the UV-vis and CD data, both regarding the helical conformation of the peptide chains, and the Λ configuration of the hexacoordinated CoIII ion. The RMD calculations, using the NMR experimental data as conformational restraints, indicated two helical peptide chains, oriented about perpendicularly.

In summary, mimochrome IV is a simple, structurally defined heme protein model, which provide an excellent opportunity for exploring the subtle mechanisms that control the heme functions. The peptide structure of mimochrome IV is such that a partially open hydrophobic cage around the imidazole ring is present. Except for the position 20 of the deuteroporphyrin ring, all the other meso positions are covered by the polypeptide chains,

which, similarly to the natural systems, may protect the deuteroporphyrin ring from degradation during catalytic cycles.

The amino acid composition of mimochrome IV can be modified in order to modulate the functionality in terms of redox potentials, trying to adapt the behavior to different applications. Substitution of serines, glutamines and asparagines, which point outward from the molecular core, with differently charged residues may alter the electrostatics, polarity and solvent accessibility of the heme site, and modulate its electronic, catalytic and binding properties.

Chapter 3: Design of new mimochromes

On the basis of results gotten by mimochromes development, we have drawn advantage from stereochemically stable structure of mimochrome IV for modulating the redox potential of the heme. Based on the mimochrome IV design, two news models were obtained: mimochrome IV 8Glu and mimochrome IV 8Lys (figure 3.1).

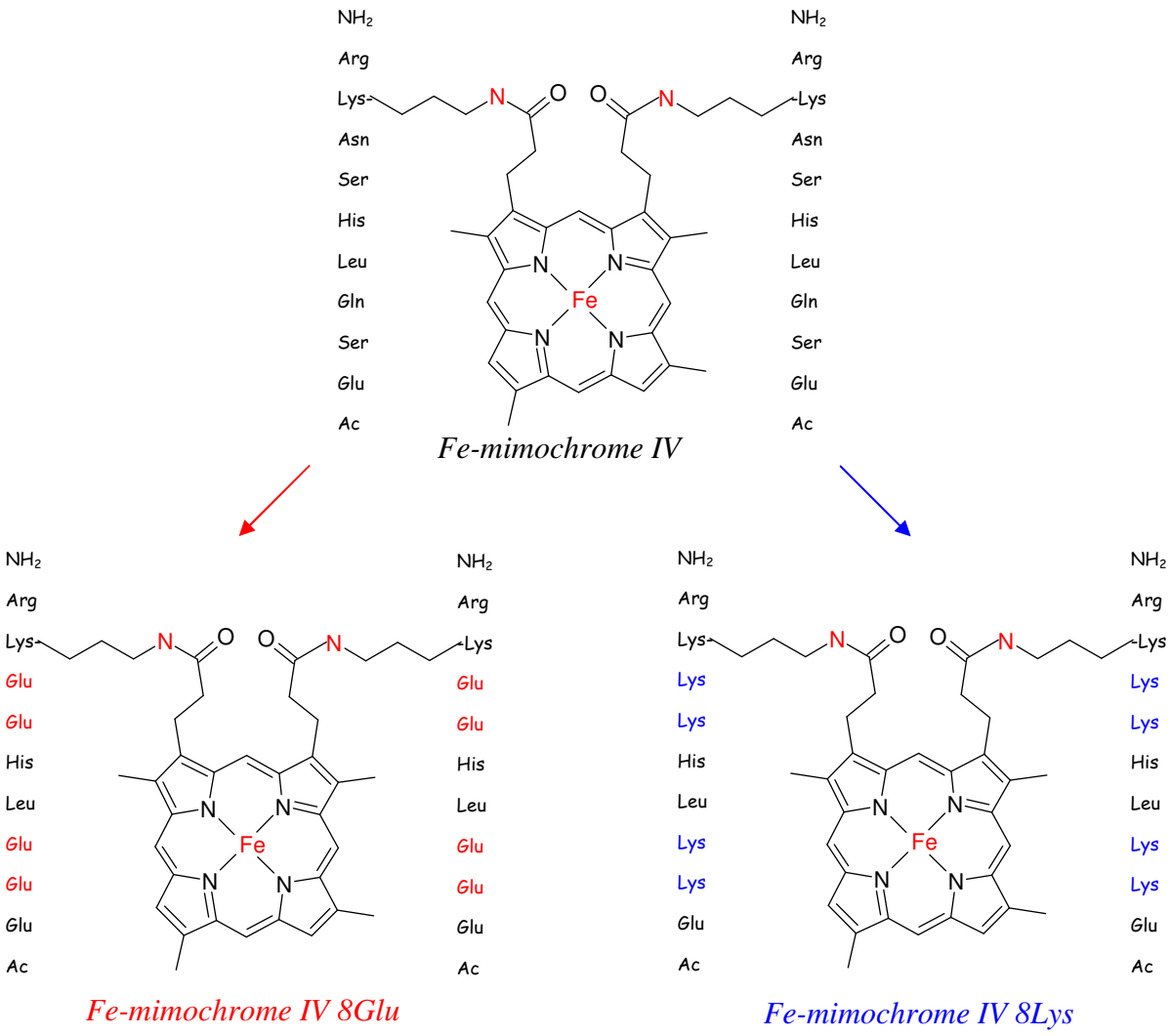

Figure 3.1: Schematic structures of mimochrome IV, mimochromeIV 8Glu , and mimochrome IV 8Lys

Mimochrome IV 8Glu and mimochrome IV 8Lys contain into their sequences differently charged residues: eight **Glu** residues and eight **Lys** residues, respectively, that replace Ser, Asn and Gln of the parent Mimochrome IV sequence. The impact of the charge on heme properties was studied in this work thesis

Results and Discussion

Chapter 4: Mimochromes synthesis

4.1 Synthetic procedure

Mimchrome IV, mimochrome IV 8 Glu and mimochrome IV 8 Lys were all synthesized using the same procedure. In scheme 1 the procedure used for the synthesis of mimochrome IV is depicted. Both solid phase and solution methods were used in the synthetic procedure. The deuteroporphyrin scaffolds was functionalized with three different peptides (figure 4.1)..

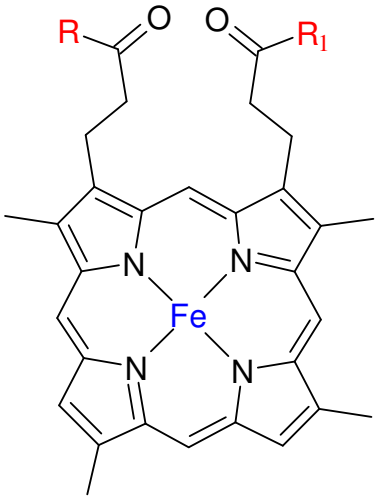

R=R_1; *Mimochromes peptide*

Mimochrome	*Peptide sequence*
8Glu	Ac-Glu-Glu-Glu-Leu-His-Glu-Glu-Lys-Arg-NH_2
8Lys	Ac-Glu-Lys-Lys-Leu-His-Lys-Lys-Lys-Arg-NH_2
IV	Ac-Glu-Ser-Gln-Leu-His-Ser-Asn-Lys-Arg-NH_2

Figure 4.1: Structure of Fe-mimochrome IV 8Glu, Fe-mimochrome IV 8Lys and Fe-mimochrome IV

The fully protected nonapeptide, except for the Lys residue, were synthesized by solid phase methodology. After removal of the peptides from the resin and deprotection of the Lys side chain, the peptide were coupled in solution to the porphyrin ring. Finally, the fully deprotection of protected group gave the desired molecules.

Solid Phase Synthesis on Sieber Amide Resin

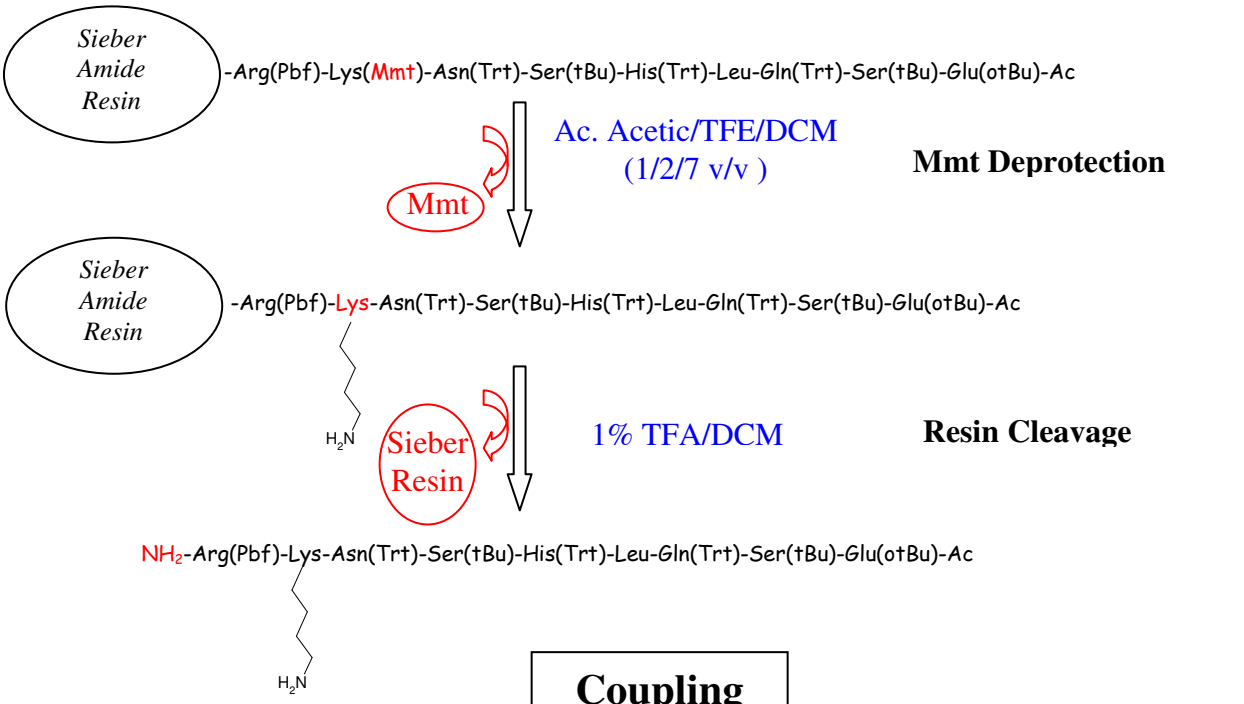

Coupling

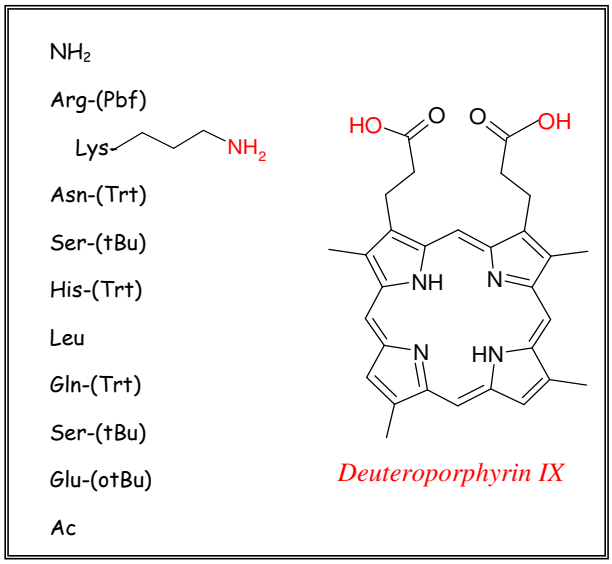

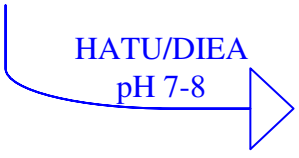

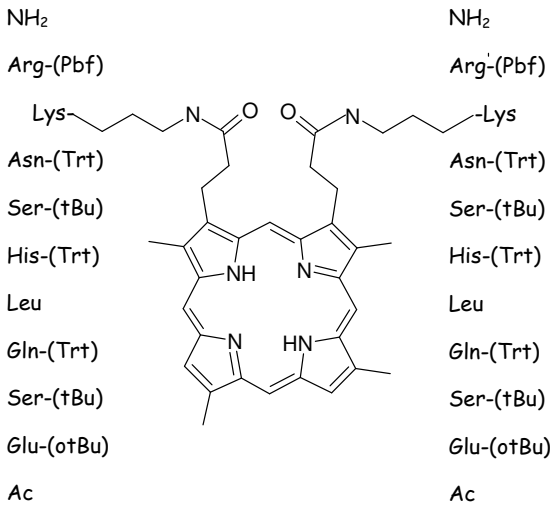

fully protected mimochrome IV

Final Deprotection

fully protected mimochrome IV

95% TFA/EDT/TIS

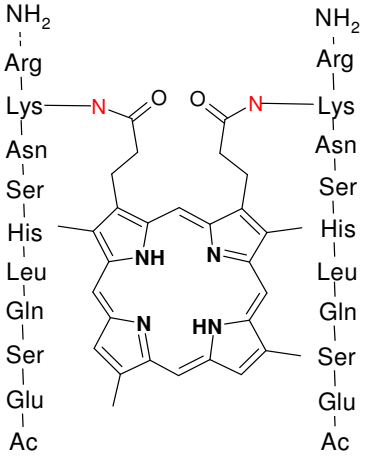

Mimochrome IV

Iron Insertion

$Fe(CH_3COOH)_2$/TFE
6/4 v/v

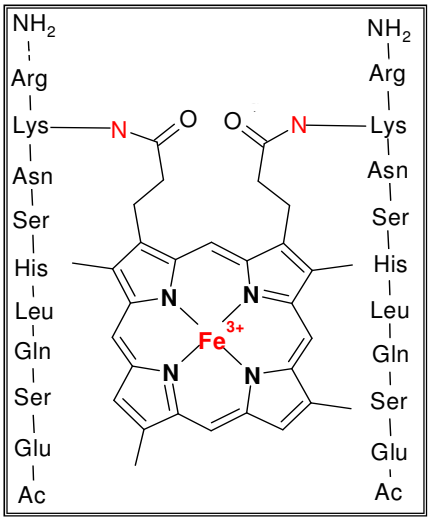

Fe^{III}-Mimochrome IV

Scheme 1: General synthetic procedure for the synthesis of Mimochrome IV

4.2 Peptides synthesis

The following peptides were synthesized:

Mimochrome IV : Ac-Glu^1-Ser^2-Gln^3-Leu^4-His^5-Ser^6-Asn^7-Lys^8-Arg^9-NH_2

Mimochrome IV 8Glu : Ac-Glu^1-Glu^2-Glu^3-Leu^4-His^5-Glu^6-Glu^7-Lys^8-Arg^9-NH_2

Mimochorme IV 8Lys : Ac-Glu^1-Lys^2-Lys^3-Leu^4-His^5-Lys^6-Lys^7-Lys^8-Arg^9-NH_2

The peptides synthesis protocol was:

1) **Automatic peptide synthesis, characterized by the following steps:**
   - Deprotection of the α- Fmoc group
   - α-carboxyl group Activation
   - Coupling
2) **Deprotection of the Lys ε-amino group**
3) **Cleavage from the resin**

The most difficult step of the mimochrome synthesis was the preparation of the nonapeptide fragment, protected at all functional groups except the ε-amino function of the Lys^8 residue.

The Sieber amide resin (shown in figure 4.2) was chosen for all three synthesized peptides, because it allows the cleavage of the peptide from the resin while leaving all protecting groups on the side-chains, as well as on the N-terminal residue, intact.

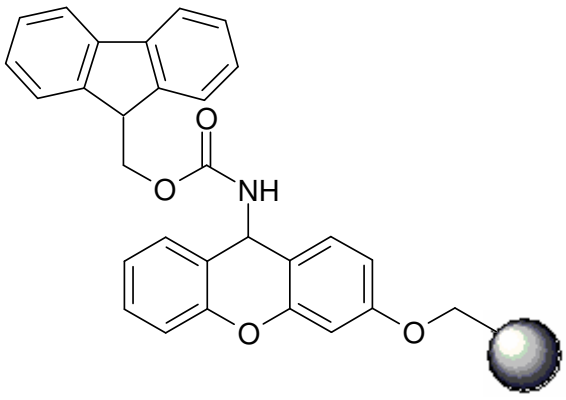

Figure 4.2: Sieber amide resin

Another fundamental point was the choice of the protecting group on N-ε function of the Lys[8], since its removal conditions had to be different than for the other side chain protecting groups. The Mmt protecting group (figure 4.3) was chosen, since it can be easily removed by repeated treatments with a solution containing 10% acetic acid and 20% trifluoroethanol (TFE) (v/v) in CH_2Cl_2, without affecting the other protecting groups.

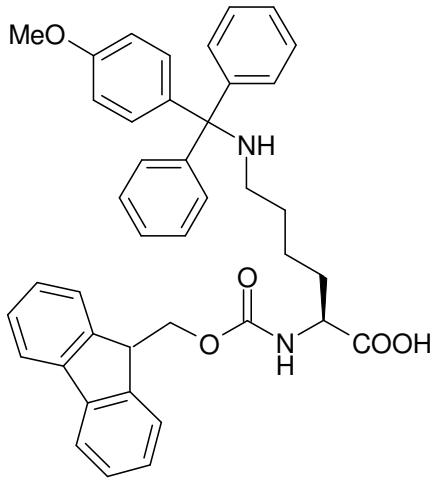

Figure 4.3: Fmoc-Lys(Mmt)-OH

For the synthesis of the three peptides the following amino acids were used:

Mimochrome IV: Fmoc-Glu(OtBu)-OH, Fmoc-Ser(tBu)-OH, Fmoc-Gln(Trt), Fmoc-Leu-OH, Fmoc-His(Trt)-OH, Fmoc-Asn(Trt)-OH, Fmoc-Lys(Mmt)-OH, Fmoc-Arg(Pbf)-OH

Mimochrome IV 8Glu : Fmoc-Glu(OtBu)-OH, Fmoc-Leu-OH, Fmoc-His(Trt)-OH, Fmoc-Lys(Mmt)-OH, Fmoc-Arg(Pbf)-OH

Mimochrome IV 8Lys : Fmoc-Glu(OtBu)-OH, Fmoc-Lys(Boc)-OH, Fmoc-Leu-OH, Fmoc-His(Trt)-OH, Fmoc-Lys(Mmt)-OH, Fmoc-Arg(Pbf)-OH

The three peptides were synthesized on a 0.25 mmol scale, using a 0.52 mmol/g resin substitution. After cleavage of the resin, the products were purified to homogeneity by RP-HPLC.

4.2.1 Synthesis of mimochrome IV peptide

As shown by the HPLC chromatogram (figure 4.4), after deprotection of the Mmt from Lys^8 and after cleavage from the resin, two products are present, with retention times of 26,00 min for species A and 28,50 min for species B, therefore the product required purification. The identity of the products was determined by mass spectroscopy:

Mass compound A: 2063.62 Da (calculated 2284.0 Da).
Mass compound B: 2304.62 Da (calculated 2284.0 Da).

From analysis of the M/z ratio, product B proved to be the desired nonapeptide + Na^+, whereas product A corresponded to the peptide without the Trt protecting group on His^5 residue .

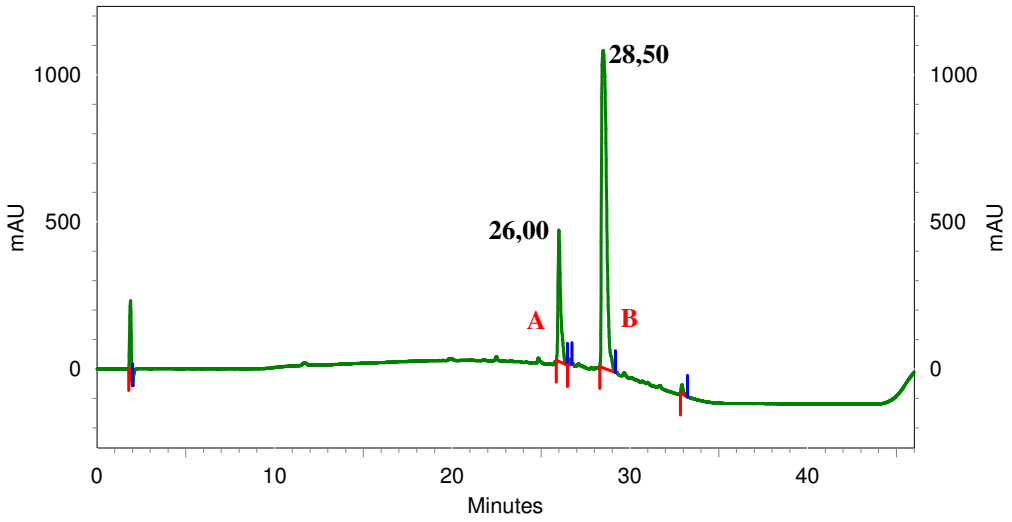

Figure 4.4: HPLC chromatogram of mimochrome IV peptide

The peptide was purified by RP-HPLC, after which the fractions containing the desired product were lyophilized

4.2.2 Synthesis of mimochrome IV 8Glu peptide

As shown by the HPLC chromatogram (figure 4.5), after deprotection of the Mmt from the Lys^8 and after cleavage from the resin, there are two main products with retention times of 13,40 min for species A and 19,34 for species B, therefore also in this case the product required purification. As for mimochrome IV, the identity of the products was determined by mass spectroscopy:

Mass compound A: 1793 (calculated 2014.0 Da).
Mass compound B: 2036 Da (calculated 2014.0 Da).

From the analysis of M/z ratio, product B, as expected, was the fully protected nonapeptide, + Na^+ , with only Lys^8 residue deprotected. Product A, again, corresponded to the fully protected nonapeptide + Na^+, except for the His^5 and Lys^8 residue.

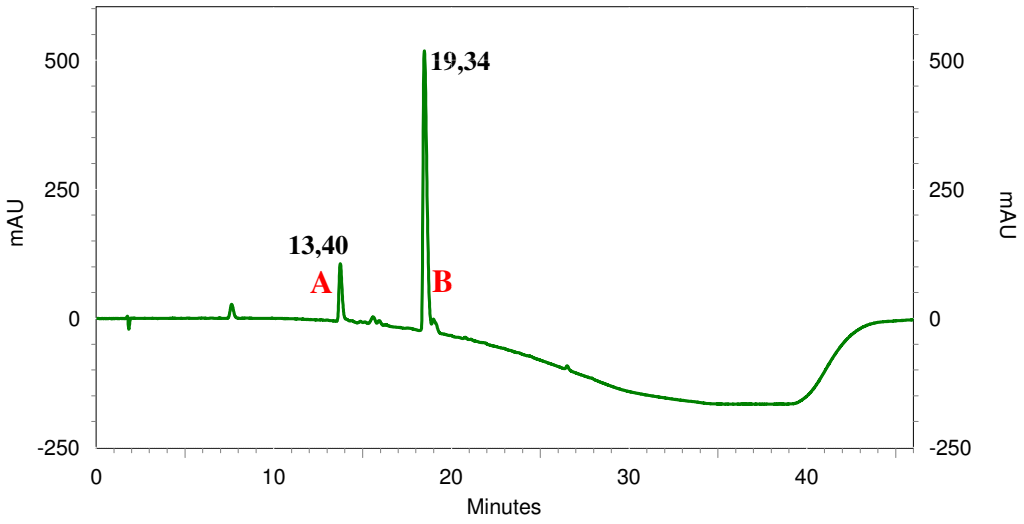

Figure 4.5: HPLC chromatogram of mimochrome IV 8Glu peptide

The product was purified by RP-HPLC, after which the fractions containing the desired product were lyophilized.

4.2.3 Synthesis of mimochrome 8Lys peptide

As shown by the HPLC chromatogram (figure 4.6), after deprotection of the Mmt from Lys^8 and after cleavage from the resin, there is one main product, with a retention time of 25,90 min. The identity of the products was determined by mass spectroscopy. No further purification was required.

Mass compound A: 2211 Da (calculated 2190 Da).

From the analysis of M/z ratio, product A, as expected, was the fully protected nonapeptide + Na^+, with only Lys^8 residue deprotected.

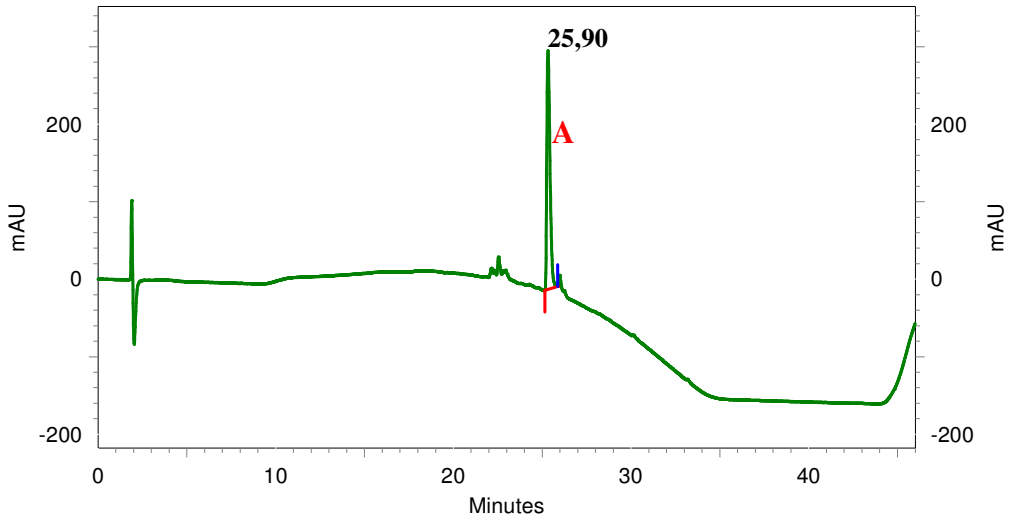

***Figure 4.6*:** HPLC chromatogram of mimochrome IV 8Lys peptide

4.3 Peptide-deuteroporphyrin coupling

The purified fully protected nonapeptides were coupled in solution to the deuteroporphyrin ring. In order to favour the formation of the *bis* sostituited deuteroporphyrin IX, the mixture of activated porphyrin was slowly added to the nonapeptide solution. This approach has lead to a good average yield for all mimochromes.

4.3.1 Coupling of mimochrome IV

As shown by the HPLC chromatogram (figure 4.7), after the coupling reaction and the subsequent complete deprotection of the side chain protecting groups, there is one main product with retention time of 20,03 min.

The identity of the product was checked by mass spectroscopy (figure 4.8), which confirmed the product to be mimochrome IV (mass: 2753,26, calculated 2753,57). Mimochrome IV was purified by HPLC. The pooled fractions containing the desired product were lyophilized

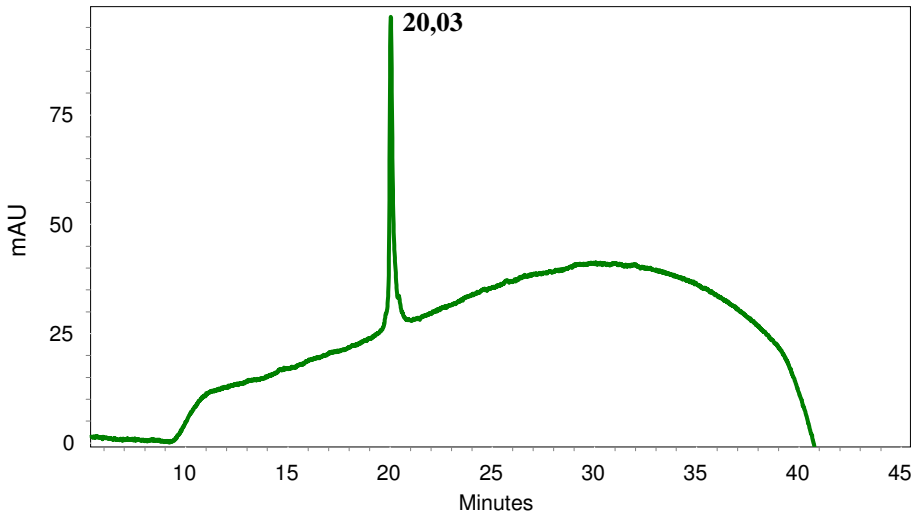

Figure 4.7: HPLC chromatogram of pure mimochrome IV free base

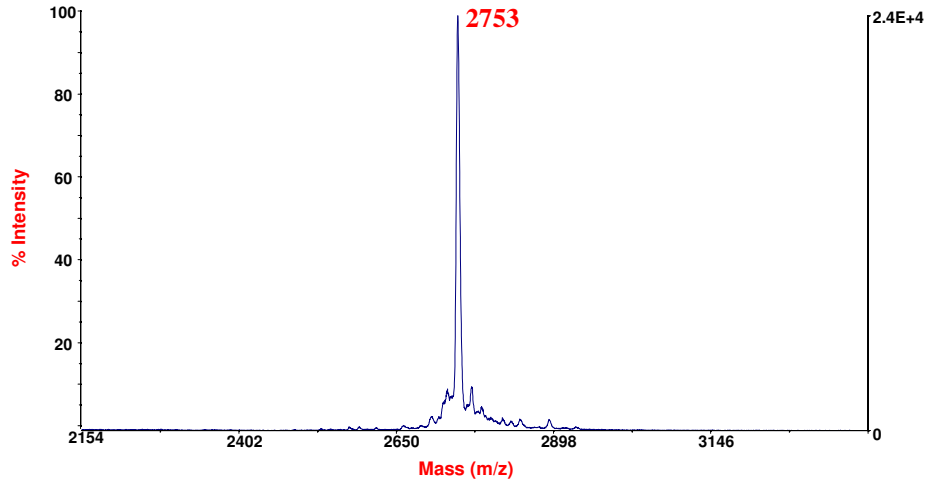

Figure 4.8: Mass spectrum of mimochrome IV free base

4.3.2 Coupling mimochrome IV 8Glu

As for mimochrome IV, after coupling and deprotection by protecting groups, the HPLC chromatogram (figure 4.9) confirmed the presence of a main peak with a retention time of 21,94 min. Mass spectroscopy (figure 4.10) confirmed the product to be mimochrome IV 8Glu (mass: 2953 Da, calculated 2953 Da).

Mimochrome IV 8Glu was purified with HPLC, the pooled fractions containing the desired product were lyophilized.

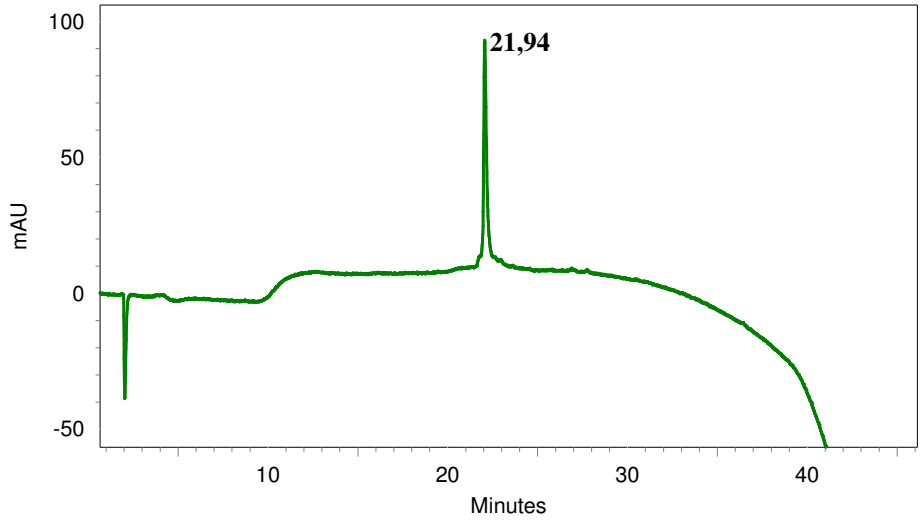

Figure 4.9: HPLC chromatogram of pure mimochrome IV 8Glu free base

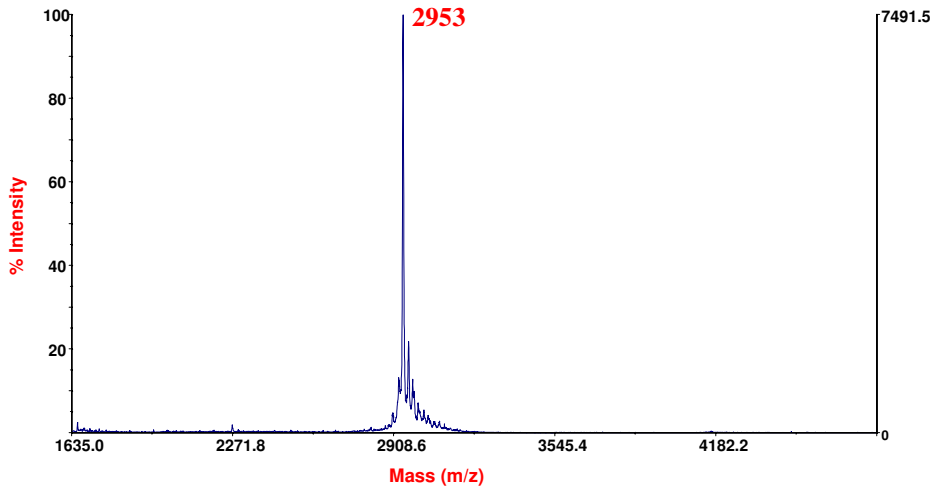

Figure 4.10: Mass spectrum of mimochrome IV 8Glu free base

4.3.3 Coupling mimochrome IV 8Lys

The same coupling procedure was also applied to Mimochrome IV 8Lys, which produced the same positive results as the others mimochromes. The HPLC chromatogram after deprotection (figure 4.11) of the side chain protecting groups showed one main peak, with retention time of 19,90 min. The identity of mimochrome IV 8Lys was confirmed by mass spectroscopy (mass 2948.26 Da, calculated 2948 Da) (figure 4.12). The product was purified by HPLC and lyophilized.

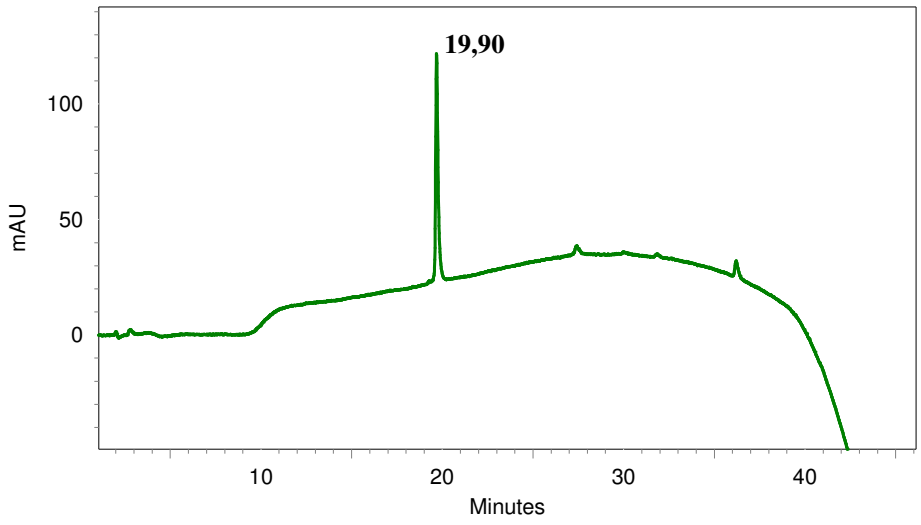

Figure 4.11: HPLC chromatogram of pure mimochrome IV 8Lys free base

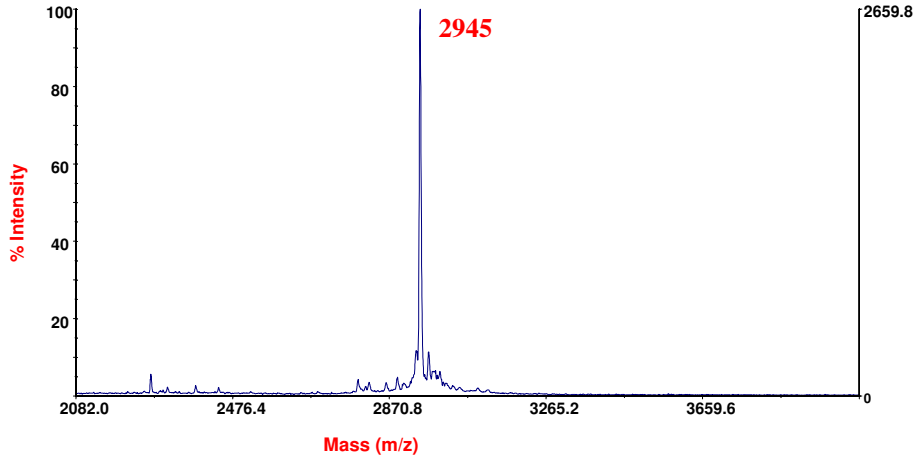

Figure 4.12: Mass spectrum of mimochrome IV 8Lys free base

4.4 Iron insertion into mimochromes

Basically, the reaction between the metal ion and a porphyrinic compound consists of *a)* the formation of the equatorial MN_4 plane; and *b)* the completion of the axial coordination sphere. However, certain considerations have to be made concerning the metalation procedure:

1. The solvent for the reaction should be able to dissolve the porphyrin as well as the metal compound, but without coordinating the metal ion with high affinity in order to avoid competition with the porphyrin.

2. The porphyrin has to be deprotonated in order to produce the negative P^{2-} ion that is present in the metal-porphyrin complex. The presence of strong acids in the reaction media will impede or even reverse metalation by shifting the protonation/ deprotonation equilibrium to the left.

   $$\mathbf{H_4(P)^{2+} \rightleftharpoons H_3(P)^{+} \rightleftharpoons H_2(P) \rightleftharpoons H(P)^{-} \rightleftharpoons (P)^{2-}}$$

3. To be able to react with the porphyrin macrocycle, the metal compound which carries the metal ion should dissociate, yielding an active (coordinatively unsaturated) species. Therefore, the metal complex should not be too stable

otherwise it will not react with the porphyrin present in the reaction mixture. Other considerations are the availability, ease of handling, and solubility of the metal complexes in organic solvents.

4. After the incorporation of a metal ion with a positive charge greater than +2, it will bind one or more anions from the reaction medium to form a neutral species. Some metal ions prefer certain defined geometries, which require the addition of a neutral ligand (solvent, H_2O, O_2) to complete their coordination sphere.

The methods commonly used for the insertion of metal ions in the porphyrin macrocycle are listed below. The systems are characterized either by the solvent or the metal carrier used, depending on the more essential component. Since metalloporphyrins have characteristic UV-VIS properties, the reaction is usually monitored by spectrophotometry.

The acetate method

$$\mathbf{Zn(OAc)_2.xH_2O + H_2P \xrightarrow[50\,^{\circ}C]{HOAc} Zn(P) + 2\,HOAc + 2\,H_2O}$$

The acetate method includes all metalation reactions in which the protons of the porphyrin are transferred to acetate or propionate ions of the metal acetates/propionates. The solvents can be glacial acetic acid, or mixtures of $CHCl_3$/MeOH. This method can be applied to all divalent metals, except those which are unstable in acetic acid, and to some tri- and tetravalent metal ions. Often sodium acetate is added to further buffer the solution and to enhance deprotonation of the porphyrins. This method is considered the method of choice for the synthesis of manganese-porphyrin complexes.

The pyridine method

$$\mathbf{Mg(ClO_4)_2 + H_2P + 4\,Py \xrightarrow{Py} Mg(P)Py_2 + 2\,[PyH][ClO_4]}$$

In those cases where the metalloporphyrin is very labile towards acids, the basic solvent pyridine is used for divalent metal ions. Pyridine is capable of dissolving the porphyrins as well as the metal salts, and the good complexing properties of pyridine allow the direct isolation of metalloporphyrin pyridinates. The same properties, however, impede the

incorporation of metal ions with higher charges by forming pyridine complexes with the metal carrier, thus retarding the dissociation of the metal ion.

The dimethylformamide method

$$4\ CrCl_4 + 4\ H_2P\ + O_2 \xrightarrow[153\ ^\circ C]{DMF} 4\ Cr(P)Cl + 2\ H_2O + 4\ HCl$$

Weakly coordinating, high boiling oxygen-donor solvents such as dimethylformamide, tetramethylurea and sulfolan are excellent solvents for the metal carriers and porphyrins. The best results have been obtained with anhydrous metal chlorides (although they can be difficult to obtain and to handle), as the high boiling temperature forces the formed HCl to escape.

The metal carbonyl method

$$Re_2(CO)_{10} + H_2P \xrightarrow[195\ ^\circ C]{decalin} [Re(CO)_3]_2(P) + H_2 + 4\ CO$$

In metal carbonyls some of the CO groups may be eliminated, resulting in a coordinatively unsaturated species. This species acts as a Lewis acid, attacking the lone pairs of the porphyrin nitrogen atoms. This method is especially useful for the preparation of porphyrins containing the metals of groups VI to VIII.

For the insertion of iron into mimochrome, the acetate method was used. The reaction took place in a 60/40 (v/v) solution of acetic acid and TFE, using iron(II) acetate as metal carrier. Upon insertion of the metal in the porphyrin ring, the Fe(II) ion was oxidized to Fe(III). During the reaction, the colour of the reaction mixture changed from red to brown, indicating the formation of the Fe(III) porphyrin complex. The reaction was monitored by HPLC and UV-vis spectroscopy.

4.4.1 Synthesis of Fe(III) mimochrome IV

After two hours the reaction mixture turned slowly brown, and the HPLC chromatogram showed the presence of a new peak at 19.79 min with the characteristic UV spectrum of Fe(III) mimochrome (figure 4.13). The mass spectrum confirmed (figure 4.14) the identity of the desired product: 2805 Da (calculated 2806.0 Da).

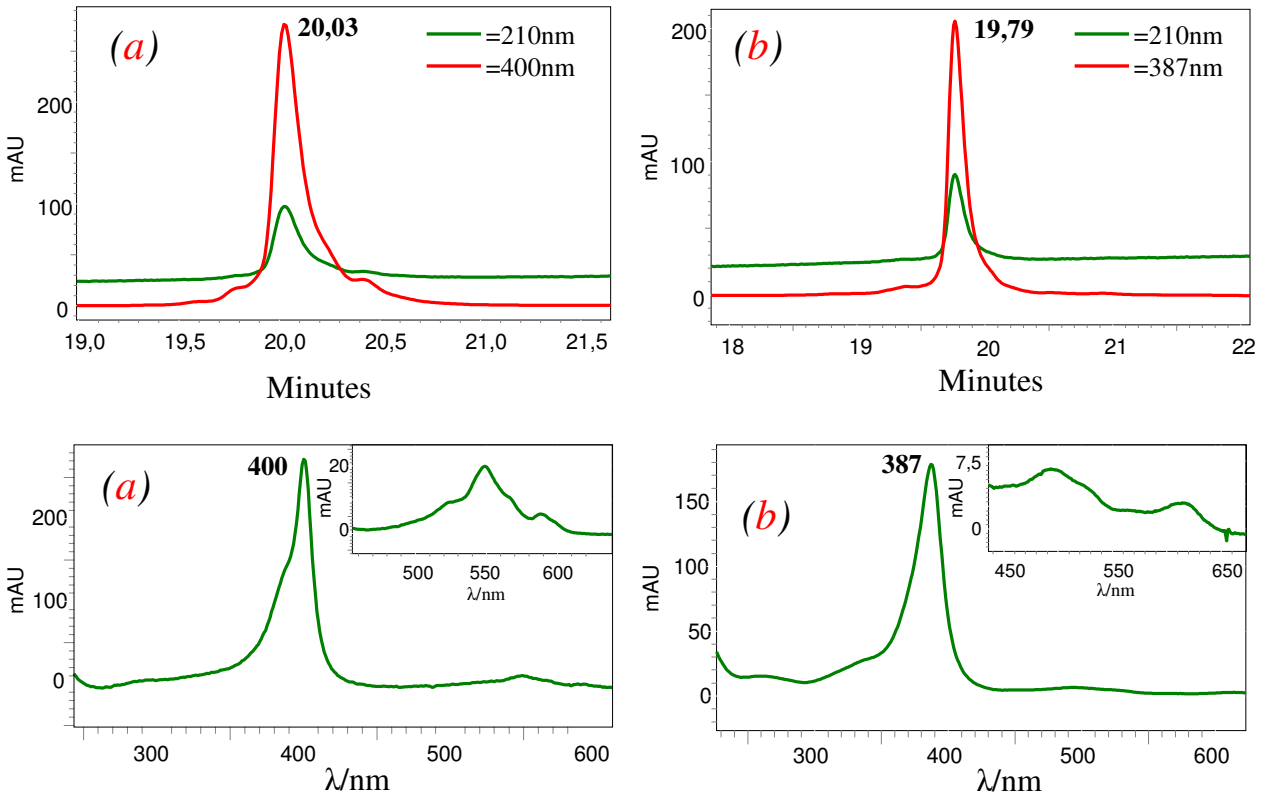

Figure 4.13: HPLC chromatogram and UV-vis spectra, at pH ≈ 1, of mimochrome IV free base (*a*) and Fe(III) mimochrome IV (*b*).

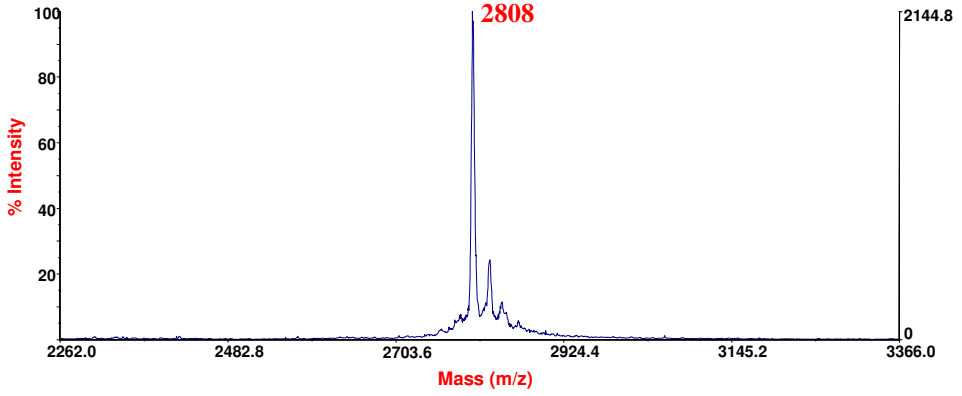

***Figure 4.14*:** Mass spectrum of Fe(III) mimochrome IV

4.4.2 Synthesis of Fe(III) mimochrome IV 8Glu

The formation of the Fe(III)-complex of mimochrome 8Glu was analogue to the synthesis of Fe(III) mimochrome IV. The same colour change was observed and the HPLC chromatogram showed the presence of a new peak at 21,20 min with the characteristic UV spectrum of Fe(III) mimochrome (figure 4.15). The identity of the desired product was confirmed by mass spectroscopy. (mass: 3008 Da; calculated; 3008 Da) (figure 4.16).

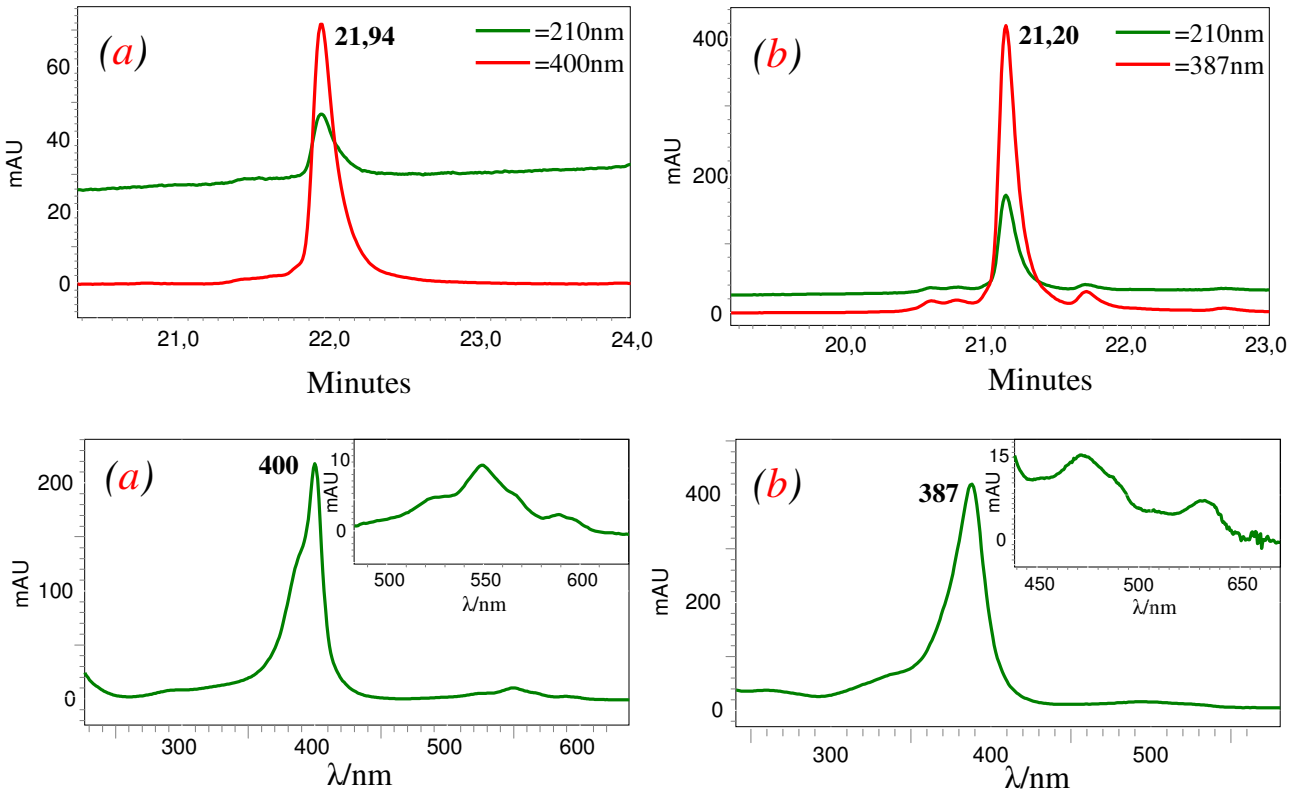

Figure 4.15: HPLC chromatogram and UV-vis spectra, at pH ≈ 1, of mimochrome IV 8Glu free base (*a*) and Fe(III) mimochrome IV 8Glu (*b*)

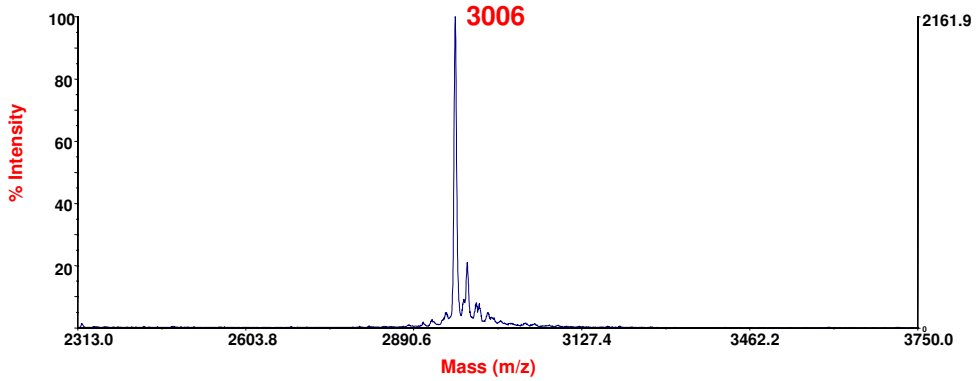

Figure 4.16: Mass spectrum of Fe(III) mimochrome IV 8Glu

4.4.3 Synthesis of Fe(III) mimochrome IV 8Lys

The same results were obtained for mimochrome IV 8Lys. The HPLC chromatogram showed the formation of a new compound with a retention time of 18.80 min, which showed the characteristic UV spectrum of Fe(III) mimochrome (figure 4.17). As for the other mimochromes, the identity of Fe(III) mimochrome IV 8Lys was confirmed by mass spectroscopy. (mass: 3001 Da; calculated: 3001 Da) (figure 4.18).

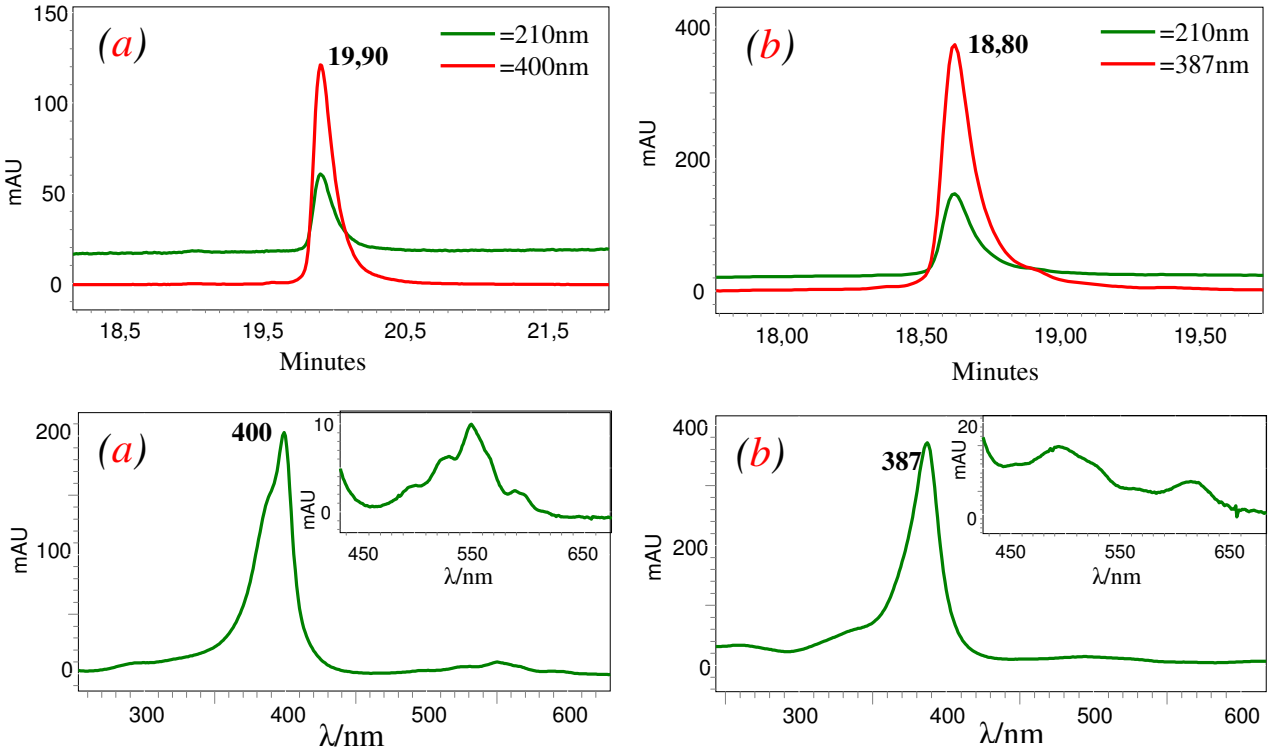

Figure 4.17: HPLC chromatogram and UV-vis spectra, at pH ≈ 1, of mimochrome IV 8Lys free base (*a*) and Fe(III) mimochrome IV 8Lys (*b*)

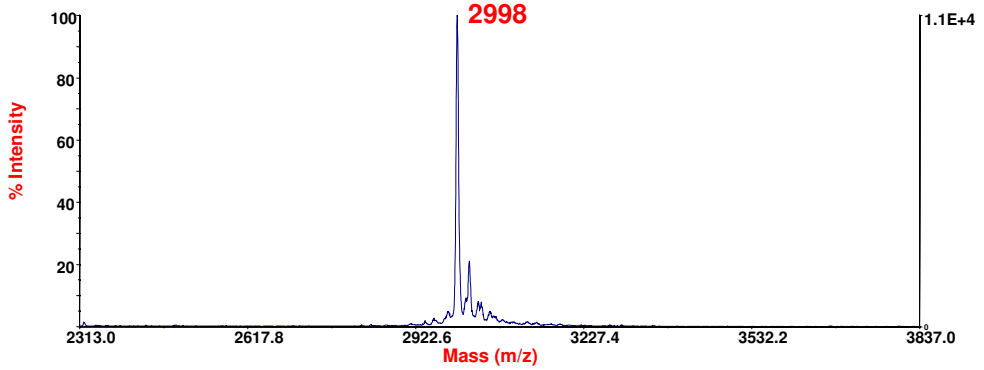

Figure 4.18: Mass spectrum of Fe(III) mimochrome IV 8Lys

Chapter 5: Spectroscopic characterization of mimochromes

5.1 UV-vis spectroscopy of mimochromes

UV-vis spectroscopy was used to verify the metal insertion into the porphyrin ring, and to determine the coordination geometry of the metal ion in both Fe(III) mimochrome IV 8Glu and Fe(III) mimochrome IV 8Lys.

5.1.1 UV-vis spectroscopy of Fe(III) mimochrome IV 8Glu

Figure 5.1a and 5.1b shows the UV-vis spectrum of 3.05 x 10^{-5} M mimochrome IV 8Glu free base, and 6.76 x 10^{-6} M Fe(III) mimochrome IV 8Glu, in 10 mM phosphate buffer solution at pH 7, respectively. The observed spectral changes in both the Soret and visible regions, upon reaction of the free-deuteroporphyrin peptide conjugate with the metal ions, clearly denoted metal insertion into mimochrome IV 8Glu. The position and the relative intensities of the Soret, β and α bands give useful information on the metal ion coordination state[76,95]. The iron derivative at pH 7, is characterized by a band at 401 (ε = 9.67 x 10^4 $M^{-1}cm^{-1}$), by a band at 522 nm (ε = 6.18 x 10^3 $M^{-1}cm^{-1}$) and a shoulder at 560 nm. This is an indication of a ferric low-spin state, with a *bis*-His axial coordination[76, 95]. All the spectral data are very similar to those found for Fe(III) mimochrome IV[110].

Table 5.1 reports the typical UV-vis parameters of Fe(III) mimochrome IV 8Glu and Fe(III) mimochrome IV.

	$\varepsilon_{(Soret)}$ M^{-1} cm^{-1}	***Soret*** *(nm)*	$\varepsilon_{(\beta)}$ M^{-1} cm^{-1}	***β and α*** *(nm)*
Fe(III)-mimochromeIV 8Glu	9.60 x 10^4	401	6.60 x 10^3	522 -560
Fe(III)-mimochrome IV[a]	1.03 x 10^5	401	6.18 x 10^3	522 -560

Table 5.1: Parameters are derived from the experimental UV-vis spectra recorded under the conditions indicated in the experimental section. (*a*), Data taken from ref.[110].

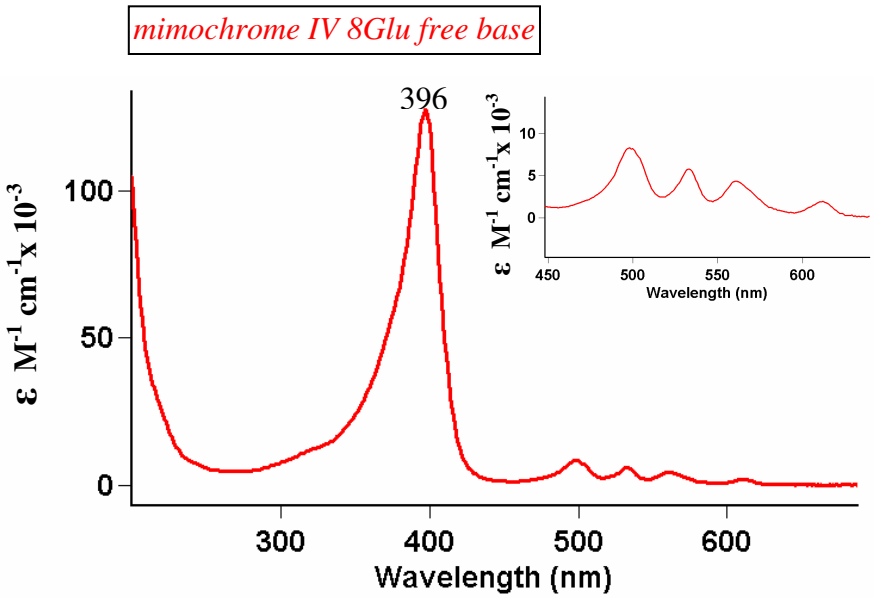

Figure 5.1a: UV-vis spectrum of 3.05 x 10^{-5} M mimochrome IV 8Glu free base, in 10 mM phosphate buffer at pH 7.

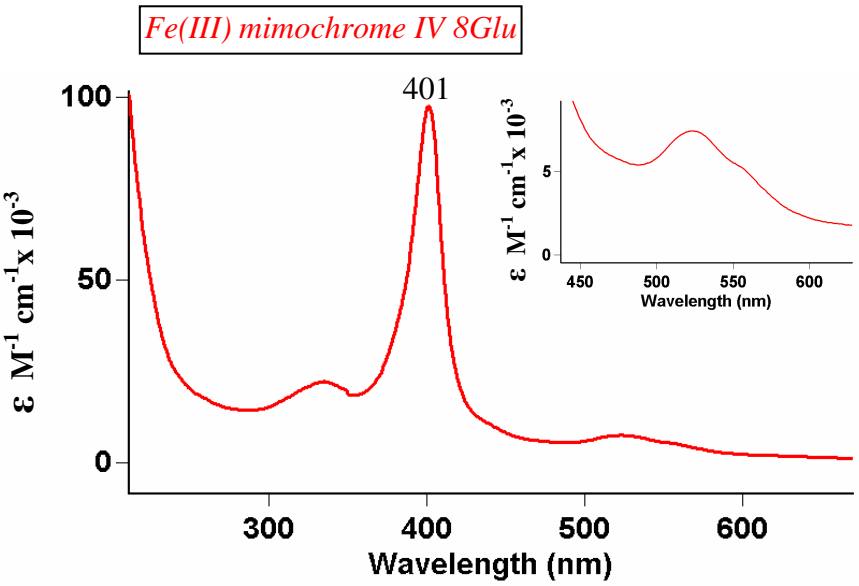

Figure 5.1b: UV-vis spectrum of 8.90 x 10^{-6} M Fe(III) mimochrome IV 8Glu, in 10 mM phosphate buffer at pH 7.

5.1.2 UV-vis Fe(III) mimochrome IV 8Glu pH titrations

The pH effect on the properties of Fe(III) mimochrome IV 8Glu was examined in aqueous solution by UV-vis spectroscopy. Figure 5.2 shows selected UV-vis spectra of Fe(III) mimochrome IV 8Glu at different pH (from pH 2 to 8). At pH ≈ 2 the spectrum is characterized by absorption maxima at 388, 494, 613 nm, for the Soret, β and α bands, respectively. This spectrum is in agreement with a high spin state for Fe(III) axially coordinated by two weak ligands (i.e., water molecules)[95]. In the pH range from 2 to 6 the Soret band is red shifted from 388 to 401 nm, while the visible bands at 522 and 560 nm appears with a simultaneous disappearance of the bands at 494 and 613 nm. At pH ≈ 8 the spectrum is characterized by absorption maxima at 401, 522, 560 nm, thus indicating the formation of a strong ligand field on the iron porphyrin, typical of a *bis*-His coordination. The absence of an isosbestic point suggests that more species are involved in the equilibrium.

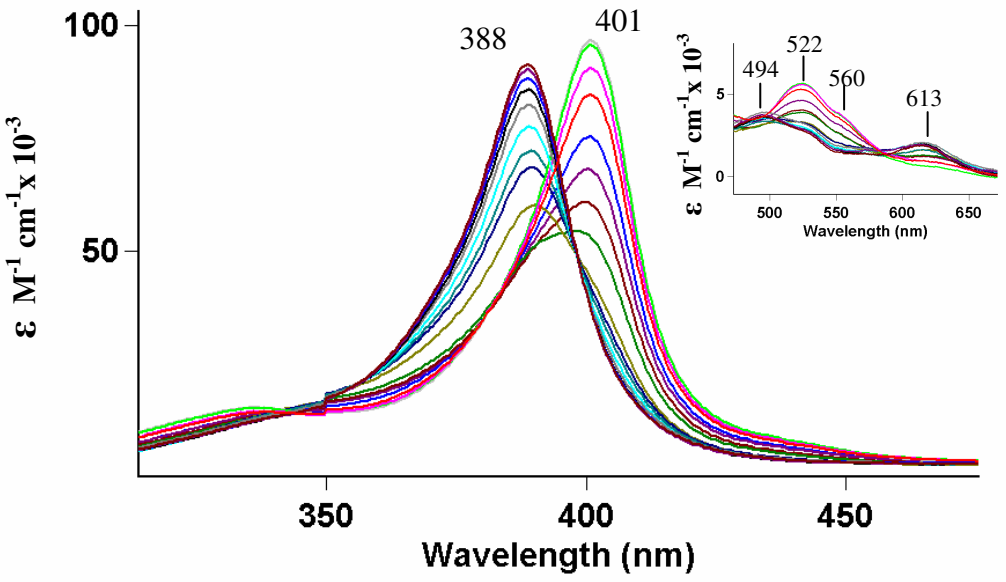

Figure 5.2: UV-vis spectrum of 3.76 x 10^{-6} M Fe(III) mimochrome IV 8Glu, in the Soret and visible region, at different pH (2-8).

Figure 5.3 reports the absorbance at 388 and 401 nm, as a function of pH. The experimental data could be fitted with two pKa values at pH 3.85 ± 0.4 and pH 5.03 ± 0.7 (see appendix A1). The first pKa value represents, in comparison with Fe(III) mimochrome IV pH tritration[110], the apparent pKa for the protonation of the axially coordinated histidines (pK_{app}), as defined by Kennedy et al.[114]. The Fe(III) imidazole complexes are know to be exchange-labile and therefore the observed pKa value accounts for the competition equilibrium between the coordination of the His to the iron and the protonation of the His in the uncoordinated form.

The pKa_2 of Fe(III) mimochrome IV 8Glu is difficult to interpret. It may be due to several protonation equilibrium of the glutammic acids that may somehow influence the geometry of the axial ligand.

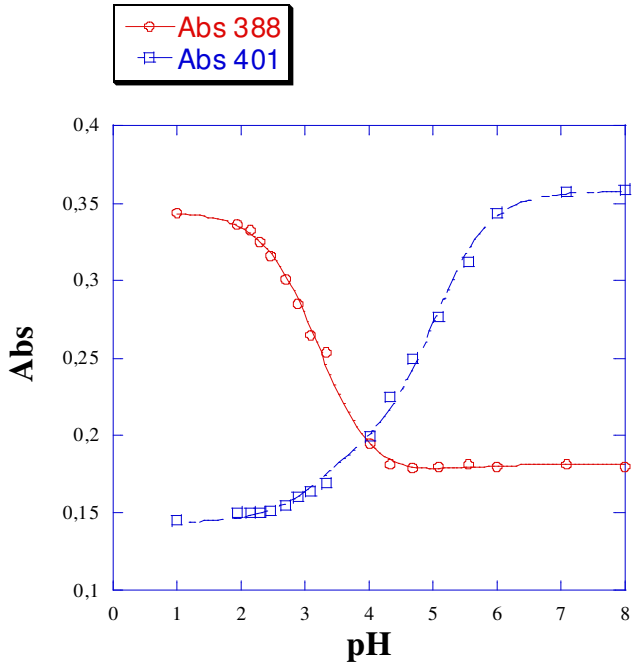

Figure 5.3: Plot of the absorbances a of 3.76 x 10^{-6} M Fe(III) mimochrome IV 8Glu at 401 (□) and 388 (o) nm as a function of pH.

5.1.3 UV-vis spectroscopy of Fe(III) mimochrome IV 8Lys

Figure 5.4a and 5.4b shows the UV-vis spectrum of 2.23 x 10^{-5} M mimochrome IV 8Lys free base and the UV-vis spectrum of 8.25 x 10^{-6} M Fe(III) mimochrome IV 8Lys, in 10 mM phosphate buffer solution at pH 7, respectively. The observed spectral changes in both the Soret and visible regions, upon reaction of the free-deuteroporphyrin peptide conjugate with the metal ions, clearly denoted metal insertion into mimochrome IV 8Lys. The iron derivative at pH 7, is characterized by a band at 402 (ε = 1.01 x 10^5 $M^{-1}cm^{-1}$), by a band at 522 nm (ε = 6.60 x 10^3 $M^{-1}cm^{-1}$) and a shoulder at 560 nm. This is an indication of a ferric low-spin state, with a *bis*-His axial coordination[76,95]. All the spectral data are very similar to those found for Fe(III) mimochrome IV[110].

Table 5.2 reports the typical UV-vis parameters of Fe(III) mimochrome IV 8Lys and Fe(III) mimochrome IV[110].

	$\varepsilon_{(Soret)}$ M^{-1} cm^{-1}	***Soret*** *(nm)*	$\varepsilon_{(\beta\text{-band})}$ M^{-1} cm^{-1}	***β and α*** *(nm)*
Fe(III)-mimochromeIV 8Lys	1.01 x 10^5	402	6.60 x 10^3	522 -560
Fe(III)-mimochrome IV[a]	1.03 x 10^5	401	6.18 x 10^3	522 -560

Table 5.2: Parameters are derived from the experimental UV-vis spectra recorded under the conditions indicated in the experimental section. (*a*), Data taken from ref.[110].

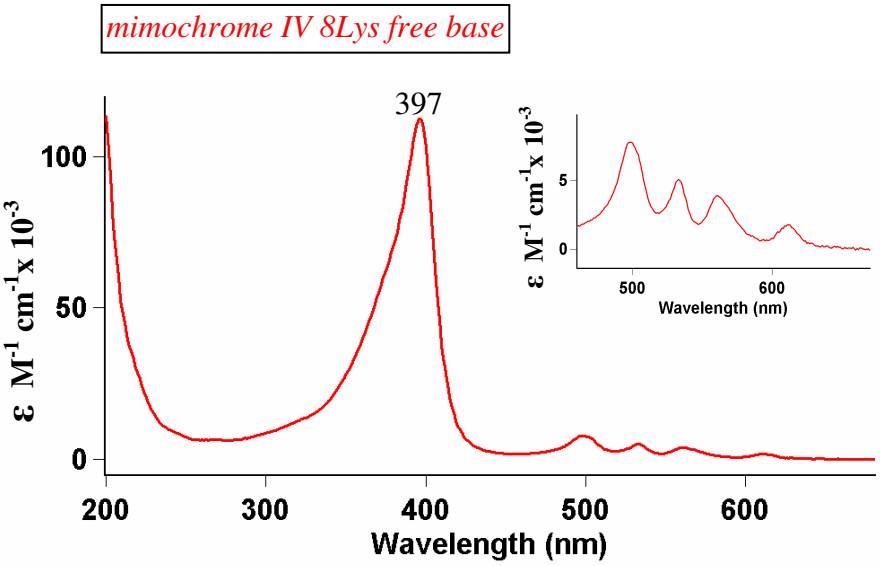

Figure 5.4a: UV-vis spectrum of 2.23 x 10^{-5} M mimochrome IV 8Lys free base, in 10 mM phosphate buffer at pH 7.

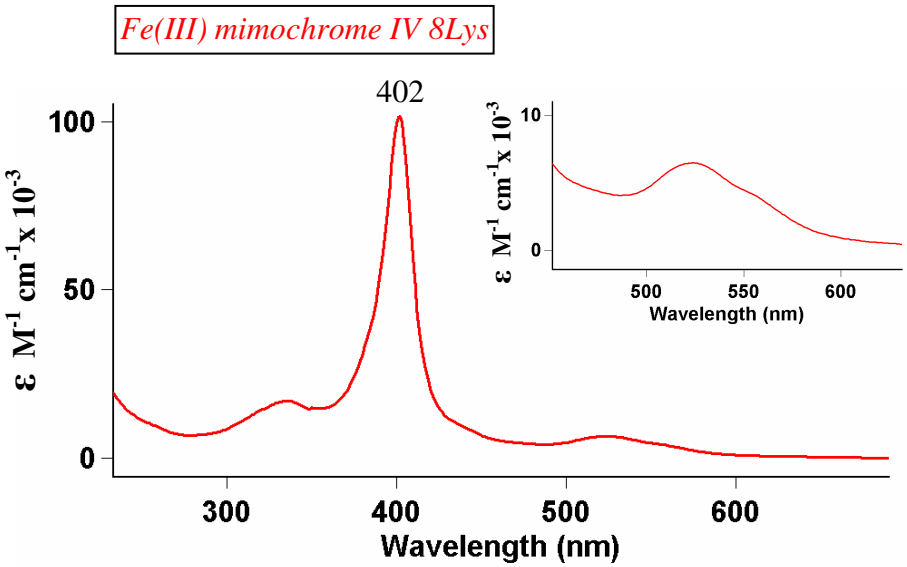

Figure 5.4b: UV-vis spectrum of 8.25 x 10^{-6} M Fe(III) mimochrome IV 8Lys, in 10 mM phosphate buffer at pH 7.

5.1.4 UV-vis Fe(III) mimochrome IV 8Lys pH titrations

The pH effect on the properties of Fe(III) mimochrome IV 8Lys was examined in aqueous solution by UV-vis spectroscopy. Figure 5.5 shows selected UV-vis spectra of Fe(III) mimochrome IV 8Lys at different pH (from pH 2 to 8). At pH ≈ 2 the spectrum is characterized by absorption maxima at 388, 494, 613 nm, for the Soret, β and α bands, respectively. This spectrum is in agreement with a high spin state for the Fe(III), axially coordinated by two weak ligands (i.e., water molecules)[95]. In the pH range from 2 to 6 the Soret band is red shifted from 402 to 388 nm while in the visible bands appears at 522 and 560 nm with a simultaneous disappearance of the bands at 494 and 613 nm. At pH ≈ 8 the spectrum is characterized by absorption maxima at 402, 522, 560 nm, thus indicating the formation of a strong ligand field on the iron porphyrin, typical of a *bis*-His coordination.. The presence of an isosbestic point suggests that only two species may predominantly be involved in the equilibrium..

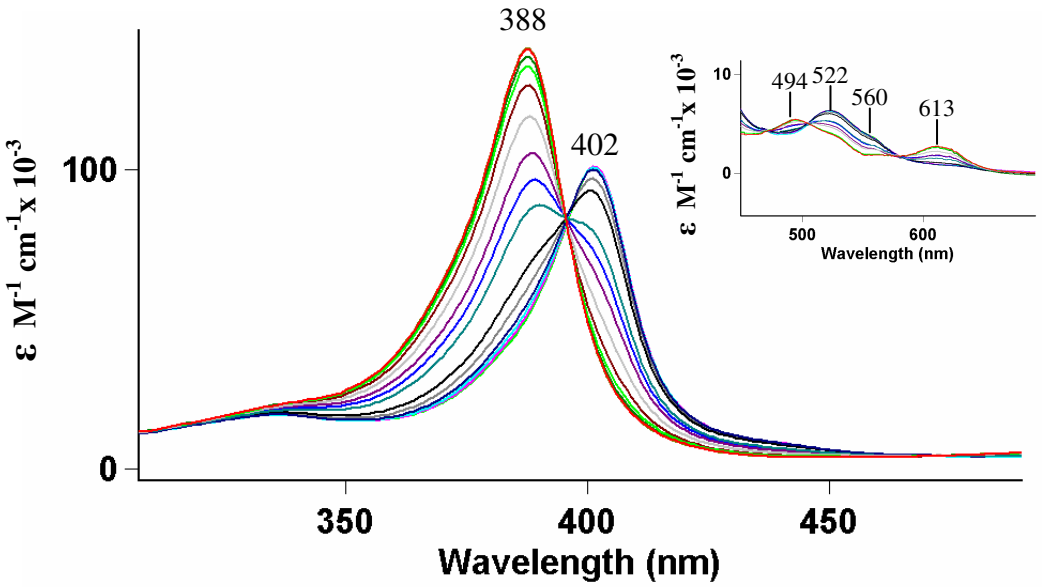

Figure 5.5: UV-vis spectrum of 7.00 x 10^{-6} M Fe(III) mimochrome IV 8Lys, in the Soret and visible region, at different pH (2-8)

Figure 5.6 reports the absorbance values at 402 and 388 nm, as a function of pH. Both titration curves exhibit one midpoint at pH 2.63 ± 0.03 (see appendix A2). The pKa value represents, in comparation with Fe(III) mimochrome IV pH titration[110], the apparent pKa for the protonation of the axially coordinated histidines (pK_{app}), as defined by Kennedy et al.[114], similarly to what found for the first pKa of Fe(III) mimochrome IV 8Glu

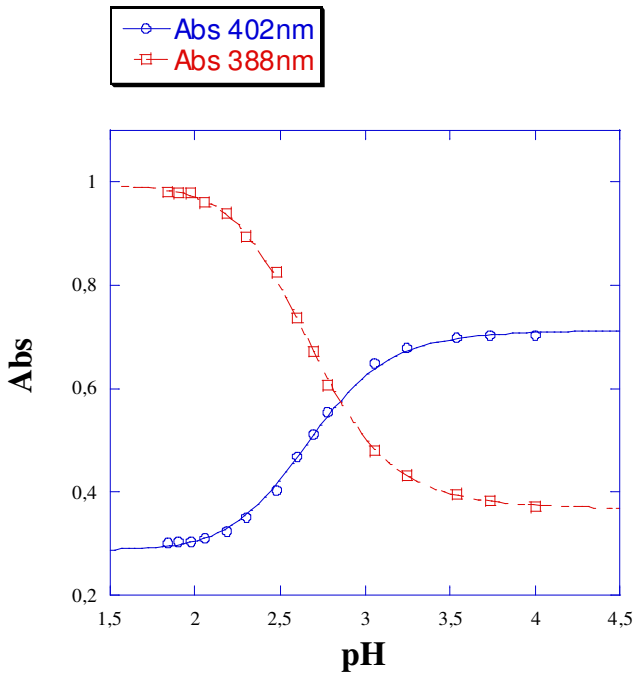

Figure 5.6: plot of the absorbance of 7.00 x 10^{-6} M Fe(III) mimochrome IV 8Lys, at 402 (□) and 388 (o) nm, as a function of the pH.

5.2 Circular dichroism spectroscopy of mimochromes

CD measurements in both the UV and Soret regions gave preliminary structural information on Fe(III) mimochrome IV 8Glu and Fe(III) mimochrome IV 8Lys. CD spectra for all the mimochromes were recorded in both far-UV and Soret regions, using a trifluoroethanol (TFE) /water solution as solvent.

5.2.1 Circular dichroism spectroscopy of Fe(III) mimochrome IV 8Glu

The 190–260 nm spectrum of Fe(III) mimochrome IV 8Glu in 10mM phosphate buffer at pH 7 (solid red line in figure 5.7) is characterized by double minima at 222 and 203 nm and a maximum below 190 nm. The [θ] value at 222 nm, the $[\theta]_{ratio}$ and the λ_o indicate the presence of a low helical content.

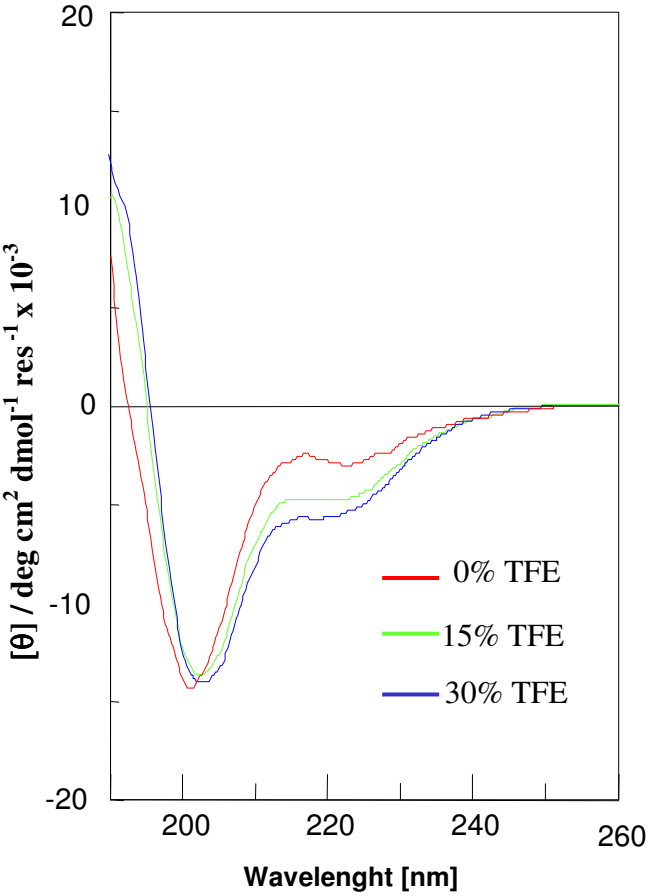

Figure 5.7: CD spectra of 5.36 x 10^{-6} M Fe(III) mimochrome IV 8Glu in the far-UV region, phosphate buffer (10 mM, pH 7.0) with 0%, 15%, 30% TFE content.

The addition of the structure inducing solvent TFE results in an small increase of the helical content for both species as expected.

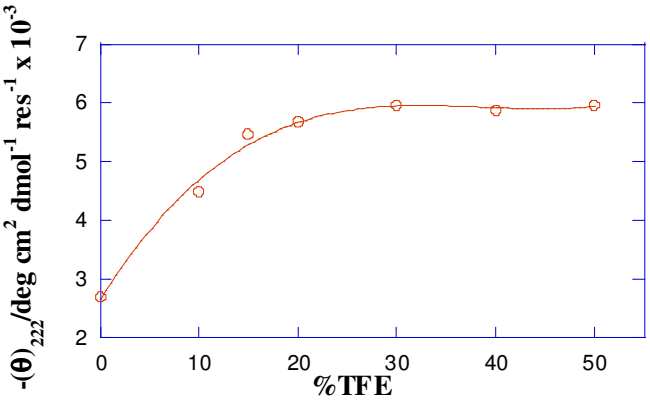

Figure 5.8: Plot of the [θ] value at 222 nm for Fe(III) mimochrome IV 8Glu as a function of the TFE concentration .

Species	***[θ]min x10^{-3}*** *(λ, nm)*	***[θ]$_{222}$ x10^{-3}***	***[θ]$_{ratio}$***	***λ$_0$(nm)***
Fe(III)-Mimochrome IV[b]	-11,20 (207)	-9,54	0,85	200,1
Fe(III)-Mimochrome IV 8Glu	-16,55 (204)	-5,76	0,35	195,8

Table 5.3: CD parameters of Fe(III) mimochrome IV 8Glu and Fe(III) mimochrome IV, in 30% TFE/phosphate buffer (10mM, pH 7.0). [*a*], [θ] are expressed as mean residue ellipticities (deg cm^{2}dmol^{-1} res^{-1}) in the UV region; λ is expressed in nm; [θ]min represents the ellipticity at the shorter wavelength minimum; [θ]ratio represents the ratio of the ellipticity at 222 nm to that at the shorter wavelength minimum. [b] Data taken from ref.[110].

The CD spectrum of Fe(III) mimochrome IV 8Glu was also recorded in the Soret region (Figure 5.9). It is characterized by the presence of a positive Cotton effect in the Soret region, with a maximum at 395 nm. We hypothesize that Fe(III) mimochrome IV 8Glu adopts a Λ configuration on the basis of the CD spectrum of Fe(III) mimochrome IV[110].

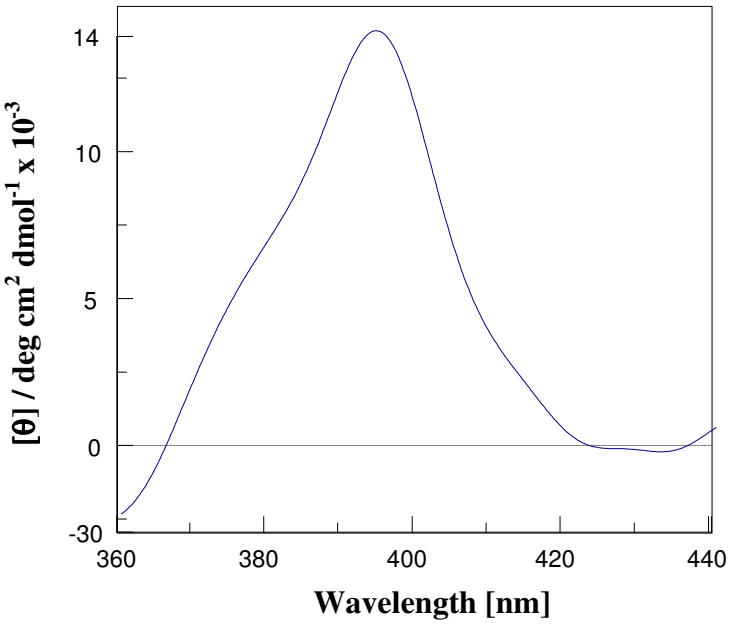

Figure 5.9: CD spectrum of 5.36 x 10^{-6} M Fe(III) mimochrome IV 8Glu in the Soret region (phosphate buffer 10 mM, pH 7.0).

5.2.2 Circular dichroism pH titration of Fe(III) mimochrome IV 8Glu

We studied the effect of pH (from 2 to 8) on the secondary structure of Fe(III) mimochrome IV 8Glu (see figure 5.10). Figure 5.11 reports the plot of the 222 nm band intensity as a function of pH. The intensity of the [θ] value at 222 nm increases by raising the pH, with a midpoint transition at pH 5.6. This value is close to the second midpoint transition observed in the UV-vis titration (pKa_2= 5.03).

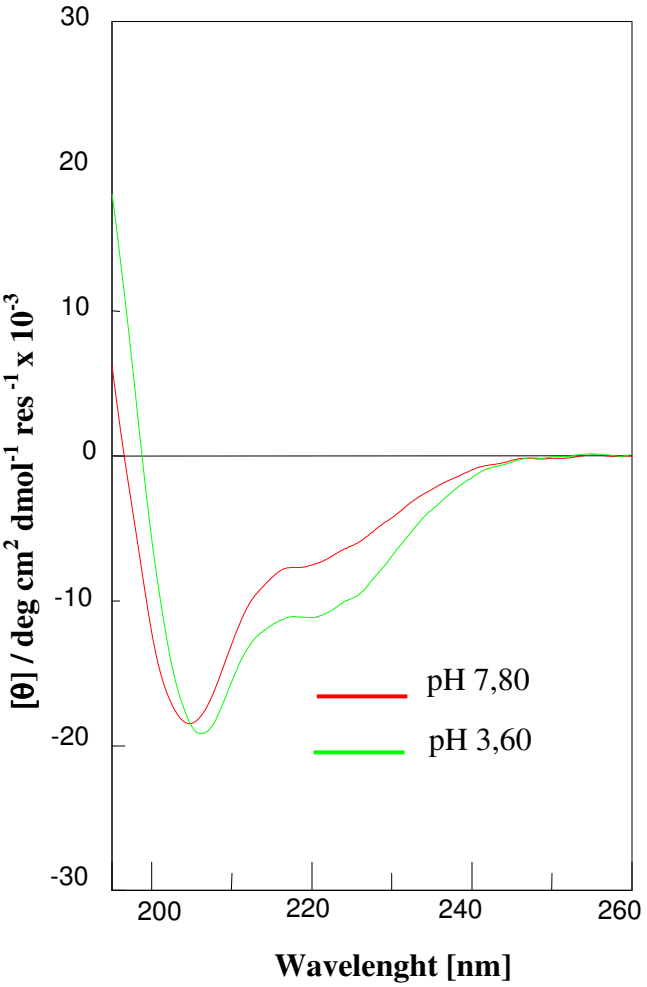

Figure 5.10 : CD spectra of 6,82 x10^{-6} M Fe(III) mimochrome IV 8Glu in the far-UV region at pH 7.80 (solid red line) and pH 3.60 (solid green line).

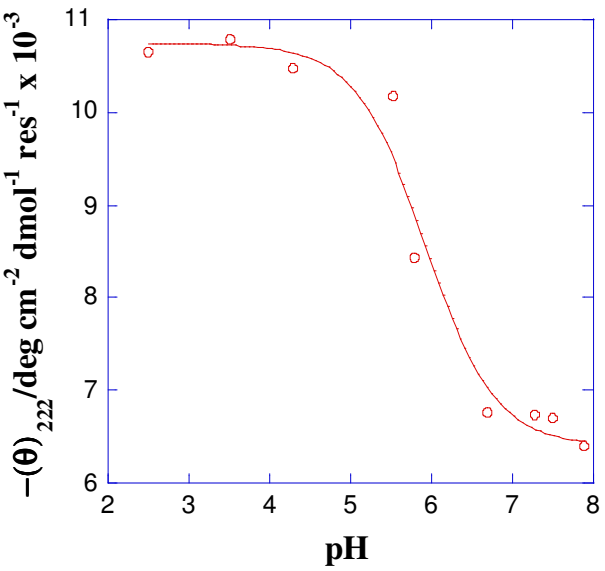

Figure 5.11: Plot of the [θ] value at 222 nm, for 6,82 x10^{-6} M Fe(III) mimochrome IV 8Glu, as a function of the pH.

5.2.3 Circular dichroism spectroscopy Fe(III) mimochrome IV 8Lys

The 190–260 nm spectra of Fe(III) mimochrome IV 8Lys in 10mM phosphate buffer at pH 7, (red line solid figure 5.12) are characterized by double minima at 222 and 203 nm and a maximum below 190 nm. The [θ] value at 222 nm, the $[\theta]_{ratio}$ and the λ_o in aqueous solution, indicate the presence of a low helical content.

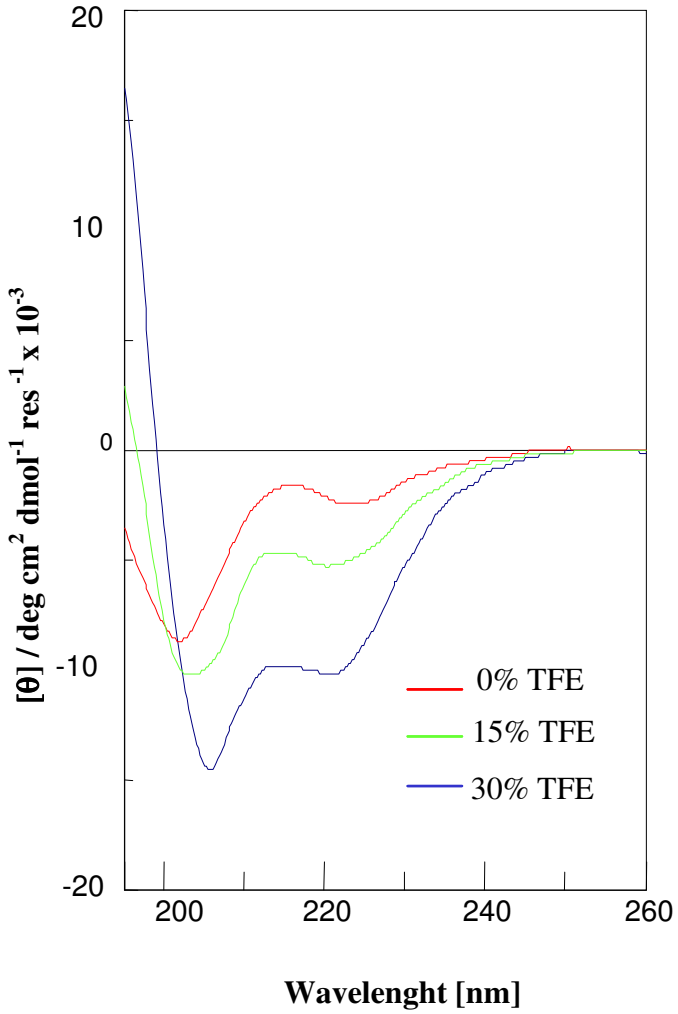

Figure 5.12: CD spectra of 3,36 x 10^{-6} M Fe(III) mimochrome IV 8Lys in the far-UV region, phosphate buffer (10 mM, pH 7.0) with 0%, 15%, 30% TFE content.

The addition of TFE results in an increase of the helical content as expected (figure 5.13).

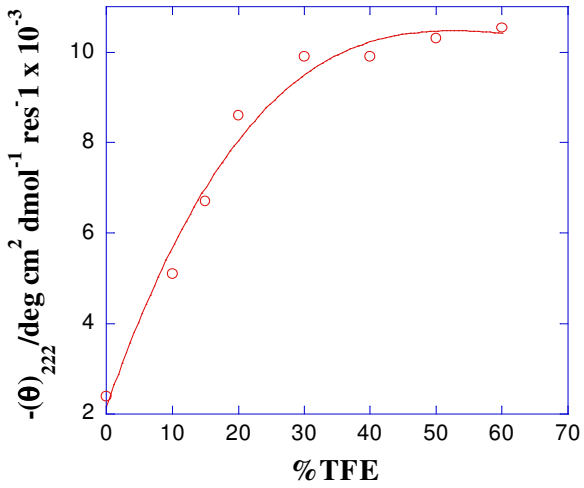

Figure 5.13: Plot of the [θ] value at 222 nm, for Fe(III) mimochrome IV 8Lys, as a function of the TFE concentrations .

Species	***(θ)min x10$^{-3(a)}$ (λ, nm)***	***(θ)$_{222}$ x10^{-3}***	***(θ)$_{ratio}$$^{(a)}$***	***λ$_0$(nm)***
Fe(III)-Mimochrome IV^{b}	-11,20 (207)	-9,54	0,85	200,1
Fe(III)-Mimochrome IV 8Lys	-14,78 (206)	-9,87	0,67	198,1

Table 5.3: CD parameters of Fe(III) mimochrome IV 8Glu and Fe(III) mimochrome IV, in 30% TFE/phosphate buffer (10mM, pH 7.0). [*a*], [θ] are expressed as mean residue ellipticities (deg cm^{2}dmol^{-1} res^{-1}) in the UV region; λ is expressed in nm; [θ]min represents the ellipticity at the shorter wavelength minimum; [θ]ratio represents the ratio of the ellipticity at 222 nm to that at the shorter wavelength minimum. [b] Data taken from ref. [5a].

The CD spectrum of Fe(III) mimochrome IV 8Lys was recorded in the Soret region (figure 5.14). It is characterized by the presence of a positive Cotton effect in the Soret region, with a maximum at 396 nm.

We hypothesize that Fe(III) mimochrome IV 8Glu adopts a Λ configuration on the basis of the CD spectrum Fe(III) mimochrome IV[110].

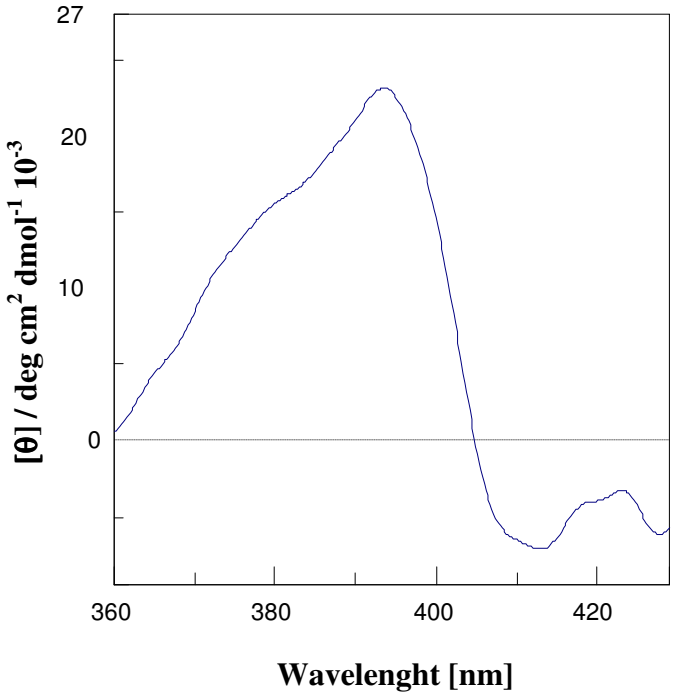

Figure 5.14: CD spectrum of 3.36 x 10^{-6} M Fe(III) mimochrome IV 8Glu in the Soret region. (phosphate buffer 10 mM, pH 7.0).

5.2.4 Circular dichroism pH titration of Fe(III) mimochrome IV 8Lys

We studied the effect of pH (from 2 to 8) on the secondary structure of Fe(III) mimochrome IV 8Lys (see figure 5.15). Figure 5.16 reports the plot of the 222 nm band intensity as a function of pH. No significant spectral changes are observed by raising of pH.

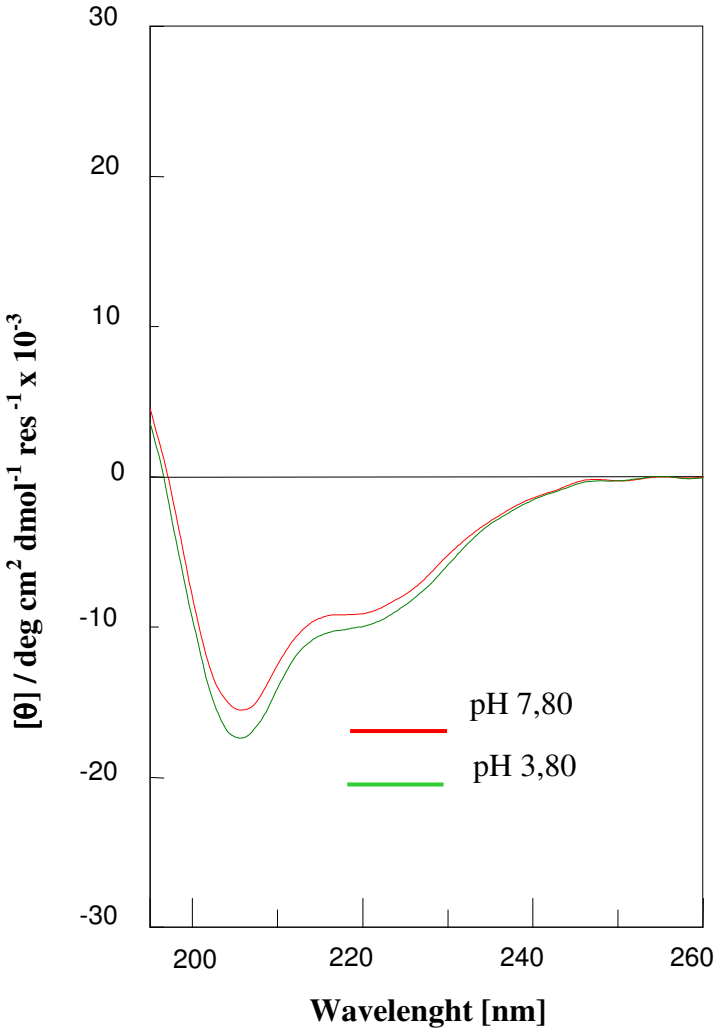

Figure 5.15 : CD spectra of 8.44 x10^{-6} M Fe(III) mimochrome IV 8Lys in the far-UV region at pH 7.80 (solid red line) and pH 3.80 (solid green line).

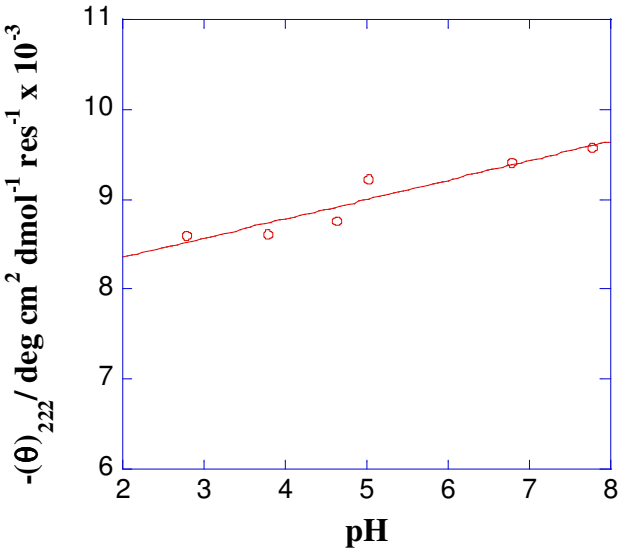

Figure 5.16 : Plot of the 222 nm band intensity, for 8.44 x 10^{-6} M Fe(III) mimochrome IV 8Lys, as a function of the pH

5.2.5 Circular dichroism pH titration of Fe(III) mimochrome IV

We also studied the effect of pH (from 2 to 8) on the secondary structure of Fe(III) mimochrome IV (see figure 5.17). Figure 5.18 reports the plot of the 222 nm band intensity as a function of the pH. The intensity of the [θ] value at 222 nm decreases up to pH 5 for then no change to pH above 5 (see figure 5.18). The same behavior was found for CD pH titration of Fe(III) mimochrome IV in the Soret region[110].

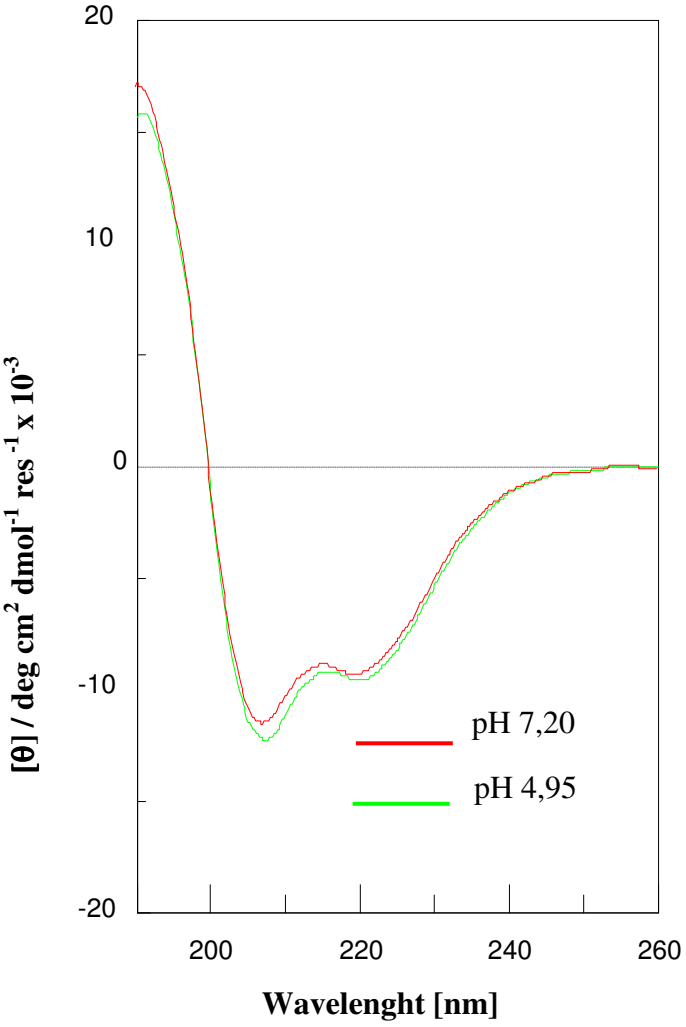

Figure 5.17 : CD spectra of 9,68 x10^{-6} M Fe(III) mimochrome IV in the far-UV region as a function of pH, at pH 7.20 (solid red line) and pH 4.95 (solid green line).

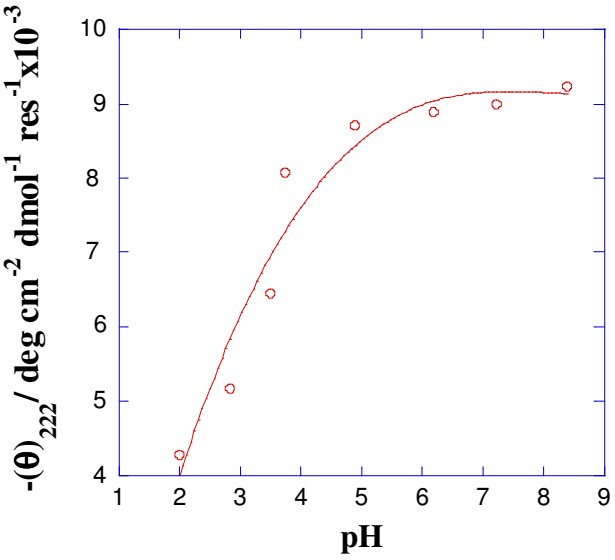

Figure 5.18: Plot of the 222 nm band intensity, for 9.68 x 10^{-6} M Fe(III) mimochrome IV, as a function of the pH.

Chapter 6: Square-Wave Voltammetry of Fe mimochromes

Square wave voltammetry experiments was performed in collaboration with the research group of professor Marco Borsari and Marco Sola at the University of Modena.

6.1 Square-Wave Voltammetry of Fe mimochrome IV 8Glu

The FeIII/FeII reduction potential (E°') of Fe-mimochrome IV 8Glu, was determined by Square-Wave Voltammetry (SWV) using a pyrolytic graphite electrode, at 25 C°.
Figure 6.1a and 6.1b show the voltammograms of Fe-mimochrome 8Glu, obtained with cathodic and anodic scans, in 10mM phosphate buffer at pH 7, and $NaClO_4$ 100 mM. They show a well-behaved voltammetric wave in both scans. A redox potential of -170 mV, *versus* the hydrogen electrode (SHE), could be evaluated from the experimental data.
This potential value is the mean between the maximum currents during cathodic and anodic scans.

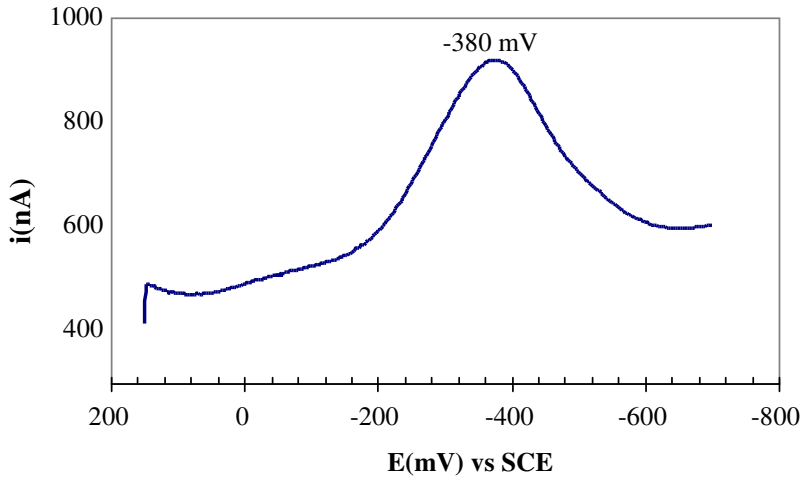

Figure 6.1a: Square wave voltammogram; cathodic scan of Fe-mimochrome IV 8Glu (25 °C, scan rate 50 mVs^{-1}), over a potential range between 0.2 and -0.8 V (against SCE), at pH 7.0

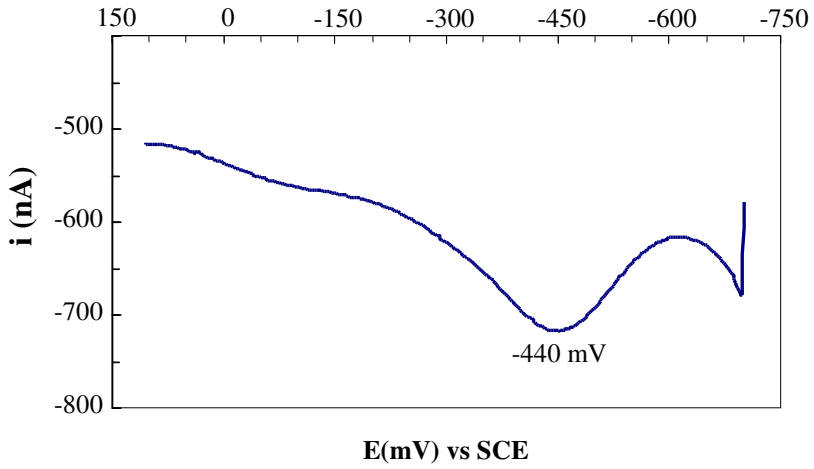

Figure 6.1b: Square wave voltammogram; anodic scan of Fe-mimochrome IV 8Glu (25 ˚C, scan rate 50 mVs^{-1}), over a potential range between 0.2 and -0.8 V (against SCE), at pH 7.0

6.2 Square-Wave Voltammetry of Fe mimochrome IV 8Lys

The FeIII/FeII reduction potential (E°') of Fe-mimochromes IV 8Lys, was determined by Square-Wave Voltammetry (SWV) using a pyrolytic graphite electrode, at 25 C°.

Figure 6.2a and 6.2b show the voltammograms of Fe-mimochrome 8Lys obtained with cathodic and anodic scans in 10mM phosphate buffer at pH 7, and $NaClO_4$ 100 mM. They show a well-behaved voltammetric wave in both scan. A redox potential of -48 mV, *versus* hydrogen electrode (SHE), could be evaluated from the experimental data.

This potential was the mean values between the maximum currents during cathodic and anodic scans.

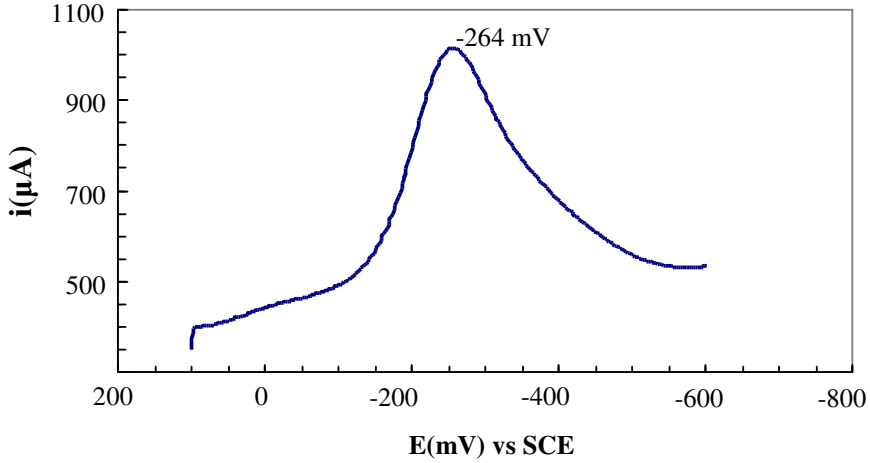

Figure 6.2a: Square wave voltammogram; catodic scan of Fe-mimochrome IV 8Lys (25 °C, scan rate 50 mVs^{-1}), over a potential range between 0.2 and -0.8 V (against SCE), at pH 7.0

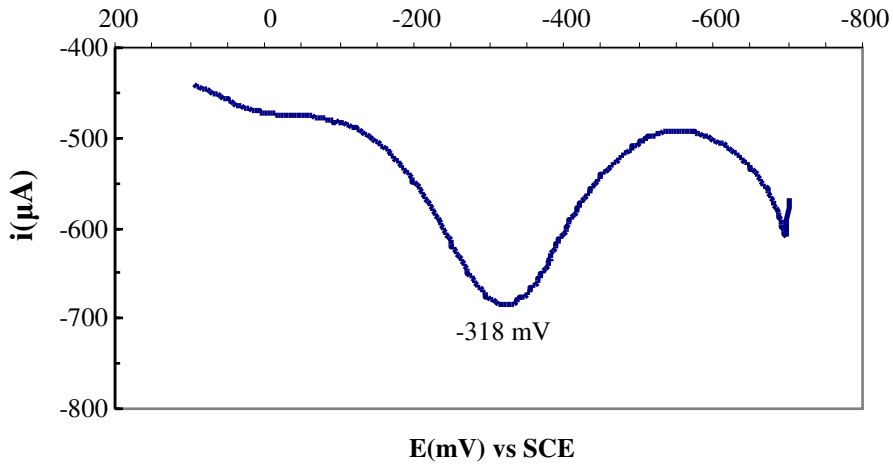

Figure 6.2b: Square wave voltammogram; anodic scan of Fe-mimochrome IV 8Lys (25 °C, scan rate 50 mVs^{-1}), over a potential range between 0.2 and -0.8 V(against SCE), at pH 7.0

6.3 Square-Wave Voltammetry of Fe mimochrome IV

The FeIII/FeII reduction potential (E°') of Fe-mimochrome IV, was determined by Square-Wave Voltammetry (SWV) using a pyrolytic graphite electrode, at 25 C°.

Figure 6.3a and 6.3b shows the voltammograms, in cathodic and anodic scan, of Fe-mimochrome IV in 10mM phosphate buffer at pH 7, and $NaClO_4$ 100 mM. They show two peaks for both scans. These peaks are characterized by differences in the maximum of current intensities that occur at quite different potentials. Usually the contribution of faradic current of adsorbed species is lower then that of the free specie in solution. Therefore the redox potential was determined on the first peak. By taking the mean currents by cathodic and anodic scan we have found a potential of -58 mV, *versus* hydrogen electrode (SHE), was calculated as the mean value of the cathodic and anodic scans.

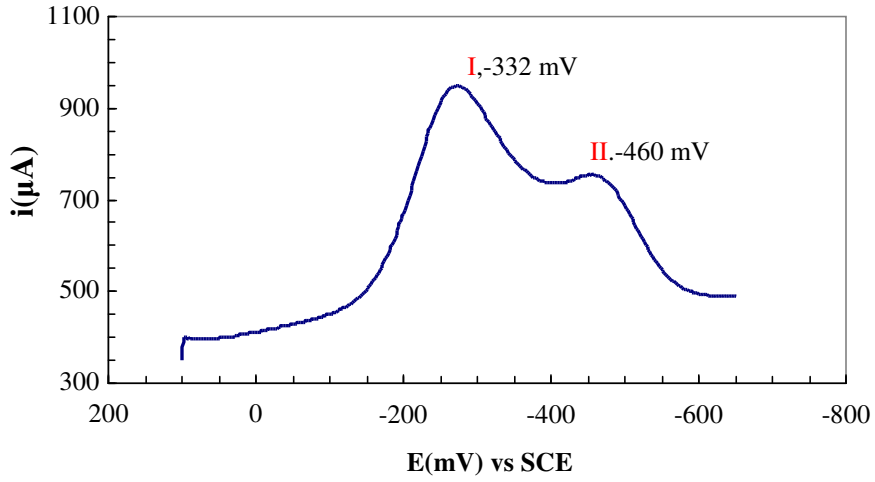

Figur 6.3a: Square wave voltammogram; cathodic scan of Fe-mimochrome IV (25 °C, scan rate 50 mVs^{-1}), over a potential range between 0.2 and -0.8 V against SCE, at pH 7.0.

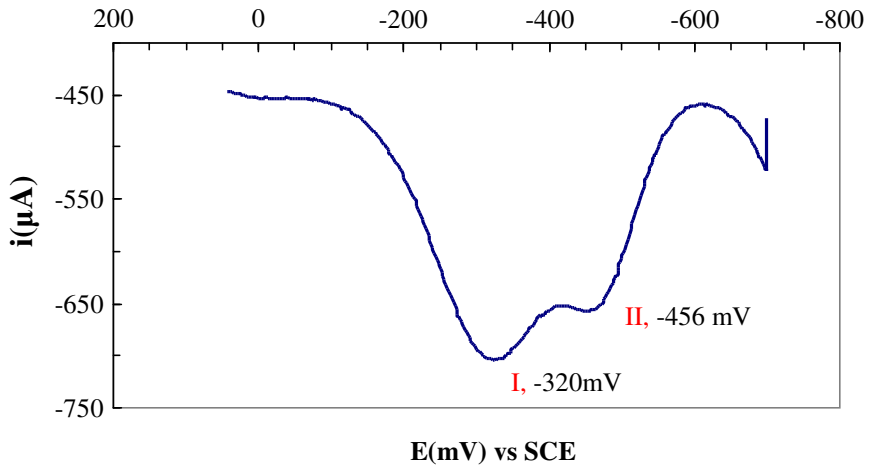

Figur 6.3b: Square wave voltammogram; catodic scan of Fe-mimochrome IV (25 ˚C, scan rate 50 mVs^{-1}), over a potential range between 0.2 and -0.8 V against SCE, at pH 7.0.

Chapter 7: Discussion

Several strategies were conceived to obtain metalloprotein models[95,115,116]. For heme-protein models, the use of two parts that associate around the heme, to give folded covalent or non-covalent self-assembled dimers was particularly successful[95,117]. Numerous models are homo-dimers with C_2 symmetry related components. The use of the symmetry is quite advantageous, on one hand, because it simplifies the design, the synthesis and the structural characterization, but, on the other hand it may lead to diastereomeric forms[108]. This problem was encountered in the study of mimochromes[91,92]. In fact, stable Λ and Δ isomers of Co(III) mimochrome I were unpredicted, but experimentally observed. One possible solution to this problem came from the study of mimochrome IV. It contains a modified sequence of mimochrome I: Leu[1] and Leu[9] were substituted with Glu and Arg residues at position 1 and 9, respectively. This strategy was successful in stabilizing the sandwich structure and in favouring the formation of the Λ isomer only[110]. On the basis of this result two new mimochromes were developed. Fe(III) mimochrome IV 8Glu and Fe(III) mimochrome IV 8Lys are characterized by a sequence containing eight **Glu** residues and eight **Lys** residues, respectively (see figure 7.1). This new compounds allowed us to correlate the different charge distributions with the redox properties of metal centre.

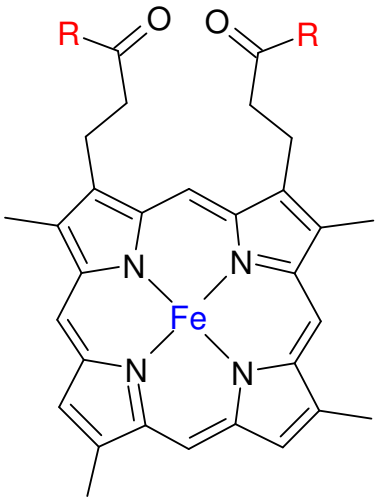

R=R_1; *Peptide mimchromes*

Mimochrome	*Sequence*
8Glu	Ac-Glu-Glu-Glu-Leu-His-Glu-Glu-Lys-Arg-NH_2
8Lys	Ac-Glu-Lys-Lys-Leu-His-Lys-Lys-Lys-Arg-NH_2
IV	Ac-Glu-Ser-Gln-Leu-His-Ser-Asn-Lys-Arg-NH_2

Figure 7.1: Structure of Fe-mimochromes

First we studied the overall structure of both compounds in solution by UV-vis and circular dichroism spectroscopy with different experimental conditions.. The UV-vis spectra of both Fe(III) mimochrome IV 8Glu (Figure 5.1a and 5.1b) and Fe(III) mimochrome IV 8Lys (figure 5.4a and 5.4b), at pH 7, are typical of octahedral *bis*-His low spin complexes, in good agreement with the spectral features previously observed for Fe(III) mimochrome I and Fe(III) mimochrome IV. *Bis*-His coordination occurs for Fe(III) mimochrome IV 8Lys even at very acidic conditions. Both imidazoles of the axially coordinating His residues display a pK_{app}=2.67, indicating that the *bis*-His coordination to the iron represents over 90% of the population at pH > 3.85 (Figure 5.6). The low pKa value of the axially coordinating His (with values very close to what observed in several myoglobins, hemoglobins and cytochromes in the oxidized and reduced forms) strongly supports the designed sandwich structure as for Fe(III) mimochrome IV complex[119,120]. For Fe(III) mimochrome IV 8Glu, in the pH range 2-8, a different behavior was observed. Two simultaneous equilibria (figure 5.2) were observed. The pKa_1 (3.85) is attributed to the protonation of the His in the uncoordinated form, as already seen for the other mimochromes, the second pKa (5.03) is more difficult to interpret. It may be due to several protonation equilibrium of the glutammic acids that may somehow influence the geometry of the axial ligand.

pH titrations also were followed by CD spectroscopy in the UV region, in order to determine the effect of the overall charge distribution on the secondary structure. No significant changes are observed in secondary structure in the pH range from 5 to 8, for Fe(III) mimochrome IV (figure 5.17) and Fe(III) mimochrome IV 8Lys (figure 5.15). This result is consistent with no substantial charge distribution changes during the titration for both species. For Fe(III) mimochrome IV at pH values below 5, protonation of the His side chain takes place[110](figure 5.18), as a consequence, the helical content decreases. Conversely no significant changes in the secondary structure are observed for Fe(III) mimochrome IV 8Lys at pH values below 5 (figure 5.16).

The CD spectroscopic pH titrations of Fe(III) mimochrome IV 8Glu (figure 5.10) show that the [θ] value at 222 nm increases from pH 2 to 8. This behavior may be attributed to deprotonation of the glutamate side chains. This may imply fewer inter and/or intra-chain unfavourable charge interactions, and as a consequence the helical content increases. The

mid-point value was observed at pH 5.8. A similar value was also derived from the Pka_2 of UV-vis pH titration of Fe(III) mimochrome IV 8Glu, this finding could indicate that both the Pka of CD and UV-vis spectroscopy pH titration refer to the same phenomenon.

CD measurements in both the UV and Soret regions gave preliminary structural information on Fe(III) mimochrome IV 8Glu (see figure 5.7) and Fe(III) mimochrome IV 8Lys (see figure 5.12). Analysis of the UV region indicates the peptides to be in helical conformation, in both Fe(III) mimochrome IV 8Glu and Fe(III) mimochrome IV 8Lys complexes at pH 7. The helical content increases upon TFE addition for Fe(III) mimochrome IV 8 Lys (Figure 5.12), reaching a maximum at 30% TFE quite similar to that observed for Fe(III) mimochrome IV[110]. The helical content increases only slightly upon TFE addition for Fe(III) mimochrome IV 8Glu (figure 5.7). The helical content is lower then that observed for Fe(III) mimochrome IV 8Lys and Fe(III) mimochrome IV.

The CD spectra in the Soret region are very interesting, in order to correlate the sign of the Cotton effect with the configuration around the metal ion. Both Fe(III) mimochrome IV 8Glu (figure 5.8) and Fe(III) mimochrome IV 8Lys (figure 5.14) exhibit positive Cotton effects. This finding, similarly to what found for Fe(III) mimochrome IV indicates that both systems adopt a Λ configuration[110]. The single positive Cotton effect gives a further indication on inter-helical interactions that reinforce the sandwich structure and drive the peptide chains to fold in a unique topology around the deuteroheme.

The effect of the charge distributions on redox properties of metal centre, was determined by experiments of square wave voltammetry. The deuteroheme redox potential of Fe-mimochromes, at pH 7, are the following:

Fe-mimochrome IV 8Glu: -170 mV *vs* SHE
Fe-mimochrome IV: -58 mV *vs* SHE
Fe-mimochrome IV 8Lys: -48 mV *vs* SHE

E°'Fe-mimohrome IV8glu < E°'Fe-mimochrome IV < E°' Fe-mimochrome IV 8 Lys

The square wave voltammograms, in cathodic and anodic scans, show for Fe-mimochrome IV 8Glu (figure 6.1a and 6.1b), Fe-mimochrome IV 8Lys (figure 6.2a and 6.2b) and

Fe-mimochrome IV (figure 6.3a and 6.3b), a well-behaved voltammetric wave in both scans. Fe-mimochrome IV voltammograms show the presence of a second peak, probably due to the electronic transfer of an adsorbed specie on the electrode. However a second species can not be ruled out.

The redox potential of -170 mV for Fe-mimochrome IV 8Glu and -48 mV for Fe-mimochrome IV 8Lys demonstrate that negatively charged residues, as for Fe-mimochrome IV 8Glu, around the molecular core, stabilize the ferric deuteroheme, while the positively charged residue of Fe-mimochrome IV 8Lys stabilize the ferrous deuteroheme. This hypothesis was further confirmed from the redox potential of the parent Mimochrome IV (-58 mV), that is intermediate between that Fe-mimochrome IV 8Glu and Fe-mimochrome IV 8Lys.

The small difference in the redox potential between Fe mimochrome IV and Fe mimochrome IV 8Lys may be due to the presence of organized phosphate ions around the molecule. Phosphate ions are know to interact with the superficial lysines of cytochrome, even at low phosphate concentrations[120,121]. Therefore the net charge on Fe mimochrome IV 8Lys is partially neutralized by specific phosphate ion interactions. It will be interesting to estimate, the changes in the redox potentials due to different buffers and ionic strength.

These redox potential values of mimochromes are significantly more positive than the reduction potential of bis-imidazole-ligated heme, as Fe(protoporphyrin IX)$(Im)_2$, -235 mV vs SHE, or Fe(mesoporphyrin IX)$(Im)_2$, -285 mV vs SHE. This result would suggest that the sandwich structure of mimochromes decreases solvent exposure, thus lead ions to positive shifts of the reduction potential.

In summary, Fe-mimochrome IV 8Glu and Fe-mimochrome IV 8Lys are a simple, structurally defined deuteroheme protein model, which may provide an excellent opportunity for exploring the subtle mechanisms that control the redox properties of the heme in natural proteins.

Experimental Section

Chapter 8: Experimental section

8.1 Design

Molecular design was performed on a Silicon Graphic 2 workstation. The program package Insight/Discover with Exstensible Systematic Force Field (ESFF), was used for energy minimization and restrained molecular dynamic (RMD) simulation. The NMR structure of Co(III) mimochrome IV were used as template for modelling the mimochrome IV 8Glu and mimochrome IV 8Lys molecules.

8.2 Equipment and materials

All amino acids, the Sieber amide resin, HATU, HOBt and HBTU were purchased from Nova Biochem; piperidine, and scavengers were from Fluka. DIEA and TFA from Applied Biosystems. All solvents used in the peptide synthesis and purification were anhydrous and HPLC grade respectively, and were supplied by LabScan Analytica. Deuteroporphyrin IX was from Porphyrin Products. Iron(II) acetate and tetramethylsilane were from Aldrich. Solvent mixtures are indicated in the respective sections.

8.3 Synthesis of Mimochrome peptides

Mimochrome IV, mimochrome IV 8Glu, and mimochrome IV 8Lys peptides were synthesized using Fmoc solid phase peptide synthesis (SPPS) on ABI 433 automatic peptide synthesizer on a 0.25 mmol scale. The used resin was the super acid labile Sieber Amide (100-200 mesh, 1% DVB, substitution level 0.52 mmol/g). For the synthesis of the three peptides the following amino acids were used:

Mimochrome IV: Fmoc-Glu(OtBu)-OH, Fmoc-Ser(tBu)-OH, Fmoc-Gln(Trt)-OH, Fmoc-Leu-OH, Fmoc-His(Trt)-OH, Fmoc-Asn(Trt)-OH , Fmoc-Lys(Mmt)- OH, Fmoc-Arg(Pbf)-OH

Mimochrome IV 8Glu: Fmoc-Glu(OtBu)-OH, Fmoc-Leu-OH, Fmoc-His(Trt)-OH, Fmoc-Glu(OtBu)-OH, Fmoc-Lys(Mmt)-OH, Fmoc-Arg(Pbf)-OH

Mimochrome IV 8Lys : Fmoc-Glu(OtBu)-OH, Fmoc-Lys(Boc)-OH, Fmoc-Leu-OH, Fmoc-His(Trt)-OH, Fmoc-Lys(Mmt)-OH, Fmoc-Arg(Pbf)-OH

For all peptides the same synthetic procedures were used (see scheme 1 pages 31 and 32). The first step was the synthesis of the fully protected peptides. This synthesis were achieved on a ABI 433 peptide synthesizer, with the Fmoc-chemistry. The synthetic procedure can be summarized as follow.

The α- Fmoc group, is removed at the beginning of every cycle with a 20% piperidine solution. After deprotection, the resin is washed with NMP to remove the piperidine. The peptide resin is then ready for coupling. All amino acids were coupled using a 0.45 M HBTU/HOBT solution in DMF. In the coupling step, the activated Fmoc aminoacid reacts with the amino-terminal of the growing peptide chain to form a peptide bond. Deprotection and coupling steps are repeated with each subsequent amino acid, until the chain assembly has been completed When the coupling is complete, the resin is washed with NMP. Mimochrome peptide N-terminal amino groups were acetylated with acid acetic (1mmol, 57 µl).

After the final assembly on the resin, the N-ε Mmt protecting group of the Lys^8 residue was removed with repeated treatments of a solution containing 10% acetic acid and 20% trifluoroethanol (TFE) in CH_2Cl_2 (10 ml) for 15min. Each step was repeated until no yellow or red trityl cations were detected in eluent . The product thus obtained, was transferred into a reactor, to cleavage the resin from the peptide. Therefore was added 1%TFA in DCM (20 ml) at the protected peptide. The mixture acid was shake for 2 minutes doing bubbling nitrogen. The solution was filtered, applying nitrogen pressure, into a flask containing 10% pyridine in methanol (2ml). The reaction was followed by TLC, each step was repeated until no product was detected. The side chain protecting groups were found to be stable in both deprotection reactions

8.4 Purification of mimochrome peptides

Mimochrome IV and mimochrome IV 8Glu peptide crude materials were purified by RP-HPLC (Shimadzu LC-8A, equipped with a SPD-M10 AV detector), on a Vydac C_{18} column (5 x 25 cm; 10 µm), eluted with water-acetonitrile (both containing 0.1 % v/v TFA) linear gradient:

- from 50 % to 90% acetonitrile concentration in 58 min; flow rate 120 ml/min

The pooled fractions containing the desired products were lyophilized. The peptides were found to be homogeneous by analytical RP-HPLC (Shimadzu LC-10 AD, equipped with a SPD-M10 AV detector and a SIL-10A Auto Sampler; Vydac C_{18} column 0.46 x 15 mm, 5µm), showing the following retention times:

mimochrome IV peptide:	28,50 min (figure 3.4),
mimochrome IV 8Glu peptide:	19,34 min (figure 3.6),

The purified compounds were analyzed by MALDI mass spectrometry (MALDI/MS) using a Voyager DE instrument (Perkin Elmer), operating at the Centro di Metodologie Chimico-Fisiche, University Federico II of Napoli. The α-cyano-4-hydroxycinnamic acid matrix was recrystallized from EtOH on a Kromasil C18 column. The analysis of mass spectroscopy confirmed the expected molecular weight

From analytical RP-HPLC analysis the mimochrome IV 8Lys peptide (figure 3.7) was pure and did not require further purification. The peptide mixture was evaporated to dryness and the mass spectroscopy confirmed the expected molecular weight. Mimochrome IV 8Lys peptide showing a retention time of 25,90 minutes.

The yield of reaction are the followings:

mimochrome IV:	538 mg of pure product (94%)
mimochrome IV 8Glu:	315 mg of pure product (63%)
mimochrome IV 8Lys:	494 mg of pure product (90%)

8.5 Coupling of mimochromes

Peptide synthesis protocols usually employ activants such as PyBop, DCC, HOBt, HATU, or HBTU in the presence of DIEA, to activate the free carboxyl groups and perform the coupling reaction to the next amino acid. The coupling reaction between the carboxyl groups of the porphyrin scaffols and the free ε amino groups of Lys[8] was achieved by using HATU as activant.

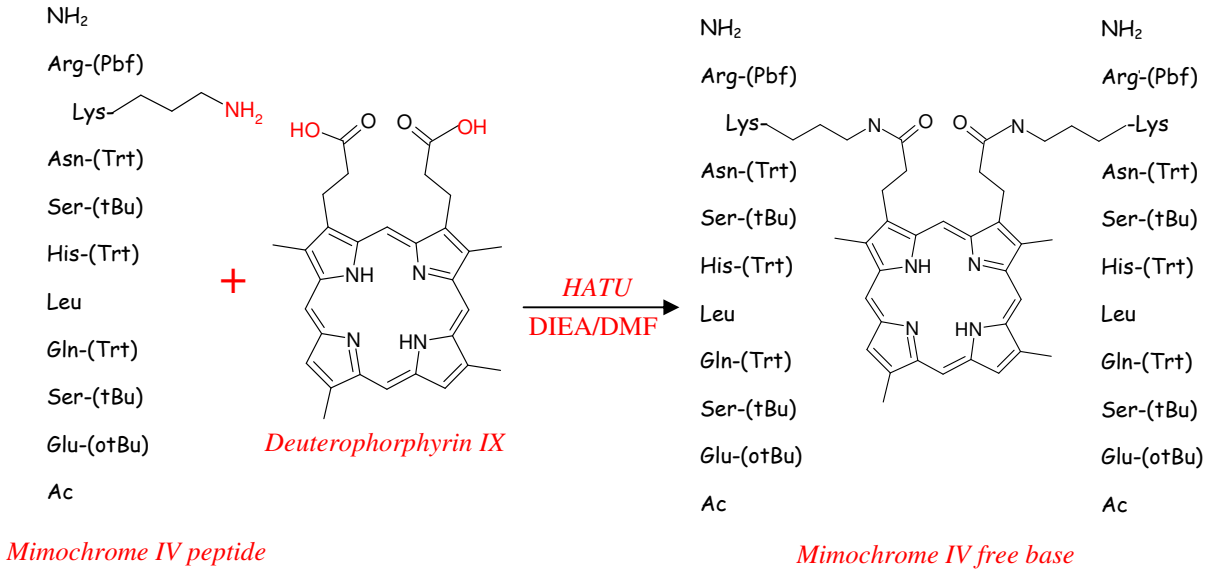

Figure 8.1: schematic representation of mimochrome coupling. The figure refers to the coupling of mimochrome IV.

The coupling was done in DMF at room temperature, at concentration of 6.6 x 10^{-3} M, and it was effected in the same conditions for the three mimochromes .

The first step was the deuteroporphyrin activation (Figure 8.2). The solid deuteroporphyrin IX dihydrocloride (1 equivalent, M.W., 583.5 g/mol), was dissolved in a small volume of DMF and DIEA (2 equivalents, M.W., 129,24 g/mol; density, 0.742 g/mL). At this solution were added 2 equivalents of HATU (M.W., 380.23 g/mol) and other 2 equivalents of DIEA, and this mixture was allowed to react for 15 min (figure 8.2).

In a following step, the activated deutheroporphyrin was added to a solution containing the peptide (3 equivalents; M.W. mimochrome IV, 2284 g/mol; M.W. mimochrome IV 8Glu,

2014 g/mol; M.W. mimochrome IV 8Lys, 2190 g/mol) in DMF and DIEA (3 equivalents), to form mimochromes. Other DIEA was added till pH ~ 7/8.

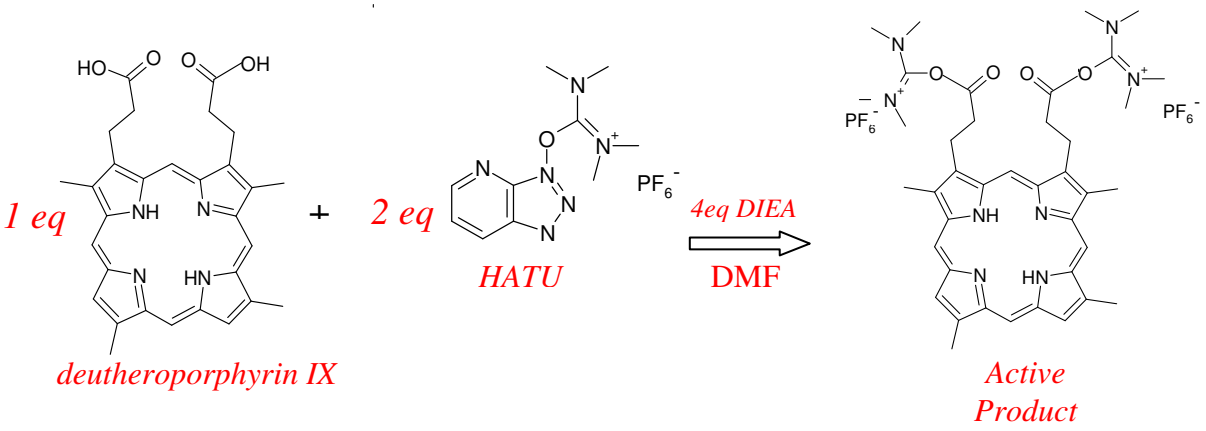

Figure 8.2: Schematic representation of deutheroporphyrin IX activation

In order to favour the formation of the *bis* substituted deutheroporphyrin IX, the mixture of the activated porphyrin was slowly added to the solution of the nonapeptide. This approach gave a good average yield for all mimochromes. The table 8.1 reports the amounts of each reagents used in the coupling reaction.

Reaction coupling	Deuteroporphyrin dihydroclhoride, 1eq	Peptide, 3eq	HATU, 2eq	DMF
mimochrome IV	9.10 x 10^{-3}g, 1.56 x 10^{-5}mol	0.100 g, 4.70 x 10^{-5}mol	1.19 x 10^{-2}g, 3.12 x 10^{-5}mol	2.35 ml
mimochrome IV 8Glu	1.17 x 10^{-2}g, 2.00 x 10^{-5}mol	0.120 g, 6.00 x 10^{-5}mol	1.52 x 10^{-2}g, 4.00 x 10^{-5}mol	3.00 ml
mimochrome IV 8Lys	1.59 x 10^{-2}g, 2.73 x 10^{-5}mol	0.180 g, 8.20 x 10^{-5}mol	1.69 x 10^{-2}g, 4.46 x 10^{-5}mol	4.10 ml

Table 8.1: kinds and quantity of reagents used in the coupling reaction

The proceeding of the reaction was followed by RP-HPLC on a Vydac C_{18} column (5 x 25 cm; 10 µm). After completion of the reaction, usually after 24 hours, the mixture was evaporated to dryness and extracted with chloroform and acid water (using citric acid

10% p/v) to eliminate the reagents (DIEA, HATU and the peptide). After completion of the extraction, the chloroform phase was evaporated. The next step was the deprotection of the protecting groups. It was achieved at room temperature in the following mixture:

9.40 ml	trifluoroacetic acid (TFA)
0.25 ml	ethanedithiol (EDT)
0.25 ml	water
0.10 ml	triisopropylsilane (TIS)

The thiol-based scavengers were added to avoid any side reactions that might occur when the protecting groups were removed from the peptide side chains. For all compounds, the deprotection was usually complete in 2 h. After completion of the reaction, the solvent that contained the crude product was evaporated under reduced pressure to 5% of the volume. Ice-cold diethyl ether added to the residue and the mixture was cooled on ice to aid precipitation of the crude product. It was isolated from the remaining part of the scavengers by centrifuges with diethyl ether, and it was further purified by HPLC. (Shimadzu LC-8A, equipped with a SPD-M10 AV detector), on a Vydac C_{18} column (2.2 x 25 cm; 10 µm), eluted with water-acetonitrile (both containing 0.1 % v/v of TFA) linear gradient:

- from 5 % to 90% acetonitrile concentration in 66 min; flow rate 22 ml/min

The pooled fractions containing the desired products were lyophilized to obtain:

mimochrome IV:	35 mg of pure product (53%)
mimochrome IV 8Glu:	52 mg of pure product (63%)
mimochrome IV 8Lys:	54 mg of pure product (40%)

The purified compounds were analyzed by MALDI mass spectrometry (MALDI/MS) using a Voyager DE instrument (Perkin Elmer), operating at the Centro di Metodologie Chimico-Fisiche, University Federico II of Napoli. The α-cyano-4-hydroxycinnamic acid was recrystallized from EtOH on a Kromasil C18 column.

8.6 Insertion of Iron in Mimochromes

For the insertion of iron acetate method was used .

$$Fe(OAc)_2.xH_2O + H_2P \longrightarrow Fe(P) + 2\ HOAc + 2\ H_2O$$

Iron II acetate (10 equivalent, M.W. 173,94) was added to a solution of pure mimochrome (M.W. mimochrome IV, 2753 g/mol, M.W. mimochrome IV 8Glu, 2953 g/mol; M.W. mimochrome IV 8Lys, 2945 g/mol) in acetic acid/TFE (6:4) for a final concentration of 2×10^{-4} M (figure 8.3). The reaction mixture was heated under reflux for 2 h at 45 °C.

	M.W.[a] (g/mol)	*mol number (mol)*	*Iron (II) Acetate (mol)*	*Volume (L)*
mimochrome IV	3209	1.8×10^{-5}	1.8×10^{-4}	9.0×10^{-2}
mimochrome IV 8Glu	3409	5.8×10^{-6}	5.8×10^{-5}	3.4×10^{-2}
mimochrome IV 8Lys	4313	7.0×10^{-6}	7.0×10^{-5}	3.5×10^{-2}

Table 8.2: iron insertion stecheometry; *(a)*, molecular weight of TFA salt

Upon insertion of the metal in the porphyrin ring, the Fe^{II} ion was oxidized to Fe^{III}. During the reaction the colour of the reaction mixture changed from purple rose to brown, indicating the formation of the iron (III) porphyrin complex. The reaction was monitored by RP-HPLC and UV-VIS, where the characteristic Fe^{III}-porphyrin spectrum became dominant. The desired product was purified to homogeneity by Gel fitration with pre-packed PD-10 columns of the GE Healthcare Bio-Science AB (Sephadex™ G-25M contains 0.15% Kathon CG as preservative). MALDI/MS confirmed the expected molecular weight (cap 3.1). The pooled fractions containing the desired products were lyophilized to obtain:

mimochrome IV :	26mg of product pure (55%)
mimochrome IV 8Glu:	12 mg of product pure (10%)
mimochrome IV 8Lys:	18 mg of product pure (72%)

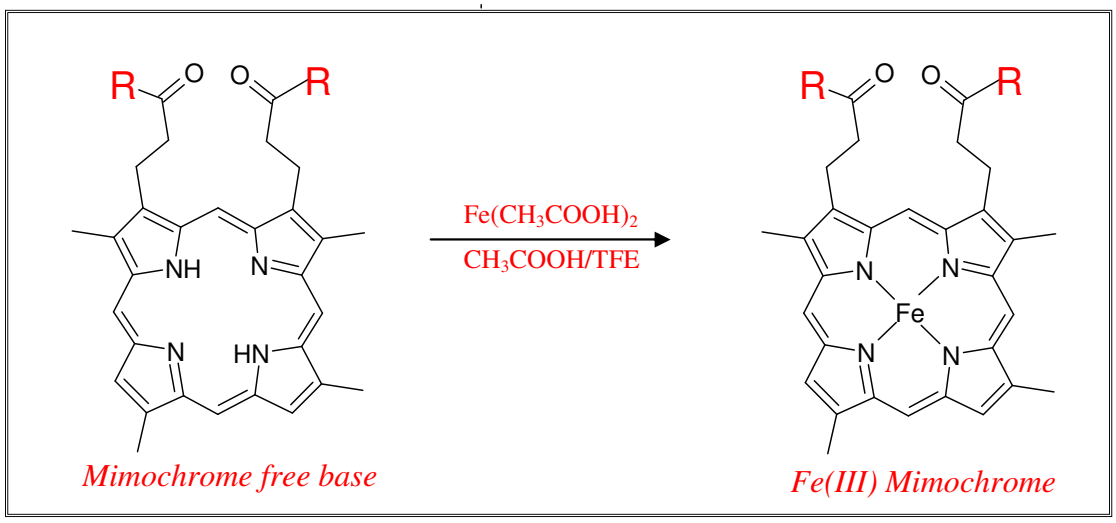

Figure 8.3 : Schematic representation of insertion of iron in mimochrome; (R), represents mimochrome peptide

8.7 Analytical methods

Total metal-reconstituted mimochrome IV concentrations were determined on the basis of the metal content, derived from flame atomic absorption spectrometry. Standard procedures, on a Varian Spectra AA 220 atomic absorption spectrometer, equipped with a MK7 burner, were used[122]. Solutions containing approximately 350 mgL^{-1} of Fe(III) mimochrome IV 8Glu and Fe(III) mimochrome IV 8Lys in ultra pure metal-free water were directly aspired into an air-acetylene flame with no prior treatment. Concentrations were obtained both by comparison with calibration curve and by standard addition. No differences, which overcome experimental uncertainty, were observed. Fe(III) mimochrome IV 8Glu and Fe(III) mimochrome IV 8Lys stock solutions, analyzed for metal contents, were appropriately diluted and used for determining the extinction coefficients at the Soret band maximum wavelength.

8.8 UV/Vis spectroscopy:

UV/Vis spectroscopy: UV/Vis spectra were recorded on a Cary Varian 5000 UV Spectrophotometer with 1 cm path length cells. Wavelength scans were performed at 25˚C from 200 to 700 nm, with a 300 nm min^{-1} scan speed. Fe(III) mimochrome IV 8Glu and Fe(III) mimochrome IV 8Lys extinction coefficients at the Soret band maximum wavelength were determined in phosphate buffered solutions (pH 7; final phosphate concentration 1.0×10^{-2}M), using a concentrations range from 1.0×10^{-6} M to 1.0×10^{-5} M. Fe(III) mimochrome IV 8Glu and Fe(III) mimochrome IV 8Lys pH titration were performed in aqueous solution, using HCl solution (0,37% and 3,7%) to lower pH. The concentrations of Fe(III) mimochrome IV 8Glu and of Fe(III) mimochrome IV 8Lys were 3.76×10^{-6} M and 7.00×10^{-6} M, respectively.

8.9 Circular dichroism spectroscopy

CD spectra were obtained at 25˚C on a Jasco J-715 dichrograph. Data were collected at 0.2 nm intervals with a 5 nm min^{-1} scan speed, a 2 nm bandwidth and a 16 s response, from 260 to 190 nm in the far-UV region. The spectra in the Soret region were collected at 0.2 nm intervals with a 10 nm min^{-1} scan speed, a 2 nm bandwidth and a 16 s response, collected from 470 to 360 nm. Cuvette path length of 1 cm was used for all spectral regions. Sample solutions at different TFE/aqueous phosphate ratio (from 0 to 50% TFE) were prepared for both Fe(III) mimochrome IV 8Glu (4.02 x 10^{-6}M) and Fe(III) mimochrome IV 8Lys (3.36 x 10^{-6} M). CD intensities in the far UV region are expressed as mean residue ellipticities (deg $cm^2 dmol^{-1} res^{-1}$); intensities in the Soret region are reported as total molar ellipticities (deg cm^2 $dmol^{-1}$).

8.10 Square wave voltammetry

Square wave voltammetry experiments were carried out under argon with a Potentiostat/Galvanostat PAR mod. 273A, using a cell designed for small volume samples (V_{min}=0.8 ml). Scan rate, 0.01 Vs^{-1} ; frequency, 5 Hz; pulse amplitude, 0.050 V. an edge-cleaved pyrolitic graphite (PGE) disc were used as working electrodes for the. A Pt sheet and a saturated calomel electrode (SCE) acted as counter and reference electrode, respectively. The electric contact between the SCE and the working solution was obtained with a Vycor set. Potentials were calibrated against the MV^{+2}/ MV^{+} couple (MV = methylviologen). The cleaning procedure of PGE electrode consisted in a treatment with anhydrous ethanol for 5 min, followed by polishing with an alumina (BDH, particle size of about 0.015 μm) water slurry on cotton wool for 3 min and a final immersion in an ultrasonic pool for about 5 min. All measurements were made in 0.01 M phosphate buffer pH 7 and $NaClO_4$ 0.1 M, at 25˚C. All mimochromes were freshly prepared before use. Equilibrium reduction potentials (E˚´) were calculated from the peak potential Ep of the square-wave voltammograms using the Parry–Osteryoung equation[123].

All reduction potentials reported in this paper are referred to the standard hydrogen electrode (SHE). For each species, the experiments were performed at least two times.

Appendix

A1: Fe mimochrome IV 8Glu UV-vis titration: Fitting equation

Figure A1 shows the pH-dependent coordination equilibria in Fe(III) mimochromes. At acid pH (≈ 2) the molecules are characterized from two protonated histidines. Fe(III) mimochrome is convert to a species in which both ligands are coordinated to Fe by increasing of the pH. The same equilibria could involve Fe-mimochrome IV 8Glu and Fe-mimochrome IV 8 Glu in pH range 2-8.

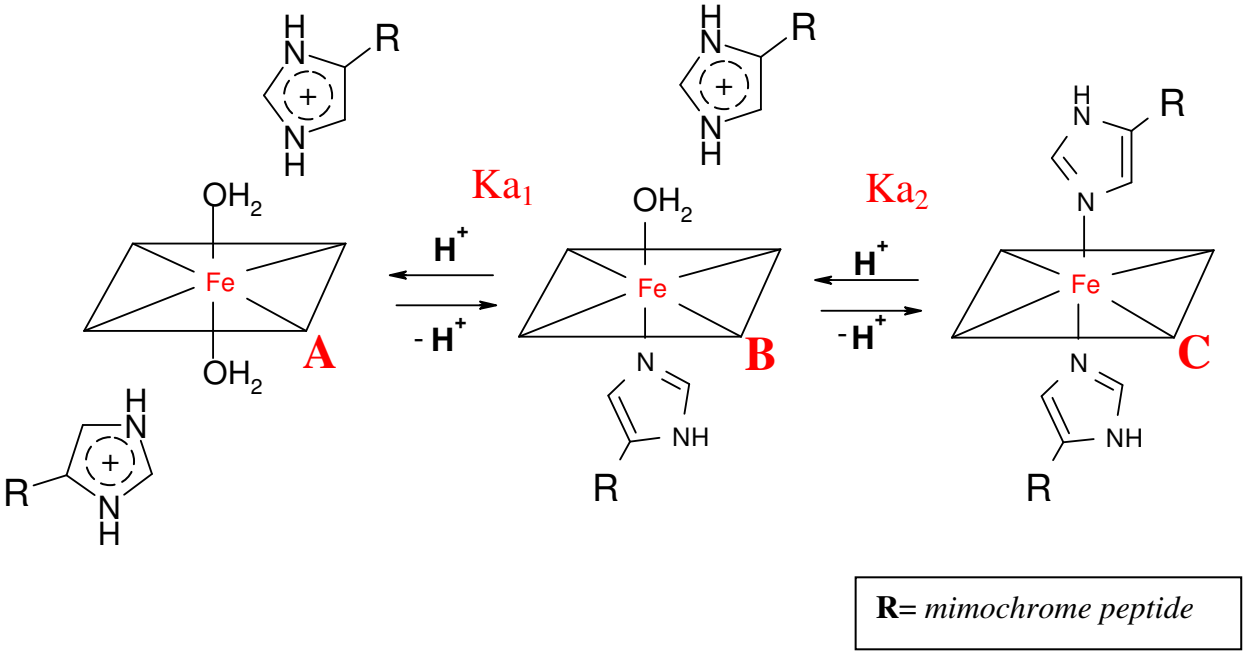

Figure A1: Coordination equilibria Fe-porphyrin Histidine as function of pH

We have prove to fit the titration curve of Fe-mimochromeIV 8Glu on the basis of Fe-histidine coordination equilibria shown above.

$$Ka_1 = \frac{[A]\,[H^+]}{[B]} \qquad (E_1)$$

The total concentration of iron porphyrin is given by eq. E_3 and the absorbance is given by eq. E_4, where ε_x is the molar extinction coefficient of each species:

$$Ct = [A] + [B] + [C]; \quad (E_3)$$

$$A = [A]\varepsilon_A + [B]\varepsilon_B + [C]\varepsilon_C \quad (E_4)$$

The total concentration can be also write how depicted in the equation T_1

$$Ct = Ct\,(X_A + X_B + X_C); \quad (T_1)$$

$$(X_A + X_B + X_C) = 1 \quad (T_2)$$

Therefore inserting equation T_1, into absorbance equation (E_4) and into equation of the first and second acids constant (E_1 and E_2), we have:

$$A = Ct\,(X_A\,\varepsilon_A + X_B\,\varepsilon_B + X_C\,\varepsilon_C) \quad (T_3)$$

$$Ka_1 = \frac{[B][H^+]}{[A]} = \frac{X_B\,[H^+]}{X_A} \quad (T_4)$$

$$Ka_2 = \frac{[C][H^+]}{[B]} = \frac{X_C[H^+]}{X_B} \quad (T_5)$$

From equation T_4 and T_5 can be determinate X_A and X_C;

$$X_A = \frac{X_B\,[H^+]}{Ka_1} \quad (T_6)$$

$$X_C = \frac{X_B\,Ka_2}{[H^+]} \quad (T_7)$$

The equations T_4 and T_5 replace X_A and X_B into absorbance equation (T_3), to give:

$$A = Ct \left(\frac{X_B [H^+] \varepsilon_A}{Ka_1} + X_B \varepsilon_B + \frac{X_B Ka_2 \varepsilon_C}{[H^+]} \right) \qquad (T_8)$$

The equation T_6 and T_7 replaced X_A and X_C into eq.T_2 to calculate X_B, how shown by the equations T_9 and T_{10}

$$\frac{X_B [H^+]}{Ka_1} + X_B + \frac{X_B Ka_2}{[H^+]} = 1; \qquad (T_9)$$

$$X_B = \frac{Ka_1[H^+]}{[H^+]^2 + Ka_1[H^+] + Ka_1Ka_2} \qquad (T_{10})$$

In final step equation T_{10} replace D_H into adsorbance equation T_8 to obtain:

$$A = Ct \left(\frac{[H^+]^2 \varepsilon_A + Ka_1[H^+]\varepsilon_B + Ka_1Ka_2 \varepsilon_C}{[H^+]^2 + Ka_1[H^+] + Ka_1Ka_2} \right) \qquad (T_{11})$$

This equation was used to fit the curve derivate by UV-vis Fe-mimochrome IV 8Glu pH titration

A2: Fe mimochrome IV 8Lys UV-vis titration: Fitting equation

For Fe-Mimochrome IV 8Lys it seen that only one equilibrium being present. This indicates that the two pKa are quite similar, therefore we can consider a single equilibrium:

$$[A] + 2[H^+] \rightleftarrows [C]$$

The total concentration of iron porphyrin is given by eq. E_1 and the absorbance is given by eq. E_2, where ε_x is the molar extinction coefficient of each species:

$$Ct = [A] + [C]; \qquad (E_1)$$

$$A = [A]\varepsilon_A + [C]\varepsilon_C; \qquad (E_2)$$

The total concentration can be also write how depicted in the equation M_1

$$Ct = Ct\,(X_A + X_C); \qquad (M_1)$$

$$(X_A + X_C) = 1 \qquad (M_2)$$

Therefore replacing equation M_1 into absorbance equation (E_2) we have:

$$A = Ct\,(X_A\,\varepsilon_A + X_C\,\varepsilon_C) \qquad (M_3)$$

Considering that

$$Ka_1 \approx Ka_2 \approx Ka$$

The Ka equation can be written:

$$Ka^2 = \frac{[H^+]^2\,[C]}{[A]} \qquad (M_4)$$

On the basis of equation M_1, Ka equation become:

$$Ka^2 = \frac{[H^+]^2\,X_C}{X_A} \qquad (M_5)$$

Which gives eq.M_6

$$X_C = \frac{Ka^2 X_A}{[H^+]^2} \qquad (M_6)$$

Replacing eq M_6 into eq M_3 and eq M_2

$$A = Ct\left(X_A \varepsilon_A + \frac{Ka^2 X_A}{[H^+]^2}\varepsilon_C\right) \qquad (M_7)$$

$$X_A + \frac{Ka^2 X_A}{[H^+]^2} = 1 \qquad (M_8)$$

X_A can be calculate by equation M_8 for give

$$X_A = \frac{[H^+]^2}{Ka^2\,[H^+]^2} \qquad (M_9)$$

In final step equation M_9 replace X_A into adsorbance equation M_7 to obtain the equation (M_{10}) that we used to fit the curve derivate by UV-vis Fe-mimochrome IV 8Lys pH titration

$$A = Ct\left(\frac{[H^+]^2 \varepsilon_A + Ka^2 \varepsilon_C}{Ka^2\,[H^+]^2}\right) \qquad (M_{10})$$

Acknowledgement

We wish to thank Profs. Sola M. and Borsari M. (University of Modena) for assistance in square wave voltammetry experiments, and Dr. Marco Trifuoggi for metal content analysis.

References

1. Lippard, S. J.; Berg, J. M. *Principles of Bioinorganic Chemistry*; University Science Books: Mill Valley, **1994**; p 349.
2. Holm, R. H.; Kennepohl, P.; Solomon, E. I. *Chem. Rev*. **1996**, *96*, 2239.
3. *The Porphyrins*; Dolphin, D., Ed.; Academic Press: New York, **1979**; Vol. 7.
4. Bertini, I.; Luchinat, C. *Curr. Opin. Chem. Biol*. **1999**, *3*, 145.
5. Perutz, M. F.; Wilkinson, A. J.; Paoli, M.; Dodson, G. G. *Annu. Rev. Biophys. Biomol. Struct*. **1998**, *27*, 1.
6. Peterson, J. A.; Graham, S. E. *Structure* **1998**, *6*, 1079.
7. Loew, G. H.; Harris, D. L. *Chem. Rev*. **2000**, *100*, 407.
8. Li, H.; Poulos, T. L. *Structure* **1994**, *2*, 461.
9. Wong, L. L. *Curr. Opin. Chem. Biol*. **1998**, *2*, 263.
10. Smith, A. T.; Veitch, N. C. *Curr. Opin. Chem. Biol*. **1998**, *2*, 269.
11. Banci, L. *J. Biotechnol*. **1997**, *53*, 253.
12. Sono, M.; Roach, M. P.; Coulter, E. D.; Dawson, J. H. *Chem. Rev*. **1996**, *96*, 2841.
13. Barker, P. D.; Ferguson, S. J. *Structure* **1999**, *7*, R281.
14. Poulos, T. L.; Li, H.; Raman, C. S. *Curr. Opin. Chem. Biol*. **1999**, *3*, 131.
15. Michel, H.; Behr, J.; Harrenga, A.; Kannt, A. *Annu. Rev. Biophys.Biomol. Struct*. **1998**, *27*, 329.
16. Lederer, F. *Biochimie* **1994**, *76*, 674.
17. Fischer, H.; Zeile, K. *Justus Liebigs Ann. Chem.* **1929**, *468*, 98.
18. Sellers, V. M.; Wu, C. K.; Dailey, T. A.; Dailey, H. A. *Biochemistry* **2001**, *40*, 9821.
19. Wu, C. K.; Dailey, H. A.; Rose, J. P.; Burden, A.; Sellers, V. M.; Wang, B. C. *Nat. Struct. Biol.* **2001**, *8*, 156.
20. Moore, G. R.; Pettigrew, G. W. *Cytochromes c: Evolutionary, Structural and Physiochemical Aspects*; Springer-Verlag: New York, 1990.
21. Drygas, M. E.; Lambowitz, A. M.; Nargang, F. E. *J. Biol. Chem.* **1989**, *264*, 17897.
22. O'Brian, M. R.; Thony-Meyer, L. *Adv. Microb. Physiol.* **2002**, *46*, 257.
23. Mogi, T.; Saiki, K.; Anraku, Y. *Mol. Microbiol.* **1994**, *14*, 391.

24. Brown, K. R.; Allan, B. A.; Do, P.; Hegg, E. L. *Biochemistry* **2002**, *41*, 10906.
25. Vainshtein, B. K.; Melikadamyan, W. R.; Barynin, V. V.; Vagin, A. A.; Grebenko, A. I.; Borisov, V. V.; Bartels, K. S.; Fita, I.; Rossmann, M. G. *J. Mol. Biol.* **1986**, *188*, 49.
26. Igarashi, N.; Moriyama, H.; Fujiwara, T.; Fukumori, Y.; Tanaka, N. *Nat. Struct. Biol.* **1997**, *4*, 276.
27. Crane, B. R.; Siegel, L. M.; Getzoff, E. D. *Science* **1995**, *270*, 59.
28. Lemberg, R.; Falk, J. E. *Biochem. J.* **1951**, *49*, 6
29. Tainer, J. A.; Roberts, V. A.; Getzoff, E. D. *Curr. Opin. Biotechnol.* **1992**, *3*, 378-387.
30. *Cytochrome c*: *Evolutionary, Structural and Physiological Aspects*; Moore, G. R.; Pettigrew, G. W., Eds.; Springer-Verlag: Berlin, **1990**.
31. Scott, R. A.; Mauk, A. G. *Cytochrome c*: *A Multidisciplinary Approach*; University Science Books: Sausalito, CA, **1996**.
32. Turano, P.; Lu, Y. In *Handbaook on Metalloproteins*; Bertini, I., Sigel, H., Sigel, A., Eds.; Marcel Dekker: New York, **2001**; pp 269-356.
33. Goodin, D. B. *J. Biol. Inorg. Chem.* **1996**, *1*, 360-363.
34. Banci, L.; Rosato, A.; Turano, P. *J. Biol. Inorg. Chem.* **1996**, *1*, 364-367.
35. Gross, Z. *J. Biol. Inorg. Chem.* **1996**, *1*, 368-371.
36. Rietjens, I. M. C. M.; Osman, A. M.; Veeger, C.; Zakharieva, O.; Antony, J.; Grodzicki, M.; Trautwein, A. X. *J. Biol. Inorg. Chem.* **1996**, *1*, 372-376.
37. Weiss, R.; Mandon, D.; Wolter, T.; Trautwein, A. X.; Muther, M.; Bill, E.; Gold, A.; Jayaraj, K.; Terner, J. *J. Biol. Inorg. Chem.* **1996**, *1*, 377-383.
38. Martinez, S. E.; Huang, D.; Szczepaniak, A.; Cramer, W. A.; Smith, J. L. *Structure* **1994**, *2*, 95-105.
39. Lanzilotta, W. N.; Schuller, D. J.; Thorsteinsson, M. V.; Kerby, R. L.; Roberts, G. P.; Poulos, T. L. *Nat. Struct. Biol.* **2000**, *7*,876-880.
40. Tezcan, F. A.; Winkler, J. R.; Gray, H. B. *J. Am. Chem. Soc*. **1998**, *120*, 13383.
41. Mauk, A. G.; Moore, G. R. *J. Biol. Inorg. Chem*. **1997**, *2*, 119.
42. Gunner, M. R.; Alexov, E.; Torres, E.; Lipovaca, S. *J. Biol. Inorg. Chem.* **1997**, *2*, 126.

43. Naray-Szabo', G. *J. Biol. Inorg. Chem*. **1997**, *2*, 135.
44. Wuttke, D. S.; Gray, H. B. *Curr. Opin. Struct. Biol.* **1993**, *3*, 555.
45. Gray, H. B.; Winkler, J. R. *Annu. Rev. Biochem*. **1996**, *65*, 537.
46. Nastri, F.; Lombardi, A.; D'Andrea, L. D.; Sanseverino M.; Maglio, O.; Pavone, V. *Biopolymers* **1998**, *47*, 5
47. Traylor, T. G. *Acc. Chem. Res.* **1981**, *14*, 102.
48. Traylor, T. G.; Chang, C. K.; Geibel, J.; Berzinis, A.; Mincey, T.;Cannon, J. *J. Am. Chem. Soc.* **1979**, *101*, 6716.
49. Collman, J. P. *Inorg. Chem*. **1997**, *36*, 5145.
50. Momenteau, M.; Reed, C. A. *Chem. Rev.* **1994**, *94*, 659.
51. Mansuy, D.; Battioni, P. *Bioinorganic Catalysis*; Marcel Dekker: New York, **1993**; p 395.
52. Mansuy, D. *Coord. Chem. Rev.* **1993**, *125*, 129.
53. Meunier, B. *Chem. Rev.* **1992**, *92*, 1411.
54. Collman, J. P.; Zhang, X.; Lee, V. J.; Uffelman, E. S.; Brauman, J. I. *Science* **1993**, *261*, 1404.
55. Bruice, T. C., Zipplies, M. F. & Lee, W. A. **1986** *Proc. Natl. Acad. Sci.* 83**,** 4646–4649.
56. Mortimer, D. N. & Lindsay Smith, J. R. **1985** *J. Chem. Soc. Perkin Trans. 2,* 1139–1149.
57. Hellinga, H. W. *Curr. Opin. Biotechnol.* **1996**, ***7***, 437.
58. Hellinga, H. W. *Folding Des.* **1998**, *3*, R1.
59. DeGrado, W. F.; Summa, C. M.; Pavone, V.; Nastri, F.; Lombardi, A. *Annu. Rev. Biochem.* **1999**, *68*, 779.
60. Regan, L. *Trends Biochem. Sci.* **1995**, *20*, 280.
61. Lu, Y.; Valentine, J. S. *Curr. Opin. Struct. Biol.* **1997**, *7*, 495.
62. Baltzer, L. *Topics Curr. Chem*. **1999**, *202*, 39.
63. Richardson, J. S.; Richardson, D. C.; Tweedy, N. B.; Gernert, K. M.; Quinn, T. P.; Hecht, M. H.; Erickson, B. W.; Yan, Y.; McClain, R. D.; Donlan, M. E.; et al. *Biophys. J.* **1992**, *63*, 1185.

64. Bryson, J. W.; Betz, S. F.; Lu, H. S.; Suich, D. J.; Zhou, H. X.; O'Neil, K. T.; DeGrado, W. F. *Science* **1995**, *270*, 935.
65. Betz, S. F.; Raleigh, D. P.; DeGrado, W. F. *Curr. Opin. Struct.Biol.* **1993**, *3*, 601.
66. Beasley, J. R.; Hecht, M. H. *J. Biol. Chem.* **1997**, *272*, 2031.
67. Balaram, P. *J. Pept. Res*. **1999**, *54*, 195.
68. Imperiali, B.; Ottesen, J. J. *Biopolymers* **1998**, *47*, 23.
69. Tuchscherer, G.; Scheibler, L.; Dumy, P.; Mutter, M. *Biopolymers* **1998**, *47*, 63.
70. Street, A. G.; Mayo, S. L. *Structure* **1999**, *7*, R105.
71. Desjarlais, J. R.; Handel, T. M. *Protein Sci*. **1995**, *4*, 2006.
72. Desjarlais, J. R.; Clarke, N. D. *Curr. Opin. Struct. Biol.* **1998**, *8*, 471.
73. Gouterman, M. *The Porphyrins*; Academic Press. New York, **1978**; Vol. 3, p 1.
74. Adar, F. *The Porphyrins*; Academic Press: New York, **1978**; Vol. 3, p 167.
75. Eaton, W. A.; Hofrichter, J. *Methods Enzymol.* **1981**, vol. 76, p 175.
76. Buchler J. W. *The Porphyrins;* Academic Press.: New York, **1979**; Vol. 1, p 389.
77. Bullock, P. A.; Myer, Y. P. *Biochemistry* **1978**, *17*, 3084.
78. Babcock, G. T.; Widger, W. R.; Cramer, W. A.; Oertling, W. A.; Metz, J. G. *Biochemistry* **1985**, *24*, 3638.
79. Sugiyama, T.; Miura, R.; Yamano, T.; Shiga, K.; Watari, H. *Biochem. Biophys. Res. Commun.* **1980**, *97*, 22.
80. Dawson, J. H.; Andersson, L. A.; Masanori, S. *J. Biol. Chem*. **1982**, *257*, 3606.
81. Spee, J. H., Boersma, M. G., Veeger, C., Samyn, B., Van Beeumen, J., Warmerdam, G., Canters, G. W., Van Dogen, W. M. A. M. & Rietjens, I. M. C. M. **1996** *Eur. J. Biochem.* 241**,** 215–220.
82. Othman, S., Le Lirzin, A. & Desbois, A. **1993** *Biochemistry* 32**,** 9781–9791.
83. Sasaki, T. & Kaiser, E. T. **1989** *J. Am. Chem. Soc.* 111**,** 380–381.
84. Akerfeldt, K. S., Kim, R. M., Camac, D., Groves, J. T., Lear, J. D. & DeGrado, W. F. **1992** *J. Am. Chem. Soc.* 114**,** 9656–9657.
85. Benson, D. R., Hart, B. R., Zhu, X. & Doughty, M. B. **1995** *J. Am. Chem. Soc.* 117**,** 8502–8510.
86. Arnold, P. A., Shelton, W. R. & Benson, D. R.**1997** *J. Am. Chem. Soc.* 119**,** 3181–3182

87. Wang, M., Kennedy, M. L., Hart, B. R. & Benson, D. R. **1997** *Chem. Commun.* 883–884.

88. Sakamoto, S., Sakurai, S., Ueno, A. & Mihara, H. **1997** *Chem. Commun.* 1221–1222.

89. Nastri, F.; Lombardi, A.; Morelli, G.; Maglio, O.; D'Auria, G.; Pedone, C.; Pavone, V. *Chem. Eur. J.* **1997**, *3*, 340.

90. D'Auria, G.; Maglio, O.; Nastri, F.; Lombardi, A.; Mazzeo, M.; Morelli, G. Paolillo, L.; Pedone, C.; Pavone, V. *Chem. Eur. J.* **1997**, *3*, 350.

91. Lombardi, A.; Nastri, F.; Sanseverino, M.; Maglio, O.; Pedone, C.; Pavone, V. *Inorg. Chim. Acta* **1998**, *275-276*, 301.

92. Nastri, F.; Lombardi, A.; Morelli, G.; Pedone, C.; Pavone, V.; Chottard, G.; Battioni, P.; Mansuy, D. *J. Biol. Inorg. Chem.* **1998**, *3*, 671.

93. D'Andrea, L. D.; Nastri, F.; Lombardi, A.; Maglio, O.; Pavone,V.; *Miniaturized Hemoproteins:* A Covalent Asymmetric Peptide- Porphyrin System. In *Peptides 98*; Bajusz, S., Hudecz, F., Eds.; Akade´mia Kiado´: Budapest, Hungary, **1999**; pp 304-305;

94. D. A. Moffet, M. H. Hecht, *Chem. Rev*. **2001**, 101, 3191 - 3203.

95. Lombardi, F. Nastri, V. Pavone, *Chem. Rev*. **2001**, 101, 3165 – 3189;

96. S. Sakamoto, A. Ueno, H. Mihara, *J.Chem. Soc. Perkin Trans*. 2 **1998**, 2395 - 2404;

97. S. Sakamoto, I. Obataya, A. Ueno, H. Mihara, *J. Chem. Soc. Perkin Trans*. 2 **1999,** 2059 - 2069;

98. M. M. Rosenblatt, D. L. Huffman, X. Wang, H. A. Remmer, K. S. Suslick, *J. Am. Chem. Soc.* **2002**, 124, 12 394 -12 395;

99. H. K. Rau, W. Haehnel, *J. Am. Chem. Soc*. **1998**, 120, 468 - 476;

100. H. K. Rau, N. DeJonge, W. Haehnel, *Proc. Natl. Acad. Sci*. USA **1998**, 95, 11526 - 11531;

101. H. K. Rau, N. DeJonge, W. Haehnel, *Angew. Chem*. **2000**, 112, 256 - 259; *Angew. Chem. Int. Ed*. **2000**, 39, 250 – 253;

102. D. E. Robertson, R. S. Farid, C. C. Moser, J. L. Urbauer, S. E.Mulholland, R. Pidikiti, J. D. Lear, A. J. Wand, W. F. DeGrado, P. L. Dutton, *Nature* **1994**, 368, 425 - 432;

103. J. M. Shifman, C. C. Moser, W. A. Kalsbeck, D. F. Bocian, P. L. Dutton, *Biochemistry* **1998**, 37, 16815 -16827;

104. J. M. Shifman, B. R. Gibney, R. E. Sharp, P. L. Dutton, *Biochemistry* **2000**, 39, 14813 - 14821

105. B. R. Gibney, P. L. Dutton, *Protein Sci.* **1999**, 8, 1888 -1898.

106. Perutz, M. F., Hasnain, S. S., Duke, P. J., Sessler, 660–663. J. L. & Hahn, J. E. **1982** *Nature* 295**,** 535–538.

107. Lombardi, A.; Summa, C.; Geremia, S.; Randaccio, L.; Pavone, V.; DeGrado, W. F. *Proc. Natl. Acad. Sci*. **2000**, *97*, 6298.

108. Lombardi, A.; Marasco, D.; Maglio, O.; Di Costanzo, L.; Nastri, F.; Pavone, V. *Proc. Natl. Acad. Sci.* **2000**, *97*, 11922.

109. W. F. DeGrado, C. M. Summa, V. Pavone, F. Nastri, A. Lombardi, *Annu. Rev. Biochem.* **1999**, 68, 779 – 819

110. Lombardi, F. Nastri, D. Marasco, O. Maglio, G. De Sanctis, F. Sinibaldi, R. Santucci, M. Coletta, and V. Pavone *Chem. Eur. J.* **2003**, 9, 5643 – 5654

111. V. Palaniappan, D. F. Bocian, *Biochemistry* **1994**, 33, 14264 -14274

112. M. Coletta, H. Costa, G. De Sanctis, F. Neri, G. Smulevich, D. L. Turner, H. Santos, *J. Biol. Chem*. **1997**, 272, 24800 - 24804.

113. W.C. Chart, P.D. White, J. Beythien and R. Steinauer. *J. Chem. Sot. Chem. Commun.* **1995** 589-592.

114. M. L. Kennedy, S. Silchenko, N. Houndonougbo, B. R. Gibney, P. L. Dutton, K. R. Rodgers, D. R. Benson*, J. Am. Chem. Soc*. **2001**, 123, 4635 - 4636.

115. K. D. Karlin, *Science* **1993**, 261, 701 - 708

116. Y. Lu, S. M. Berry, T. D. Pfisterand, *Chem. Rev*. **2001**, 101, 3047 - 3080.

117. D. A. Moffet, M. H. Hecht, *Chem. Rev.* **2001,** 101, 3191 - 3203.

118. V. Palaniappan, D. F. Bocian, *Biochemistry* **1994**, 33, 14264 - 14274

119. M. Coletta, H. Costa, G. De Sanctis, F. Neri, G. Smulevich, D. L. Turner, H. Santos*, J. Biol. Chem*. **1997**, 272, 24800 - 24804.

120. G. Battistuzzi, M. Borsari, M. Sola, *Eur. J. Inorg. Chem.* **2001**, 2989-3004;

121. N. Osheroff, D. L. Brautigantt, And E. Margollasht, *Proc. Natl Acad. Sci. USA* **1980**, *77*, 4439-4443

122. J. D. Winefordner, A Practical Guide to Graphite Furnace Atomic Absorption Spectrometry, *Chemical Analysis*, Vol. 149, Wiley, NY, **1998**
123. Parry E, Osteryoung R **1965** *Anal Chem* 37:1634–1637